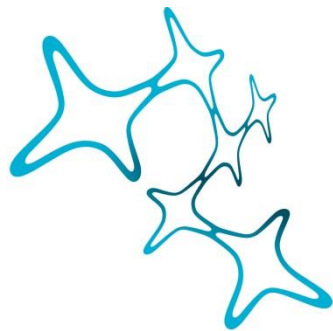

The role of TREM2 in pathogenesis and treatment of Alzheimer's disease

XIANG, Xianyuan



Graduate School of
Systemic Neurosciences

LMU Munich



Dissertation der Graduate School of Systemic
Neurosciences der Ludwig-Maximilians-Universität München

30.04.2019

Supervisor

Prof. Dr. Dr. h.c. Christian Haass

Biomedical Center (BMC), Biochemistry, Ludwig-Maximilians- University
Munich, 81377 Munich, Germany

First Reviewer: Prof. Dr. Dr. h.c. Christian Haass

Second Reviewer: Prof. Dr. Harald Steiner

Date of Defense: 17.07.2019

Introduction.....	1
Alzheimer’s disease	1
1. The amyloid cascade hypothesis.....	1
2. Proteolytic processing of the amyloid precursor protein	2
3. Mutations associated with familial Alzheimer’s disease.....	4
4. Neuropathology of Alzheimer’s disease.....	6
5. The role of microglia in Alzheimer’s disease	9
Therapeutic strategies for Alzheimer’s disease	12
1. β -secretase inhibitors and γ -secretase inhibitors and modulators	12
2. Anti-A β immunotherapy for Alzheimer’s disease	15
Triggering receptor expressed on myeloid cells 2 (TREM2)	22
1. Expression and processing of TREM2	22
2. The function of TREM2 in microglia.....	25
3. TREM2 variants are risk factors of Alzheimer’s disease.....	28
Goals of the study	33
References.....	34
Paper I: TREM2 deficiency reduces the efficacy of immunotherapeutic amyloid clearance (EMBO molecular medicine 2016)	44
Title page.....	45
Abstract.....	46
Introduction	47
Results	50

1. TREM2-deficiency reduces uptake efficacy of antibody-bound A β by phagocytic cells	50
2. Increased Fcy-receptors expression and enhanced Syk phosphorylation in TREM2-deficient BMDM	53
3. TREM2-deficiency reduces antibody-mediated amyloid plaque clearance	54
4. Improvement of amyloid plaque clearance by elevated antibody concentrations	56
Discussion	57
Materials and Methods.....	60
1. Mice.....	60
2. CRISPR/Cas9-mediated genome engineering in N9.....	60
3. Bone marrow derived macrophages culture.....	61
4. Primary microglial culture	62
5. Flow Cytometry.....	62
6. Cell lysis and immunoblotting.....	63
7. Antibodies	64
8. <i>In vitro</i> A β phagocytosis assay	66
9. <i>Ex vivo</i> plaque clearance assay	66
10. Quantitative real-time PCR analysis	68
11. Statistics.....	69
Acknowledgements.....	70
Author contributions.....	70
Conflict of interest.....	71

References.....	72
Figure legends.....	75
Figures	81
Paper II: The TREM2 R47H Alzheimer's risk variant impairs splicing and reduces TREM2 mRNA and protein in mice but not in humans (Molecular neurodegeneration 2018)	87
Title Page	88
Abstract.....	89
Background	91
Materials and Methods.....	94
1. Mice.....	94
2. Generation of TREM2 R47H knock-in mice	94
3. Off target analysis of TREM2 R47H mice.....	95
4. Bone marrow derived macrophages culture.....	96
5. Microglia isolation	96
6. Cell lysis and immunoblotting.....	97
7. iPSC generation.....	98
8. iPSC-derived microglia (iMG)	98
9. Isolation of human blood derived-monocytes	101
10. Microglia signature gene array.....	101
11. Immunocytochemistry	103
12. Cellular splicing assay	104
13. Reverse transcription polymerase chain reaction.....	105
14. Quantitative real-time polymerase chain reaction.....	106

Results	108
1. Reduced mRNA and protein level in TREM2 R47H knock-in mice	108
2. Aberrant splicing of exon1/2 in TREM2 R47H knock-in mice ..	110
3. The R47H variant does not affect splicing and mRNA levels in humans.....	111
Discussion	115
Conclusions.....	117
Abbreviations	118
Declarations.....	118
1. Ethics approval.....	118
2. Consent for publication	119
3. Availability of data and materials	119
4. Competing interests	119
5. Funding	120
6. Authors' contributions	120
7. Acknowledgements	121
Publisher's Note	121
References	122
Figure legends.....	125
Figures	131
Summary and general Discussion	141
TREM2 contributes to antibody-mediated uptake	141

The TREM2 R47H variant impairs TREM2 splicing in mice but not in humans.....	146
References.....	149
Acknowledgments	151
Curriculum Vitae	1
List of publications	2
Eidesstattliche Versicherung / Affidavit	3
Declaration of author contributions	4

Introduction

Alzheimer's disease

1. The amyloid cascade hypothesis

In 1984, Glenner and Wang published a landmark report identifying the cerebrovascular amyloidogenic protein from patients with Alzheimer's disease (AD) ¹. One year later, the amyloid protein from brain parenchyma of individuals with AD or Down syndrome (DS) was characterized, showing that the cerebrovascular and parenchymal amyloid protein share the same origin ². The amyloid protein from AD and DS is derived from the amyloid precursor protein (APP) ³. These findings formed the basis of the amyloid cascade hypothesis. It proposes that amyloid- β (A β) deposits in the brain drive multiple downstream effects and eventually lead to neurodegeneration ⁴⁻⁷ (Fig. 1). Microglia activation is downstream of A β aggregation, but it also could be the driving force for the disease progression when microglia functions are compromised ⁸ (Fig. 1). The amyloid cascade hypothesis moved the focus from descriptive research to mechanistic studies and is now the most widely accepted basis for drug development.

The most powerful evidence supporting the amyloid cascade hypothesis comes from human genetics. DS patients (trisomy 21) have three copies of chromosome 21, where the APP gene locates. These patients often develop dementia due to AD complete with the two main AD pathological features,

amyloid plaques and neurofibrillary tangles, at early age ⁹. Moreover, DS patients with a third copy of chromosome 21 lacking the APP gene do not exhibit plaque and tangle pathologies ¹⁰.

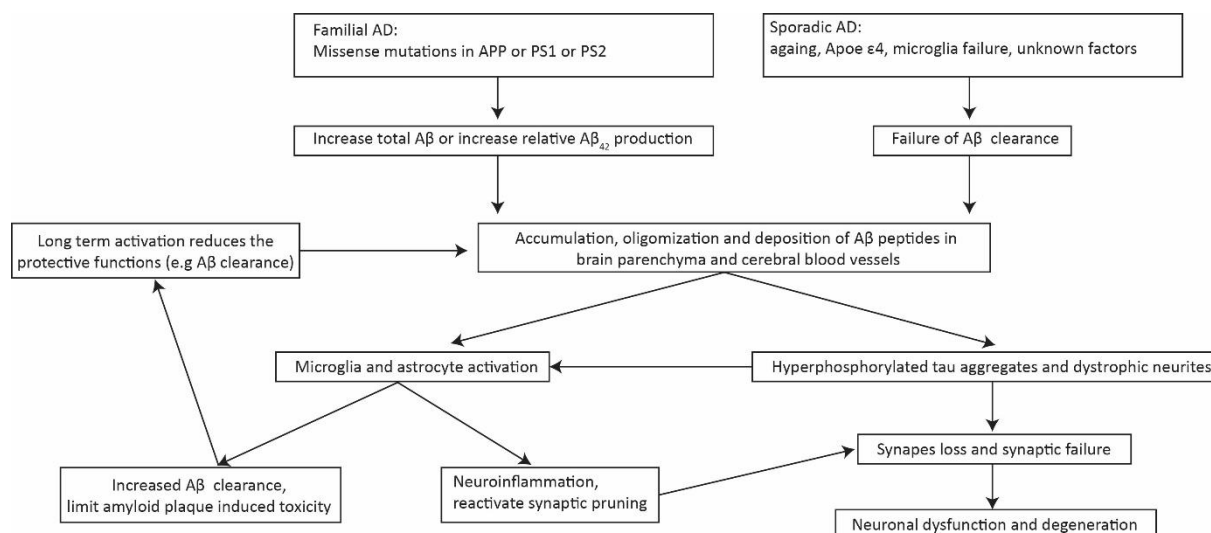


Fig. 1 The major pathological events in AD proposed by the amyloid cascade hypothesis

Accumulated Aβ initiates downstream effects, including glial cells activation and neuronal tau aggregates. The serial events finally lead to neurodegeneration.

2. Proteolytic processing of the amyloid precursor protein

APP is a type-I transmembrane protein ³. APP undergoes proteolytic processing to generate multiple fragments, including the pathogenic Aβ peptides. Three processing pathways were discovered; the anti-amyloidogenic pathway, the amyloidogenic pathway and the η-secretase pathway ^{11,12} (Fig. 2). In the anti-amyloidogenic pathway, a disintegrin and metalloproteinase 10 (ADAM10), also known as α-secretase, cleaves APP to generate soluble

APP α (sAPP α) and membrane-bound CTF α (C83) ¹³. Subsequently, γ -secretase processes CTF α to liberate p3 into the lumen and APP intracellular domain (AICD) into the cytosol ¹¹. γ -secretase is a large protein complex with four essential subunits: nicastrin (NCT), anterior pharynx defective 1a (APH-1a) or APH-1b, presenilin enhancer-2 (PEN-2) ¹⁴⁻¹⁹ and the catalytic subunit presenilin 1 (PS1) or PS2 ²⁰⁻²⁵. p3 is a truncated form of A β lacking the N-terminal amino acid 1-16, and it is considered as a non-pathogenic peptide ²⁶. Alternatively, A β is generated via the amyloidogenic pathway. β -site APP-cleaving enzyme 1 (BACE1) cleaves full-length APP to generate soluble APP β (sAPP β) and a slightly longer form of membrane-bound CTF β (C99) ^{11,27-30}. The CTF β is also processed by γ -secretase to liberate pathogenic A β and AICD ¹¹. In the η -secretase pathway, an additional cleavage site was identified primarily at 504-505 of APP₆₉₅ ¹². MT5-MMP exerts this cleavage, although it might not be the unique η -secretase enzyme ¹². With this additional cleavage, sAPP η and CTF η are generated. Subsequently, CTF η is further processed by α -secretase or BACE1 to release A η - α or A η - β ¹² (Fig. 2).

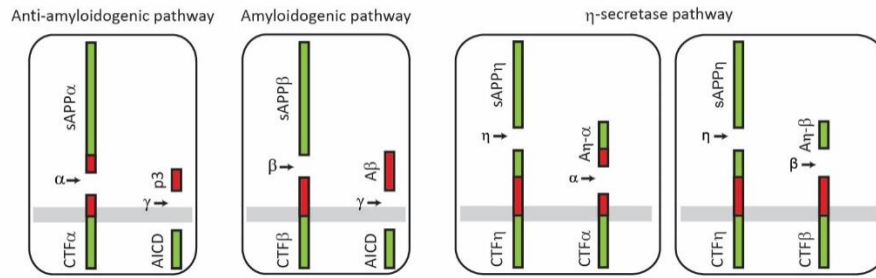


Fig. 2 Processing of the amyloid precursor protein

Anti-amyloidogenic pathway: APP is sequentially cleaved by α-secretase and γ-secretase to liberate sAPPα, p3 and AICD. Amyloidogenic pathway: APP is sequentially processed by BACE1 and γ-secretase to secrete sAPPβ and Aβ and to release AICD. η-secretase pathway: η-secretase cleaves the full-length APP to generate sAPPη and CTFη. CTFη is further cleaved by α-secretase or BACE1. APP: amyloid precursor protein; sAPP: soluble amyloid precursor protein; AICD: APP intracellular domain; CTF: C terminal fragment.

3. Mutations associated with familial Alzheimer's disease

Soon after the identification of APP, mutations were found in familial AD (FAD) patients. The first identified APP mutation was V717I (reference isoform: APP 770 amino acid), close to the C-terminus of Aβ peptide³¹. It elevates the Aβ₄₂ / Aβ₄₀ ratio by increasing formation of the peptide Aβ₄₂, which is more prone to aggregate³². Thereafter, additional mutations in APP were found, some of which alter the proteolytic cleavage of APP or Aβ peptide aggregation properties. For example, the Swedish mutations substitute asparagine (N) and leucine (L) for lysine (K) and methionine (M) (KM670/671NL)^{33–35}. The Swedish mutations strongly enhance total Aβ production^{33–35}. The Arctic mutation (APP E693G) substitutes glycine for glutamic acid, resulting in a faster aggregation rate of Aβ₄₂³⁶. In addition to pathogenic mutations, a very

rare protective coding mutation (A673T) has been identified in Icelanders (Icelandic mutation) ³⁷. In vitro studies show that this protective mutation reduces A β production by about 40% ³⁷ and alters the aggregation properties of either A β ₄₀ ³⁸ or A β ₄₂ ³⁹ peptides. A673T carriers have 28% less plasma A β ₄₀ and A β ₄₂ than non-carriers ⁴⁰, indicating that lifelong A β suppression protects against AD.

Most early-onset familial AD cases have mutations in PS1 ⁴¹. PS1 and PS2 encode presenilins, the catalytic subunits of the γ -secretase ²⁰⁻²⁵. More than 180 mutations were reported in PS1. Most pathogenic PS1 mutations increase the proportion of longer A β species like A β ₄₂, which have higher aggregation properties leading to enhanced A β deposition in mid-life ⁴². For example, the L166P mutation in PS1 reduces A β ₄₀ production and dramatically increases the ratio of A β ₄₂ / A β ₄₀ ⁴³. Patients with the L166P mutation show early-onset AD and have numerous neuritic plaques throughout the cortical region ⁴⁴. Some presenilin mutations, like the FAD-causing mutation L435F in PS1, are loss-of-function mutations and decrease total A β production without significantly altering the level of A β ₄₂ ⁴⁵. This provides evidence that the loss of functional presenilin and not the accumulation of A β underlies FAD ⁴⁵. However, the nearly inactive PS1 L435F mutation primarily produces the highly amyloidogenic A β ₄₃ ⁴⁶. Substantial amounts of A β ₄₃-positive plaques were detected in brains of AD patients with PS1 L435F mutations, indicating that the large amount of A β ₄₃ produced in L435F mutation carriers might induce FAD rather than by a loss of γ -secretase function ⁴⁶. The pathogenic

and protective mutations strongly support that A β dyshomeostasis is necessary and sufficient to cause AD.

4. Neuropathology of Alzheimer's disease

In a short report, Dr. Alois Alzheimer described the neuropathological features of the brain of Auguste D. The brain showed atrophy along with the major lesions, plaques and tangles, which we now know as the two major pathological hallmarks for AD ^{47,48}.

The accumulation of amyloid plaques in CNS is the unique feature for AD. Senile plaques are extracellular deposits containing mainly the A β_{40} and A β_{42} peptides, although A β_{43} is detected in some mutation carriers (Fig. 3 A & B) ^{46,49}. Based on morphology, plaques are classified into two main categories: diffuse plaques and dense-core plaques, also known as neuritic plaques. Dense-core plaques can be easily stained by several dyes like Congo red, Thioflavin-S and Methoxy-X04, which mainly bind to β -sheet structure. Abnormal axons called dystrophic neurites are frequently found around the neuritic plaques. These contain paired helical filaments ^{49,50}, degenerating mitochondria and mitochondria-derived autophagosomes ⁵¹. Ubiquitin and lysosomal-associated membrane protein 1 (LAMP1) are also accumulated in most of these dystrophic neurites ^{52,53}, indicating that retrograde trafficking and lysosomal function might be affected. AD related proteins like APP and BACE1 are found in dystrophic neurites as well, suggesting that axonal transport

defects accelerate A β production locally^{54,55}. Other pathological features, for example, activated microglia⁵⁶, reactive astrocytes⁵⁷, and synaptic and neuronal loss^{58,59}, are associated with neuritic plaques. These features suggest that neuritic plaques are closely related to neuronal injury.

Unlike neuritic plaques, diffuse plaque usually can be detected by immunohistochemistry using antibodies against A β ⁶⁰. Most of them lack the accompanying dystrophic neurites and gliosis^{49,61}. Diffuse plaques are frequently detected in cognitively normal elders^{49,61}. These pathological changes might be the first indication of the disease progression because they may later develop into neuritic plaques⁶². Therefore, the cognitively normal elders with diffuse plaques are considered to be in the presymptomatic stage⁶².

In addition to the parenchymal accumulation, A β also deposits in the vessel walls to form cerebral amyloid angiopathy (CAA). The major component of CAA is A β_{40} ^{49,61}. A β_{40} usually accumulates in the walls of capillaries, small arteries in grey matter and arterioles of the leptomeninges^{49,61}. About 20% of AD patients are CAA negative⁴⁹.

Neurofibrillary tangles (NFTs) are the second important feature of AD, although they do not exclusively appear in AD cases (Fig. 3 A & C). NFTs can be also found in other tauopathies, like Pick disease and certain forms of frontotemporal dementia⁶³. NFTs are intracellular aggregates containing misfolded and hyperphosphorylated microtubule-associated protein tau (p-tau)⁶⁴. In the physiological situation, tau is a highly soluble protein that promotes

the assembly of the microtubule network⁶³. The abnormal phosphorylation of tau changes its conformation and causes it to dissociate from microtubules and accumulate into somatodendritic compartment⁴⁹. Tau phosphorylation also promotes self-aggregation⁶⁵.

In addition to these two main pathological hallmarks, AD brains also exhibit broad glial responses. Activated microglia and astrocytes are associated with neuritic plaques. Microglia activation markers, for example microglial lysosomal protein CD68 and cell surface protein CD11c, are increased with the accumulation of neuritic plaques in entorhinal cortex⁶⁶. However, even after amyloid plaque burden reaches a plateau, microgliosis continues to increase linearly⁶⁷, indicating that glial responses are associated with both amyloid plaques and neurofibrillary tangles. The brain's innate immune system actively responds to any change within the CNS, and these reactions are a double-edged sword (discussed in later chapter).

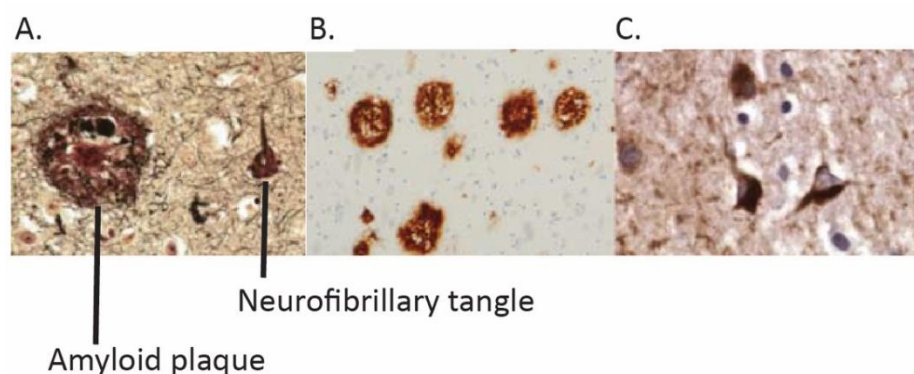


Fig. 3 Neuropathological hallmarks in Alzheimer's diseases

A. Silver staining highlights amyloid plaques and neurofibrillary tangles; B. Amyloid plaques presented by immunostaining using anti-A β antibody; C. Neurofibrillary tangles highlighted by immunostaining using anti-phosphorylated tau antibody. Figure adapted from⁴⁹.

5. The role of microglia in Alzheimer's disease

Microglia are the resident innate immune cells of the central nervous system (CNS) and account for about 5-20% cells of the total mouse brain ⁶⁸. They originate from progenitors in the embryonic yolk sac that migrate into the brain during development ^{69,70}. In the resting stage, microglia appear to be ramified with multiple thin processes that constantly monitor the neighboring area ⁷¹. In response to small injury like microlesions, microglial processes rapidly protrude toward and around the injury site ⁷². Long-term stimulations, for example, amyloid plaques and neurofibrillary tangles, induce morphological changes in microglia from ramified to amoeboid shapes ⁷³ and changes in microglial gene expression and microglial functions ^{74,75}. How do microglia contribute to AD progression? Are they protective or detrimental to the disease?

Recent genome-wide association studies (GWAS) and whole-exome microarray experiments identified variants of multiple genes that are specifically expressed or highly enriched in microglia that increase the risk for late onset Alzheimer's disease (LOAD), including *TREM2*, *ABCA7*, *CD33*, *CR1*, *MS4A*, *PLCG2*, and *ABI3* ^{76,77}. These genetic data indicate that microglia are not a bystander of AD, but rather actively contribute to the disease progression.

Reduced microglia function is deleterious in AD. An important function of microglia is the engulfment and clearance of apoptotic cells and protein

aggregates. The phagocytic capacity of microglia is compromised by risk variants in the gene encoding *triggering receptor expressed on myeloid cells 2* (*TREM2*; discussed in next chapter). Another AD risk variant in *CD33* increases the expression level of CD33, which negatively regulates microglia phagocytic capacity⁷⁸. Microglia constantly change their expression profiles in response to the extracellular environments. In mouse models with plaque pathology, three subpopulations were found: homeostatic, intermediate, and disease-associated microglia (DAM)⁷⁴. In the DAM, certain pathways are highly upregulated, for example, the *TREM2-ApoE* pathway, the phagocytic and the lipid metabolism pathways^{74,75}. Alternatively, homeostatic genes like *P2RY12*, *TMEM119*, and *HEXB* as well as some inhibitory checkpoints like *CX3CR1* are downregulated in this subset of microglia^{74,75}. DAM closely interact with amyloid plaques and also actively engulf A β ⁷⁴. Downregulation of *CX3CR1* might be required for acquiring higher phagocytic capacity, as *CX3CR1* signaling inhibits phagocytosis and *CX3CR1*-deficient mice show reduced A β deposition⁷⁹. Full activation of the DAM signature is Trem2-dependent⁷⁴. Trem2-deficient microglia stay in the intermediate state and lack plaque-clustering capacity, thus they cannot abrogate amyloid pathology-induced toxicity^{74,80,81}. In this context, DAM have protective functions that clear protein aggregates and damaged neurons, as well as shield amyloid plaque to reduce toxicity^{74,80,81}.

Activated microglia can be also deleterious in AD. Although the increased phagocytic capacity of microglia is beneficial for clearing toxic aggregates, aberrant and excessive synaptic engulfment by microglia is detrimental.

Indeed, abnormal synaptic loss is the first sign for neurodegeneration and positively correlates with cognitive decline⁸²⁻⁸⁴. During development, microglia shape neural circuits by eliminating redundant synapses. Developmental synaptic pruning mainly relies on the complement cascade and fractalkine CX3CR1-CX3CL1 interactions⁸⁵⁻⁸⁷. Complement protein C3 and C1q tag immature synapses and mediate phagocytosis via C3 receptors expressed in microglia⁸⁶. During progression of AD, this developmental process appears to be re-activated. C3 and C1q are upregulated in AD mouse models, enhancing synaptic engulfment by activated microglia⁸⁴. This synaptic loss can be blocked by inhibition of C3, or its receptor, CR3⁸⁴.

Another harmful aspect of microglial activation is the excessive secretion of inflammatory cytokines. Activated microglia release many factors, like the pro-inflammatory cytokines TNF α and IL-1 β , microglial proteases, and neurotoxic reactive oxygen⁸⁸. High levels of the pro-inflammatory cytokines TNF α and IL1 β suppress long-term potentiation and induce neurotoxicity⁸⁹. However, TNF α and IL1 β can also be beneficial. Overexpression of either TNF α or IL1 β reduces amyloid pathology^{90,91}. Another harmful aspect of activated microglia is that they also induce neurotoxic reactive astrocytes by secreting TNF α , IL-1 α and C1q⁹². These reactive astrocytes lack neuroprotective functions and induce death of neurons and oligodendrocytes⁹².

Microglia activation induced by amyloid pathology is a double-edged sword. Activated microglia clear A β by elevating phagocytic capacity; however,

chronic interactions between microglia and A β induces proinflammatory cytokines and activates astrocytes, leading to neuronal damage. For developing therapeutic approaches that modify microglia functions, it is crucial to study how to promote microglial protective functions like phagocytosis and prevent harmful effects.

Therapeutic strategies for Alzheimer's disease

The amyloid cascade hypothesis provides multiple intervention opportunities for modifying disease onset and progression. Inhibition and modification of β - and γ -secretases are straightforward strategies for lowering A β production. Anti-A β immunotherapy aims to increase A β clearance and is the most advanced treatment for AD in clinical trials.

1. β -secretase inhibitors and γ -secretase inhibitors and modulators

Because the last step for A β generation is mediated by γ -secretase¹¹, γ -secretase inhibition was a very attractive therapeutic approach. However, γ -secretase cleaves more than 90 intramembrane proteins other than APP, some of which are involved in important signaling cascades⁹³. For example, the γ -secretase cleavage-dependent Notch signaling pathway regulates cell

proliferation, differentiation, and apoptotic programs (Fig. 4)⁹⁴. Non-selective γ -secretase inhibitors, like semagacestat, have failed in clinical trials due to significant adverse events, including skin cancers, infections and gastrointestinal symptoms^{95,96}. To make matters worse, cognitive decline was accelerated in patients receiving semagacestat⁹⁶. These adverse events may be partially due to the non-selective inhibition of γ -secretase resulting in impaired Notch signaling⁹⁵. To avoid non-selective inhibition of γ -secretase function, γ -secretase modulators (GSMs) are in development. GSMs modulate the processivity of γ -secretase, thereby shifting the $A\beta$ production line to shorter species⁹⁷.

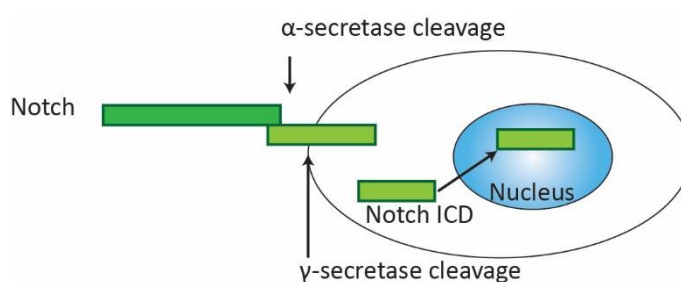


Fig. 4 Illustration of Notch proteolytic processing and signaling

Notch is a cell surface protein that is first cleaved by α -secretase followed by cleavage by γ -secretase to generate the intracellular domain (ICD). Notch ICD translocates to the nucleus where it modulates target gene expression.

Another therapeutic target of AD is β -secretase, also known as BACE1. BACE1 is the rate-limiting enzyme for $A\beta$ generation. Similar to γ -secretase, BACE1 has many substrates⁹⁸. The non-selective inhibition of BACE1 might cause side effects due to affecting the biological functions of its substrates. Dendritic spine density and synaptic plasticity were reduced upon treatment

with a high dose of BACE inhibitors^{99,100}. These alterations result from abolishing the processing of seizure protein 6^{99,100}. Moreover, BACE inhibition alters APP processing, leading to an accumulation of A η - α , which inhibits the neuronal activity in the hippocampus¹². A disruption of axonal organization in the hippocampus was found in adult conditional BACE1 knockout mice, suggesting adulthood complete BACE inhibition might cause deficits in the hippocampus, the region that is important for learning and memory¹⁰¹. The on-target side effects induced by BACE inhibition might be responsible for the recent failure of the BACE inhibitor in a phase III clinical trial. In this trial, prodromal AD patients with positive amyloid positron emission tomography (PET) imaging were recruited for a two-year treatment with the BACE inhibitor verubecestat. Verubecestat caused a small but statistically significant cognitive deficit in a dose-dependent manner (Alzforum news 02 Nov 2018; <https://www.alzforum.org>). A lower dose of BACE inhibitor could be used to avoid the adverse effects, although this might only lower A β production less than 50% (Alzforum news 02 Nov 2018; <https://www.alzforum.org>). In preventive trials with subjects at risk for AD, low doses of BACE inhibitors might have a chance to prevent or delay AD onset, as even small decreases in A β can be protective. For instance, the protective *APP* rare variant A673T lowers plasma A β levels by 28%, indicating lifelong small A β reductions are sufficient to prevent AD⁴⁰. Additionally, the cocktail therapy combining a low dosage of BACE inhibitors with anti-A β immunotherapy can be considered.

2. Anti-A β immunotherapy for Alzheimer's disease

A pivotal study by Schenk and colleagues initiated the anti-A β immunotherapy approach for AD. Immunization of young, pre-plaque PDAPP mice (Table 2) ¹⁰² with A β ₄₂ prevented amyloid plaque pathology ¹⁰³. Amyloid plaque burden was largely reduced in aged PDAPP mice after immunization ¹⁰³. Most importantly, immunotherapy prevented age-related learning and memory deficits in an AD mouse model ¹⁰⁴. These striking preclinical studies inspired the first active immunotherapy clinical trial for AD, which involves intravenous injections of amyloid peptides in patients. In the AN1792 trial (Table 1), A β ₁₋₄₂ was injected into mild to moderate AD patients. However, it had to be terminated at early 2002 after 6% of subjects developed symptoms of T cell-mediated aseptic meningoencephalitis and leukoencephalopathy ^{105,106}. This might be due to the presence of T-cell epitopes in the middle region and the carboxyl terminus of A β ₄₂ ¹⁰⁷. Furthermore, no significant improvement on cognitive performance was detected in patients with an antibody response ¹⁰⁶. A follow-up study from the AN1792 phase I trial examined eight vaccine-recipients neuropathologically ¹⁰⁸. A β load was significantly lower in the A β ₄₂-injected group compared to placebo controls, and the degree of A β reduction correlated with mean anti-A β antibody titer ¹⁰⁸. Despite A β removal in all examined patients in the A β ₄₂-injected group, they had severe end-stage dementia at the time of death ¹⁰⁸. This study is often cited in arguments against the amyloid cascade hypothesis. However, most patients had moderate dementia at the time of vaccination, and plaque removal at this stage may not

be sufficient to reverse the established deficits. Another follow-up study from the AN1792 trial showed that about 4.6 years after immunization with A β ₄₂, most of the antibody responders (17 of 19 individuals tested) still had a low but detectable anti-A β titer ¹⁰⁹. Moreover, these individuals showed reduced functional decline compared to placebo-treated subjects, although brain volumes were the same between the two groups ¹⁰⁹. This follow-up study may suggest that, although anti-A β antibody does not prevent neurodegeneration, daily-life performance of antibody responders may improve. However, the small sample size limited clear conclusions from antibody responders.

The second-generation of A β vaccines are currently being tested in clinical trials (Table 1). The main goals of the second-generation vaccines are to avoid the T-cell mediated cellular immune response and to increase the antibody response titer. For example, ACC-001 (A β ₁₋₆) from Janssen/Pfizer, was tested in two phase IIa trials. Mild to moderate AD patients (n=245) were enrolled to validate the safety, tolerability and anti-A β IgG immunogenicity ¹¹⁰. Amyloid-related imaging abnormalities (ARIAs), which represent vasogenic edema or cerebral microhemorrhages, occurred in 0.8% of patients ^{110,111}. A β ₁₋₆ immunization induced higher and sustained anti-A β IgG titers. In this phase IIa study, cognitive performance did not increase in treatment groups compared to placebo, although the functional measurements are exploratory ¹¹⁰.

Different from active immunotherapy, passive immunotherapy for AD involves immunizing patients with anti-A β antibodies. Peripheral injection of

anti-A β antibody 3D6 decreased amyloid burden in an AD mouse model ¹¹². Although the antibody level in plasma is relative high, only 0.1-0.2% of antibody enters the CNS and decorates amyloid plaques, allowing A β clearance via Fc γ receptor-mediated microglial phagocytosis ¹¹². Compared to active vaccines, passive immunization is easier to stop if adverse events occur and allows for more easily managed antibody concentrations in serum. However, disadvantages to passive immunity are high cost and repeated injections. Several monoclonal antibodies (mAb) are testing in advanced clinical trials (Table 1).

Bapineuzumab is the humanized version of mouse mAb 3D6 and targets the A β ₁₋₅ epitope ^{113,114}. The biggest complication in the phase II trial of Bapineuzumab was ARIAs, which are associated with high antibody doses and the *ApoE* ϵ 4 allele ¹¹³. *ApoE* ϵ 4 is the strongest genetic risk factor for AD ¹¹⁵ and it has been linked to higher degree of cerebral amyloid angiopathy (CAA) in AD mouse models and in AD patients ¹¹⁶. It is possible that vascular integrity is further compromised in *ApoE* ϵ 4 carriers after anti-A β immunotherapy. The primary efficacy analysis did not show significant differences; however, a *post hoc* study analyzing the patients who received all infusion and non-*ApoE* ϵ 4 carriers showed potential cognitive and functional improvements ¹¹⁷. In the phase III trial of Bapineuzumab, *ApoE* ϵ 4 carriers received lower antibody dosage. Unfortunately, no statistically significant cognitive improvement was observed in treatment groups ^{113,114}. ARIAs limited the usage of high antibody dosage in patients, especially in the *ApoE* ϵ 4

carriers. One possible mechanism for ARIAs is that the fast removal of A β from cerebral vessels compromised vessel integrity due to strong Fc effector function ¹¹³. By introducing mutations in the Fc region, the second generation of Bapineuzumab has less binding efficacy to the Fc γ receptor and complement C1q ¹¹⁸. It decreases antibody effector functions, including reduced antibody–FcR interaction-triggered cytotoxicity, slower phagocytosis, and reduced complement cascade-induced cell death ¹¹⁸.

Gantenerumab, a humanized IgG1 anti-A β mAb, preferentially binds to A β fibrils and oligomers ¹¹⁹. Peripheral administration of gantenerumab in PS2APP mice (Table 2) reduced amyloid plaque burden and prevented new plaque formation by eliciting microglia-mediated A β clearance ¹¹⁹. The phase I trial of gantenerumab shows that it was well tolerated in human subjects: only six participants in the high dosage group showed ARIAs ¹²⁰. However, gantenerumab did not meet the primary outcome in the phase II/III trial ¹²¹. There were no significant differences in multiple cognitive tests between treated and placebo subjects ¹²¹, though subgroup analysis indicated that it might benefit patients with fast disease progression during the treatment, especially the ones with high exposure to gantenerumab ¹²¹. This may suggest that high doses of gantenerumab would potentially provide clinical benefits. Serious adverse events were also reported in placebo groups ¹²¹. Again, the prevalence of ARIAs was dose- and *ApoE* $\epsilon 4$ allele-dependent ¹²¹. Currently, gantenerumab is being used in the Dominantly Inherited Alzheimer Network (DIAN), which is a prevention trial enrolled with individuals at risk for developing autosomal dominant AD ¹¹⁴.

Aducanumab is another human IgG1 mAb. It was developed by screening human B-cell clones from healthy aged individuals for reactivity against aggregated A β . Upon peripheral injection of aducanumab into Tg2576 mice (Table 2), A β depositions were decreased, including the thioflavinS-positive compact plaques¹²². The number of amyloid plaque-clustered microglia was increased upon aducanumab treatment, suggesting anti-A β antibody treatment elicited microglia-mediated plaque clearance¹²². In the phase 1b trial, intravenous infusion of aducanumab reduced amyloid plaque in dose- and time-dependent manner in prodromal or mild AD patients measured by amyloid PET¹²². In the highest dose (10 mg/kg) group, amyloid PET signal was comparable to the negative scan after 54 weeks of treatment¹²². Although this trial was not powered for clinical analysis, the exploratory analysis of efficacy indicates a slower cognitive decline in the one-year treatment group¹²². The correlation between amyloid plaque removal and cognitive improvement might suggest microglia-mediated antibody-dependent plaque clearance is important for clinical benefits. Similar to other mAbs, dose- and *ApoE* ϵ 4 allele-dependent ARIAs were the most common adverse effect, and the occurrence is higher than for many other mAbs^{114,122}. Now, two phase III clinical trials were launched to test the efficacy of aducanumab in prodromal or mild AD patients¹¹⁴.

Small amount of antibodies enter the CNS and elicit amyloid clearance by multiple potential mechanisms, including (i) triggering Fc γ receptor-mediated A β clearance by microglia, (ii) binding and removing A β in plasma to generate a net efflux from CNS to plasma, and (iii) binding to A β oligomers to inhibit the

toxicity ¹²³. These mechanisms are not mutually exclusive, and different antibodies might rely more on particular mechanisms. For example, 3D6 (the murine form of bapineuzumab), gantenerumab and aducanumab elicit clearance of plaque by microglia via Fcγ receptor-mediated uptake ^{112,119,122}. For this type of antibody, the phagocytic capacity of microglia is crucial for the optimal outcome of immunotherapy.

Table 1 **Amyloid-related active and passive immunization for Alzheimer's disease**

Active			
Trial	A β target	Stage	Status
AN1792	full-length A β_{1-42} peptide	Phase 2	Terminated; No improvement
ACC-001	A β_{1-7} peptide	Phase 2	Terminated; Not reported
Affitope AD02	six amino acids mimotope mimics the N-terminus of A β	Phase 2	Terminated; Not reported
ABvac 40	C terminus of A β_{40}	Phase 2	Ongoing; safe, well-tolerated, antibody titers in phase I trail
CAD106	A β_{1-6} peptide coupled to a Q β virus-like particle	Phase 2/3	Ongoing; safe, well-tolerated, antibody titers in phase I and II trail; No report on cognitive measurement.
UB 311	A β_{1-14} linked to different helper T-cell peptide epitopes	Phase 2	Ongoing; Not reported
Passive			
Trial	Monoclonal Antibody/Target	Stage	Status
Bapineuzumab (AAB-001)	Humanized IgG1; Anti-A β_{1-5}	Phase 3	Terminated; No cognitive improvement; ARIA
Bapineuzumab (AAB-003)	Humanized IgG4 to minimize ARIA; Anti-A β_{1-5}	Phase 1	Terminated; safe, well tolerated; No significant changes in CSF biomarkers
Crenezumab	Humanized IgG4; Recognizes oligomeric and fibrillar	Phase 3	Terminated; The treatment is unlikely to have positive effects on cognition. It is studied in API*.
Ponezumab	Humanized IgG2a; Binds to the C terminal of A β	Phase 2	Terminated; No change on brain A β and no clinical improvement
Solanezumab	Humanized IgG1; Recognizes soluble monomeric A β	Phase 3	Ongoing in DIAN and A4 Study*; No clinical improvement overall but slight improvement in patients with early AD
Gantenerumab	Human IgG1; High affinity to fibrillar A β	Phase 3	Ongoing; also used in DIAN; No clinical benefits overall but toward a benefit in high dose group with fast progression
Aducanumab	Human IgG1; Binds to aggregated forms of A β	Phase 3	Ongoing; dose-dependent amyloid removal and slowing cognitive decline in exploratory analysis

* API: The Alzheimer's Prevention Initiative; DIAN: Dominantly Inherited Alzheimer Network; A4 Study: Anti-Amyloid Treatment in Asymptomatic Alzheimer's disease; ARIA: Amyloid-related imaging abnormalities; CSF: cerebral spinal fluid

Triggering receptor expressed on myeloid cells 2 (TREM2)

TREM2 is cell surface receptor exclusively expressed on myeloid cells ¹²⁴. TREM2 is required for microglial functions, for example, phagocytosis, migration, and proliferation ^{125–129}. Rare coding variants in *TREM2* increase the risk of AD ^{130,131}, implicating microglia as a pivotal factor in AD progression. In addition to disease progression, microglia functions are crucial for the outcome of immunotherapy. It is valuable for future immunotherapeutic approaches to study if and how TREM2 affects the efficacy of immunotherapeutic approaches.

1. Expression and processing of TREM2

TREM2 localizes at the short arm of chromosome 6 in humans and chromosome 17C3 in mice ¹³². Two isoforms of TREM2 are generated due to alternative splicing, encoding either membrane-bound TREM2 or soluble TREM2 (Fig. 5). In humans, the transcript variant 2 lacks the entire exon 4 coding for the transmembrane region; hence, this transcript encodes soluble TREM2 (Fig. 5). In mouse, soluble TREM2 lacking the transmembrane region is generated due to alternative splicing at the 5' end of the exon 4 ¹³³ (Fig. 5).

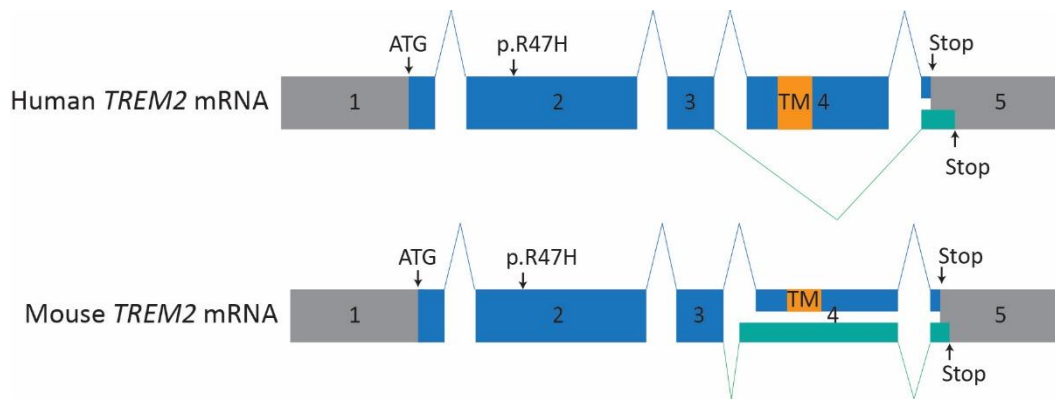


Fig. 5 Alternative splicing of TREM2 mRNA

Alternative splicing of human TREM2 skips the entire exon 4 and shifts the reading frame of exon 5 (green) to generate transcript variant 2 lacking the coding information for the transmembrane region. In mouse, a different splicing acceptor site is used in the alternative spliced mouse TREM2, and it lacks the transmembrane domain due a frame shift (green). TM: transmembrane domain.

The major transcript encodes the membrane-bound TREM2. The membrane bound TREM2 is a type I transmembrane glycoprotein, and it belongs to the immunoglobulin 'superfamily'. It consists of a immunoglobulin-like ligand-binding region in its large extracellular domain, a transmembrane region and a very short intracellular domain (Fig. 6) ^{124,132}.

TREM2 is mainly expressed in the myeloid cell lineage, including macrophages, neutrophils, microglia, and osteoclasts ¹²⁴. The expression level of TREM2 is tightly regulated; for example, proinflammatory stimuli lipopolysaccharide (LPS) reduces TREM2 expression in macrophages and microglia ^{129,134}. TREM2 is highly upregulated in amyloid plaque-associated myeloid cells ^{81,128}, suggesting that amyloid plaques are important inducers for

the expression of TREM2, although it is still unclear if this upregulation is directly induced by A β or by other signals in the near plaque region.

Membrane-bound TREM2 undergoes regulated intramembrane proteolysis similar to APP. The large extracellular domain of TREM2 is shed by ADAM10/17, releasing soluble TREM2 (sTREM2) into the extracellular space (Fig. 6)¹²⁷. Since membrane-bound TREM2 is capable of inducing downstream signaling (discussed in the next section), TREM2 signaling can be blocked by this shedding. The remaining TREM2 CTF is further degraded by γ -secretase (Fig. 6)¹³⁵. When this degradation is impaired, the accumulated TREM2 CTF also interacts with the signaling adaptor protein DNAX-activating protein 12 (DAP12) (discussed in the next section). Thereby, the accumulated TREM2 CTF might limit the interaction between full length TREM2 and DAP12 resulting in decreased TREM2 signaling¹³⁵.

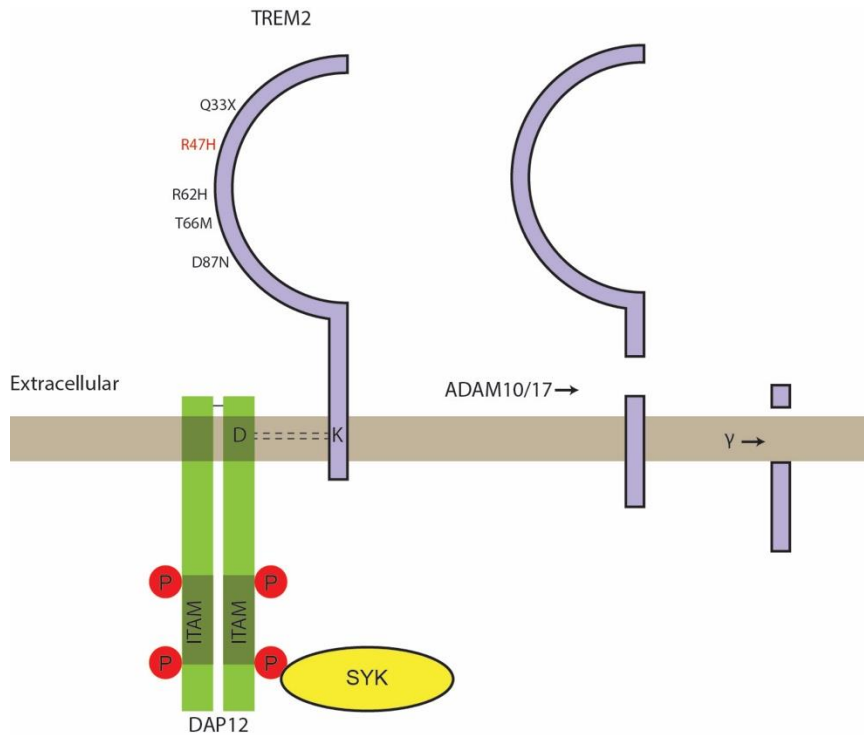


Fig. 6 Illustration of membrane-bound TREM2 and DAP12

TREM2 interacts with DAP12 through an electrostatic interaction between aspartic acid and lysine. DAP12 contains an immunoreceptor tyrosine-based activation motif (ITAM) for signaling. TREM2 is processed by ADAM10/17 and release the soluble TREM2. The membrane-attached fragment is further cleaved by γ -secretase for final degradation.

2. The function of TREM2 in microglia

TREM2 is a lipid sensor and it binds to anionic and zwitterionic lipids ¹²⁵. It also binds to ApoE ^{136,137}, ApoJ ¹³⁶ and A β ¹³⁸. Upon ligand binding, the signal transduction of TREM2 requires the adapter protein DAP12 (Fig. 6). Two cysteine residues in the short extracellular domain of DAP12 allow for the formation of homodimers by disulfide bridges ¹³⁹. A negatively charged aspartic acid residue is located in the transmembrane segment of DAP12, which interacts with the positively charged lysine of TREM2 via electrostatic

interaction¹⁴⁰. In the cytosolic region, DAP12 has an immunoreceptor tyrosine-based activation motif (ITAM) for signaling¹⁴¹ (Fig. 6). When ligands bind to TREM2, the tyrosine residues in the DAP12 ITAM motif are phosphorylated by Src kinases¹²⁴. The phosphorylated ITAM recruits and phosphorylates spleen tyrosine kinase (Syk) or/and Zeta chain-associated protein kinase 70 (ZAP70) to initiate downstream signal cascades¹²⁴.

TREM2 signaling regulates several important microglial functions such as inflammation, phagocytosis, chemotaxis and microglial activation. TREM2/DAP12 signaling plays an anti-inflammatory role by inhibiting cytokine production in response to Toll-like receptors (TLRs) activation¹²⁹.

TREM2/DAP12 signaling is important for phagocytosis. Human embryonic kidney cells 293 (HEK 293) and Chinese hamster ovary cells (CHO), the non-phagocytic cells, were capable of internalizing apoptotic cells and bacteria after TREM2 and DAP12 co-expression^{127,142}. *TREM2* knockout (ko) microglia and macrophages engulf less bacteria, apoptotic neurons, A β fibers and amyloid plaques^{127,136,142}. However, TREM2-dependent A β phagocytosis is controversial. Two groups showed that the phagocytic uptake of A β in TREM2-deficient microglia is comparable to wt microglia^{125,138}. This discrepancy will be further discussed in the summary and general discussion chapter.

TREM2 also regulates chemotaxis and injury response¹⁴³. When TREM2-deficient microglia are challenged by chemotactic signals, such as amyloid deposits, aging or focal laser injury, they are partially activated, and

their migration towards stimuli was impaired ^{74,143}. Some homeostatic check point genes, such as *P2RY12*, *TMEM119*, *CX3CR1*, were downregulated; however, most of phagocytic and lipid metabolism genes related to DAM were unchanged ⁷⁴. This may explain why they show impaired chemotactic motility and phagocytosis.

TREM2 is crucial for maintaining microglia metabolism and autophagy ¹⁴⁴. Mammalian target of rapamycin (mTOR) signaling, which is a central regulator of metabolism and autophagy, is impaired in TREM2-deficient phagocytes ¹⁴⁴. These findings are in line with our results, showing that glucose metabolism was reduced in loss-of-function mutant TREM2 T66M knock-in (ki) mice ¹⁴⁵. However, the reduced glucose consumption in TREM2 T66M ki mice may not only represent the metabolic defects in microglia. Since neurons and astrocytes are the main consumers of glucose, the metabolic status of neurons or astrocytes might be also altered in TREM2-deficient mice. TREM2 is exclusively expressed in microglia within the CNS, suggesting that metabolic changes in neurons or astrocytes might be mediated by sTREM2 generated by shedding of full length TREM2 (Fig. 6).

sTREM2 can be detected in human plasma and cerebrospinal fluid (CSF) ^{127,146}. Two independent studies showed sTREM2 levels are higher in AD patients than in controls ^{147,148}. With a detailed patient characterization, Suárez-Calvet and colleagues found that sTREM2 peaks in patients with mild cognitive impairment due to AD ¹⁴⁹. Moreover, this increase positively correlated with the neurodegeneration markers total tau and

phosphorylated-tau in CSF ¹⁴⁹. Using CSF samples from autosomal dominant AD patients, Suárez-Calvet and colleagues revealed that CSF sTREM2 levels are elevated at 5 years before the expected symptom onset and after A β deposition and neuronal injury ¹⁵⁰. All these data suggest that sTREM2 could be an indicator for microglia activation in response to neuronal injury during disease progression ^{147–150}.

3. TREM2 variants are risk factors of Alzheimer's disease

Homozygous loss-of-function variants in TREM2 or DAP12 lead to a rare autosomal disorder called Nasu-Hakola disease (NHD) ¹⁵¹. NHD is a fatal disease characterized by bone and brain phenotypes. Patients with NHD have bone cysts, frequent bone fractures and joint pain. They also show frontotemporal dementia, followed by death in their fourth or fifth decade of life. Heterozygous mutations in TREM2, on the other hand, increase the risk for several neurodegenerative diseases, including AD, frontotemporal dementia, and Parkinson's disease ^{130,131,152–154}. Most of these variants locate at the immunoglobulin-like ligand-binding region, such as Q33X, Y38C, R47H, R62H, T66M, D78N (Fig. 6). The NHD-related homozygous mutation at position 191 of the TREM2 gene changes glutamine 33 to a stop codon (Q33X), resulting in a premature truncated protein ¹⁵⁵. The same mutation in a heterozygous state is significantly associated with AD ¹³⁰ and frontotemporal dementia ¹⁵², which indicates that impaired TREM2 functions may promote disease onset and progression. Studies from certain variants, like T66M, indicate they result in a

loss of function suggesting that TREM2 has protective roles. TREM2 T66M maturation and transport are impaired, leading to a dramatic accumulation of mutant immature TREM2 in the endoplasmic reticulum^{127,145}. Therefore, cell surface, mature TREM2, sTREM2 and TREM2 CTF are all reduced^{127,145}. TREM2 T66M ki mice show enhanced proinflammatory responses upon LPS stimulation¹⁴⁵, similar to *TREM2* ko mice¹²⁹. The age-dependent microglia activation was reduced in TREM2 T66M ki mice as shown by a longitudinal study using the 18kD microglia activity tracer, translocator protein ligand (TSPO), for small animal PET (μ PET)¹⁴⁵. In line with the TSPO μ PET data, the number of microglial nodules, which are associated with removing myelin/axonal debris, was reduced in TREM2 T66M ki mice¹⁴⁵. Structural analysis suggests T66 is buried within the core of the immunoglobulin fold, and thus the T66M variant may impair protein folding (Fig. 6)¹⁵⁶. These data strongly support that T66M is a loss-of-function mutation and TREM2 is protective against disease progression.

Although several variants of TREM2 contribute to a higher risk for AD¹⁵⁷, TREM2 R47H (rs75932628-T) is the most important disease variant, tripling the risk for AD^{130,131}. It is comparable to the strongest common genetic risk factor for LOAD, the *ApoE* ϵ 4 allele^{158,159}. Structural analyses revealed that arginine 47 is required for stabilizing conformation and maintaining the positive charge binding surface¹⁶⁰. As a result, the R47H variant attenuates ligand (APOE, APOJ, A β etc.) binding^{136,137} and TREM2 signaling¹⁶¹. In line with these findings, overexpression of human TREM2 R47H in *TREM2*^{-/-}:5x*FAD* mice failed to rescue TREM2 loss-of-function phenotypes¹⁶², indicating that

the R47H variant impairs TREM2 functions. Using the CRISPR/Cas9 technique, Cheng-Hathaway and colleagues generated TREM2 R47H ki mice¹⁶³. These mice showed a reduced TREM2 mRNA level and TREM2 loss-of-function phenotypes, including reduced microgliosis, reduced TREM2 upregulation in plaque-associated microglia and reduced microglial clustering around amyloid plaques¹⁶³. This may indicate that the TREM2 loss-of-function in R47H ki mice is due to TREM2 mRNA reduction.

To study the impact of TREM2 loss-of-function on the onset and progression of AD pathology, *TREM2*^{-/-} mice were crossed with different AD mouse models. TREM2 deficiency ameliorated plaque pathology in 4-month-old APP/PS1 mice (Table 2)¹²⁸. However, in another AD mouse model, namely 5xFAD (Table 2), TREM2 deficiency worsens the amyloid burden in hippocampus at 8.5-month of age¹²⁵. Jay and colleagues attempted to clarify the conflict by studying the plaque pathology in *TREM2*^{-/-}: APP/PS1 mice at different ages¹⁶⁴. The results show that the plaque pathology is reduced in young but increased in old TREM2-deficient APP/PS1 mice¹⁶⁴. However, other studies showed that TREM2 deficiency has no impact on the burden of amyloid deposition, but the amyloid plaques are more diffuse and associated with more dystrophic neurites^{80,81}. The increased neuritic damage around amyloid plaques in TREM2 ko mice maybe due to lack of protective microglia barriers^{80,81}. Another factor that interferes with the amyloid aggregation is the A β co-aggregation protein, ApoE. ApoE is strongly upregulated in the subset of microglia with disease associated mRNA signature, which is in the vicinity of plaques⁷⁴. Interestingly, ApoE is heavily

reduced in TREM2 deficient microglia ⁷⁵. Parhizkar and colleagues used an *in vivo* amyloid seeding paradigm to study how TREM2 modified amyloid plaque formation ¹⁶⁵. At the plaque seeding stage, TREM2-dependent microglial activation limits plaque formation ¹⁶⁵. Amyloidogenesis is limited by the phagocytic CD68-positive microglia clustered around the newly seeded plaque ¹⁶⁵. Meanwhile, the plaque-associated microglia upregulate ApoE in a TREM2-dependent fashion ^{75,165}. Amyloid plaque aggregation and compaction might be promoted by TREM2-dependent microglia-derived ApoE, since ApoE is a well-described factor that accelerates A β accumulation and aggregation ^{166–168}. TREM2-deficiency worsens amyloid pathology at the plaque seeding stage due to lack of chemotaxis and phagocytosis; however, the difference on amyloid pathology is compensated by the lack of microglia-derived ApoE during plaque development ¹⁶⁵. TREM2 may have protective functions at the seeding stage by reducing seeding activity.

Table 2 **Research models** (<https://www.alzforum.org>)

Models Names	Overexpressed genes	Plaques deposition begins	Tangles appears after	Cognitive deficits show up at
PDAPP	APP V717F	6-month-old	Absent; but phosphorylated tau spears at 14-month-old	4-month-old
PS2APP	APP KM670/671NL; PSEN2 N141I	6-month-old	Absent	4-month-old
APP/PS1	APP KM670/671NL; PSEN1 L166P	6-weeks-old	Absent; but phosphorylated tau positive	7-month-old
5xFAD	APP KM670/671NL; I716V; V717I; PSEN1 M146L; L286V	Begins at 1.5 months of age	Absent	4-month-old
Tg2576	APP KM670/671NL	12-month-old	Absent	6-month-old
Tau P301S (Line PS19)	Human MAPT P301S	Absent	Appears after 6 months of age	6-month-old
Human Tau ^{+/-} ; mouse Tau ^{-/-}	Human MAPT	Absent	Appears after 9 months of age	6-month-old

MAPT: microtubule-associated protein tau

Goals of the study

Disease-associated rare coding variants in TREM2 most likely are loss-of-function mutations. At least some of the mutant proteins, such as T66M and Y38C, are misfolded and retained within ER ¹²⁷. One of the major impacts of TREM2 loss-of-function on microglia is the phagocytic defect. A complete knockout of TREM2, as well as the T66M variant, reduce the ability of microglia to phagocytose A β fibers, bacteria and beads ^{127,145}. Similarly, myelin debris removal is impaired in TREM2^{-/-} animals after cuprizone-induced acute demyelination ¹⁶⁹. The phagocytic defects of TREM2-deficient microglia may also influence the microglia-mediated antibody-dependent plaque clearance. Amyloid clearance is an essential prerequisite for potential cognitive improvement after anti- A β immunotherapy. The first goal of the thesis was to investigate if the efficacy of anti-A β immunotherapy dependent on TREM2 activity and determine how the disease-associated variants T66M interfere with the immunotherapeutic outcome. Although T66M is a lost-of-function variant, it has been identified to cause FTD-like syndrome but not AD ¹⁷⁰. The AD-associated TREM2 variant, namely R47H has been much less investigated. The second goal of my study was to generate TREM2 R47H ki mouse model and to understand the R47H related dysfunctions responsible for the enhanced risk for late onset AD.

References

1. Glenner, G. G. & Wong, C. W. Alzheimer's disease: initial report of the purification and characterization of a novel cerebrovascular amyloid protein. *Biochem. Biophys. Res. Commun.* **120**, 885–90 (1984).
2. Masters, C. L. *et al.* Amyloid plaque core protein in Alzheimer disease and Down syndrome. *Proc. Natl. Acad. Sci. U. S. A.* **82**, 4245–9 (1985).
3. Kang, J. *et al.* The precursor of Alzheimer's disease amyloid A4 protein resembles a cell-surface receptor. *Nature* **325**, 733–6 (1987).
4. Beyreuther, K. & Masters, C. L. Amyloid precursor protein (APP) and β A4 amyloid in the etiology of Alzheimer's disease: precursor-product relationships in the derangement of neuronal function. *Brain Pathol.* **1**, 241–51 (1991).
5. Hardy, J. A. & Higgins, G. A. Alzheimer's disease: the amyloid cascade hypothesis. *Science* **256**, 184–5 (1992).
6. Hardy, J. & Allsop, D. Amyloid deposition as the central event in the aetiology of Alzheimer's disease. *Trends Pharmacol. Sci.* **12**, 383–8 (1991).
7. Selkoe, D. J. The molecular pathology of Alzheimer's disease. *Neuron* **6**, 487–98 (1991).
8. Hansen, D. V, Hanson, J. E. & Sheng, M. Microglia in Alzheimer's disease. *J. Cell Biol.* **217**, 459–472 (2018).
9. Lemere, C. A. *et al.* Sequence of deposition of heterogeneous amyloid β -peptides and APOE in Down syndrome: implications for initial events in amyloid plaque formation. *Neurobiol. Dis.* **3**, 16–32 (1996).
10. Prasher, V. P. *et al.* Molecular mapping of Alzheimer-type dementia in Down's syndrome. *Ann. Neurol.* **43**, 380–3 (1998).
11. Haass, C., Kaether, C., Thinakaran, G. & Sisodia, S. Trafficking and proteolytic processing of APP. *Cold Spring Harb. Perspect. Med.* **2**, a006270 (2012).
12. Willem, M. *et al.* η -Secretase processing of APP inhibits neuronal activity in the hippocampus. *Nature* **526**, 443–7 (2015).
13. Esch, F. S. *et al.* Cleavage of amyloid β peptide during constitutive processing of its precursor. *Science* **248**, 1122–4 (1990).
14. Yu, G. *et al.* Nicastrin modulates presenilin-mediated notch/glp-1 signal transduction and β APP processing. *Nature* **407**, 48–54 (2000).
15. Lee, S.-F. *et al.* Mammalian APH-1 interacts with presenilin and nicastrin and is required for intramembrane proteolysis of amyloid- β precursor protein and Notch. *J. Biol. Chem.* **277**, 45013–9 (2002).
16. Steiner, H. *et al.* PEN-2 is an integral component of the γ -secretase complex required for coordinated expression of presenilin and nicastrin. *J. Biol. Chem.* **277**, 39062–5 (2002).
17. Edbauer, D. *et al.* Reconstitution of γ -secretase activity. *Nat. Cell Biol.* **5**, 486–8 (2003).

18. Kimberly, W. T. *et al.* γ -secretase is a membrane protein complex comprised of presenilin, nicastrin, Aph-1, and Pen-2. *Proc. Natl. Acad. Sci. U. S. A.* **100**, 6382–7 (2003).
19. Takasugi, N. *et al.* The role of presenilin cofactors in the γ -secretase complex. *Nature* **422**, 438–41 (2003).
20. Steiner, H. *et al.* A loss of function mutation of presenilin-2 interferes with amyloid β -peptide production and notch signaling. *J. Biol. Chem.* **274**, 28669–73 (1999).
21. Esler, W. P. *et al.* Transition-state analogue inhibitors of γ -secretase bind directly to presenilin-1. *Nat. Cell Biol.* **2**, 428–34 (2000).
22. Li, Y. M. *et al.* Photoactivated γ -secretase inhibitors directed to the active site covalently label presenilin 1. *Nature* **405**, 689–94 (2000).
23. Kimberly, W. T., Xia, W., Rahmati, T., Wolfe, M. S. & Selkoe, D. J. The transmembrane aspartates in presenilin 1 and 2 are obligatory for γ -secretase activity and amyloid β -protein generation. *J. Biol. Chem.* **275**, 3173–8 (2000).
24. Steiner, H. *et al.* Glycine 384 is required for presenilin-1 function and is conserved in bacterial polytopic aspartyl proteases. *Nat. Cell Biol.* **2**, 848–51 (2000).
25. Wolfe, M. S. *et al.* Two transmembrane aspartates in presenilin-1 required for presenilin endoproteolysis and γ -secretase activity. *Nature* **398**, 513–7 (1999).
26. Haass, C., Hung, A. Y., Schlossmacher, M. G., Teplow, D. B. & Selkoe, D. J. β -Amyloid peptide and a 3-kDa fragment are derived by distinct cellular mechanisms. *J. Biol. Chem.* **268**, 3021–4 (1993).
27. Lin, X. *et al.* Human aspartic protease memapsin 2 cleaves the β -secretase site of β -amyloid precursor protein. *Proc. Natl. Acad. Sci. U. S. A.* **97**, 1456–60 (2000).
28. Vassar, R. *et al.* β -secretase cleavage of Alzheimer's amyloid precursor protein by the transmembrane aspartic protease BACE. *Science* **286**, 735–41 (1999).
29. Sinha, S. *et al.* Purification and cloning of amyloid precursor protein β -secretase from human brain. *Nature* **402**, 537–40 (1999).
30. Hussain, I. *et al.* Identification of a novel aspartic protease (Asp 2) as β -secretase. *Mol. Cell. Neurosci.* **14**, 419–27 (1999).
31. Goate, A. *et al.* Segregation of a missense mutation in the amyloid precursor protein gene with familial Alzheimer's disease. *Nature* **349**, 704–6 (1991).
32. Eckman, C. B. *et al.* A new pathogenic mutation in the APP gene (I716V) increases the relative proportion of A β 42. *Hum. Mol. Genet.* **6**, 2087–9 (1997).
33. Cai, X. D., Golde, T. E. & Younkin, S. G. Release of excess amyloid β protein from a mutant amyloid β protein precursor. *Science* **259**, 514–6 (1993).
34. Citron, M. *et al.* Excessive production of amyloid β -protein by peripheral cells of symptomatic and presymptomatic patients carrying the Swedish familial Alzheimer disease mutation. *Proc. Natl. Acad. Sci. U. S. A.* **91**, 11993–7 (1994).
35. Citron, M. *et al.* Mutation of the β -amyloid precursor protein in familial Alzheimer's disease increases β -protein production. *Nature* **360**, 672–4 (1992).

36. Nilsberth, C. *et al.* The 'Arctic' APP mutation (E693G) causes Alzheimer's disease by enhanced A β protofibril formation. *Nat. Neurosci.* **4**, 887–93 (2001).
37. Jonsson, T. *et al.* A mutation in APP protects against Alzheimer's disease and age-related cognitive decline. *Nature* **488**, 96–9 (2012).
38. Benilova, I. *et al.* The Alzheimer disease protective mutation A2T modulates kinetic and thermodynamic properties of amyloid- β (A β) aggregation. *J. Biol. Chem.* **289**, 30977–89 (2014).
39. Maloney, J. A. *et al.* Molecular mechanisms of Alzheimer disease protection by the A673T allele of amyloid precursor protein. *J. Biol. Chem.* **289**, 30990–1000 (2014).
40. Martiskainen, H. *et al.* Decreased plasma β -amyloid in the Alzheimer's disease APP A673T variant carriers. *Ann. Neurol.* **82**, 128–132 (2017).
41. Sherrington, R. *et al.* Cloning of a gene bearing missense mutations in early-onset familial Alzheimer's disease. *Nature* **375**, 754–60 (1995).
42. Selkoe, D. J. & Hardy, J. The amyloid hypothesis of Alzheimer's disease at 25 years. *EMBO Mol. Med.* **8**, 595–608 (2016).
43. Li, N. *et al.* Effect of presenilin mutations on APP cleavage; insights into the pathogenesis of FAD. *Front. Aging Neurosci.* **8**, 51 (2016).
44. Moehlmann, T. *et al.* Presenilin-1 mutations of leucine 166 equally affect the generation of the Notch and APP intracellular domains independent of their effect on A β 42 production. *Proc. Natl. Acad. Sci. U. S. A.* **99**, 8025–30 (2002).
45. Xia, D. *et al.* Presenilin-1 knockin mice reveal loss-of-function mechanism for familial Alzheimer's disease. *Neuron* **85**, 967–81 (2015).
46. Kretner, B. *et al.* Generation and deposition of A β 43 by the virtually inactive presenilin-1 L435F mutant contradicts the presenilin loss-of-function hypothesis of Alzheimer's disease. *EMBO Mol. Med.* **8**, 458–65 (2016).
47. Alzheimer, A., Stelzmann, R. A., Schnitzlein, H. N. & Murtagh, F. R. An English translation of Alzheimer's 1907 paper, 'Über eine eigenartige Erkrankung der Hirnrinde'. *Clin. Anat.* **8**, 429–31 (1995).
48. Hardy, J. A hundred years of Alzheimer's disease research. *Neuron* **52**, 3–13 (2006).
49. Serrano-Pozo, A., Frosch, M. P., Masliah, E. & Hyman, B. T. Neuropathological alterations in Alzheimer disease. *Cold Spring Harb. Perspect. Med.* **1**, a006189 (2011).
50. KIDD, M. Paired helical filaments in electron microscopy of Alzheimer's disease. *Nature* **197**, 192–3 (1963).
51. Fiala, J. C., Feinberg, M., Peters, A. & Barbas, H. Mitochondrial degeneration in dystrophic neurites of senile plaques may lead to extracellular deposition of fine filaments. *Brain Struct. Funct.* **212**, 195–207 (2007).
52. Dickson, D. W. *et al.* Ubiquitin immunoelectron microscopy of dystrophic neurites in cerebellar senile plaques of Alzheimer's disease. *Acta Neuropathol.* **79**, 486–93 (1990).

53. Barrachina, M., Maes, T., Buesa, C. & Ferrer, I. Lysosome-associated membrane protein 1 (LAMP-1) in Alzheimer's disease. *Neuropathol. Appl. Neurobiol.* **32**, 505–516 (2006).
54. Zhao, J. *et al.* β -site amyloid precursor protein cleaving enzyme 1 levels become elevated in neurons around amyloid plaques: implications for Alzheimer's disease pathogenesis. *J. Neurosci.* **27**, 3639–49 (2007).
55. Cras, P. *et al.* Senile plaque neurites in Alzheimer disease accumulate amyloid precursor protein. *Proc. Natl. Acad. Sci. U. S. A.* **88**, 7552–6 (1991).
56. Itagaki, S., McGeer, P. L., Akiyama, H., Zhu, S. & Selkoe, D. Relationship of microglia and astrocytes to amyloid deposits of Alzheimer disease. *J. Neuroimmunol.* **24**, 173–82 (1989).
57. Pike, C. J., Cummings, B. J. & Cotman, C. W. Early association of reactive astrocytes with senile plaques in Alzheimer's disease. *Exp. Neurol.* **132**, 172–9 (1995).
58. Masliah, E. *et al.* Synaptic and neuritic alterations during the progression of Alzheimer's disease. *Neurosci. Lett.* **174**, 67–72 (1994).
59. Masliah, E., Terry, R. D., Mallory, M., Alford, M. & Hansen, L. A. Diffuse plaques do not accentuate synapse loss in Alzheimer's disease. *Am. J. Pathol.* **137**, 1293–7 (1990).
60. Yamaguchi, H., Hirai, S., Morimatsu, M., Shoji, M. & Nakazato, Y. Diffuse type of senile plaques in the cerebellum of Alzheimer-type dementia demonstrated by β protein immunostain. *Acta Neuropathol.* **77**, 314–9 (1989).
61. Perl, D. P. Neuropathology of Alzheimer's disease. *Mt. Sinai J. Med.* **77**, 32–42 (2010).
62. Morris, J. C. *et al.* Cerebral amyloid deposition and diffuse plaques in 'normal' aging: Evidence for presymptomatic and very mild Alzheimer's disease. *Neurology* **46**, 707–19 (1996).
63. Wippold, F. J., Cairns, N., Vo, K., Holtzman, D. M. & Morris, J. C. Neuropathology for the neuroradiologist: plaques and tangles. *AJNR. Am. J. Neuroradiol.* **29**, 18–22 (2008).
64. Grundke-Iqbal, I. *et al.* Abnormal phosphorylation of the microtubule-associated protein tau (τ) in Alzheimer cytoskeletal pathology. *Proc. Natl. Acad. Sci. U. S. A.* **83**, 4913–7 (1986).
65. Iqbal, K., Liu, F., Gong, C.-X. & Grundke-Iqbal, I. Tau in Alzheimer disease and related tauopathies. *Curr. Alzheimer Res.* **7**, 656–64 (2010).
66. Xiang, Z., Haroutunian, V., Ho, L., Purohit, D. & Pasinetti, G. M. Microglia activation in the brain as inflammatory biomarker of Alzheimer's disease neuropathology and clinical dementia. *Dis. Markers* **22**, 95–102 (2006).
67. Serrano-Pozo, A. *et al.* Reactive glia not only associates with plaques but also parallels tangles in Alzheimer's disease. *Am. J. Pathol.* **179**, 1373–84 (2011).
68. Lawson, L. J., Perry, V. H. & Gordon, S. Turnover of resident microglia in the normal adult mouse brain. *Neuroscience* **48**, 405–15 (1992).
69. Schulz, C. *et al.* A lineage of myeloid cells independent of Myb and hematopoietic stem cells. *Science* **336**, 86–90 (2012).

70. Ginhoux, F. *et al.* Fate mapping analysis reveals that adult microglia derive from primitive macrophages. *Science* **330**, 841–5 (2010).
71. Nimmerjahn, A., Kirchhoff, F. & Helmchen, F. Resting microglial cells are highly dynamic surveillants of brain parenchyma in vivo. *Science* **308**, 1314–8 (2005).
72. Davalos, D. *et al.* ATP mediates rapid microglial response to local brain injury in vivo. *Nat. Neurosci.* **8**, 752–8 (2005).
73. Colonna, M. & Butovsky, O. Microglia function in the central nervous system during health and neurodegeneration. *Annu. Rev. Immunol.* **35**, 441–468 (2017).
74. Keren-Shaul, H. *et al.* A Unique microglia type associated with restricting development of Alzheimer's Disease. *Cell* **169**, 1276–1290.e17 (2017).
75. Krasemann, S. *et al.* The TREM2-APOE pathway drives the transcriptional phenotype of dysfunctional microglia in neurodegenerative diseases. *Immunity* **47**, 566–581.e9 (2017).
76. Sims, R. *et al.* Rare coding variants in PLCG2, ABI3, and TREM2 implicate microglial-mediated innate immunity in Alzheimer's disease. *Nat. Genet.* **49**, 1373–1384 (2017).
77. Efthymiou, A. G. & Goate, A. M. Late onset Alzheimer's disease genetics implicates microglial pathways in disease risk. *Mol. Neurodegener.* **12**, 43 (2017).
78. Bradshaw, E. M. *et al.* CD33 Alzheimer's disease locus: altered monocyte function and amyloid biology. *Nat. Neurosci.* **16**, 848–50 (2013).
79. Lee, S. *et al.* CX3CR1 deficiency alters microglial activation and reduces β -amyloid deposition in two Alzheimer's disease mouse models. *Am. J. Pathol.* **177**, 2549–62 (2010).
80. Wang, Y. *et al.* TREM2-mediated early microglial response limits diffusion and toxicity of amyloid plaques. *J. Exp. Med.* **213**, 667–75 (2016).
81. Yuan, P. *et al.* TREM2 haploinsufficiency in mice and humans impairs the microglia barrier function leading to decreased amyloid compaction and severe axonal dystrophy. *Neuron* **92**, 252–264 (2016).
82. Terry, R. D. *et al.* Physical basis of cognitive alterations in Alzheimer's disease: synapse loss is the major correlate of cognitive impairment. *Ann. Neurol.* **30**, 572–80 (1991).
83. DeKosky, S. T. & Scheff, S. W. Synapse loss in frontal cortex biopsies in Alzheimer's disease: correlation with cognitive severity. *Ann. Neurol.* **27**, 457–64 (1990).
84. Hong, S. *et al.* Complement and microglia mediate early synapse loss in Alzheimer mouse models. *Science* **352**, 712–716 (2016).
85. Hoshiko, M., Arnoux, I., Avignone, E., Yamamoto, N. & Audinat, E. Deficiency of the microglial receptor CX3CR1 impairs postnatal functional development of thalamocortical synapses in the barrel cortex. *J. Neurosci.* **32**, 15106–11 (2012).
86. Stevens, B. *et al.* The classical complement cascade mediates CNS synapse elimination. *Cell* **131**, 1164–78 (2007).

87. Schafer, D. P. *et al.* Microglia sculpt postnatal neural circuits in an activity and complement-dependent manner. *Neuron* **74**, 691–705 (2012).
88. Hickman, S., Izzy, S., Sen, P., Morsett, L. & El Khoury, J. Microglia in neurodegeneration. *Nat. Neurosci.* **21**, 1359–1369 (2018).
89. Heneka, M. T. *et al.* Neuroinflammation in Alzheimer's disease. *Lancet. Neurol.* **14**, 388–405 (2015).
90. Ghosh, S. *et al.* Sustained interleukin-1 β overexpression exacerbates tau pathology despite reduced amyloid burden in an Alzheimer's mouse model. *J. Neurosci.* **33**, 5053–64 (2013).
91. Chakrabarty, P., Herring, A., Ceballos-Diaz, C., Das, P. & Golde, T. E. Hippocampal expression of murine TNF results in attenuation of amyloid deposition in vivo. *Mol. Neurodegener.* **6**, 16 (2011).
92. Liddelow, S. A. *et al.* Neurotoxic reactive astrocytes are induced by activated microglia. *Nature* **541**, 481–487 (2017).
93. Haapasalo, A. & Kovacs, D. M. The many substrates of presenilin/ γ -secretase. *J. Alzheimers. Dis.* **25**, 3–28 (2011).
94. Artavanis-Tsakonas, S., Rand, M. D. & Lake, R. J. Notch signaling: cell fate control and signal integration in development. *Science* **284**, 770–6 (1999).
95. Godyń, J., Jończyk, J., Panek, D. & Malawska, B. Therapeutic strategies for Alzheimer's disease in clinical trials. *Pharmacol. Rep.* **68**, 127–38 (2016).
96. Doody, R. S. *et al.* A phase 3 trial of semagacestat for treatment of Alzheimer's disease. *N. Engl. J. Med.* **369**, 341–50 (2013).
97. Imbimbo, B. P. Therapeutic potential of γ -secretase inhibitors and modulators. *Curr. Top. Med. Chem.* **8**, 54–61 (2008).
98. Kuhn, P.-H. *et al.* Secretome protein enrichment identifies physiological BACE1 protease substrates in neurons. *EMBO J.* **31**, 3157–68 (2012).
99. Filser, S. *et al.* Pharmacological inhibition of BACE1 impairs synaptic plasticity and cognitive functions. *Biol. Psychiatry* **77**, 729–39 (2015).
100. Zhu, K. *et al.* β -Site amyloid precursor protein cleaving enzyme 1 inhibition impairs synaptic plasticity via seizure protein 6. *Biol. Psychiatry* **83**, 428–437 (2018).
101. Ou-Yang, M.-H. *et al.* Axonal organization defects in the hippocampus of adult conditional BACE1 knockout mice. *Sci. Transl. Med.* **10**, eaao5620 (2018).
102. Games, D. *et al.* Alzheimer-type neuropathology in transgenic mice overexpressing V717F β -amyloid precursor protein. *Nature* **373**, 523–7 (1995).
103. Schenk, D. *et al.* Immunization with amyloid- β attenuates Alzheimer-disease-like pathology in the PDAPP mouse. *Nature* **400**, 173–7 (1999).
104. Morgan, D. *et al.* A β peptide vaccination prevents memory loss in an animal model of Alzheimer's disease. *Nature* **408**, 982–5 (2000).

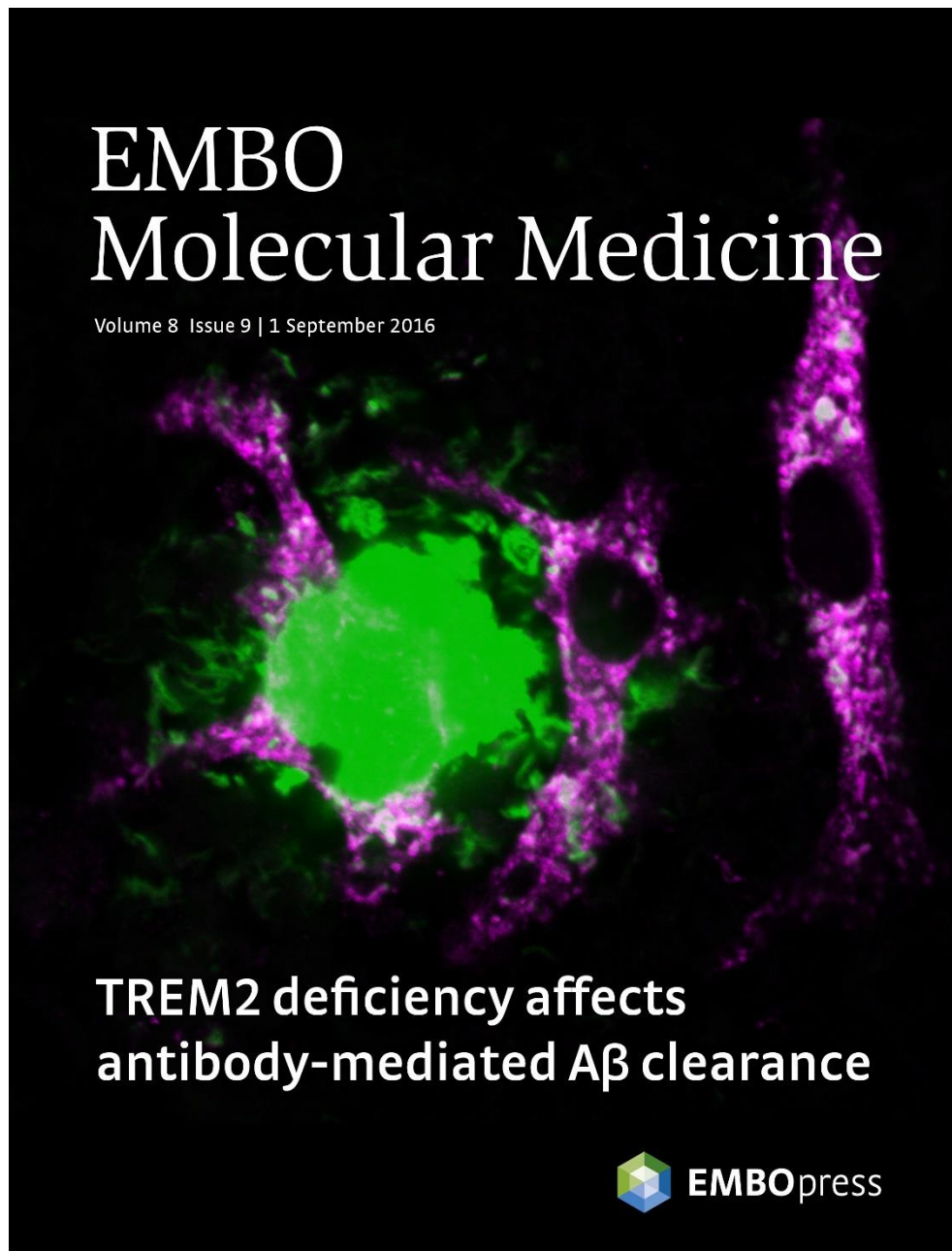
105. Orgogozo, J.-M. *et al.* Subacute meningoencephalitis in a subset of patients with AD after A β 42 immunization. *Neurology* **61**, 46–54 (2003).
106. Gilman, S. *et al.* Clinical effects of A β immunization (AN1792) in patients with AD in an interrupted trial. *Neurology* **64**, 1553–62 (2005).
107. Monsonego, A. *et al.* Increased T cell reactivity to amyloid β protein in older humans and patients with Alzheimer disease. *J. Clin. Invest.* **112**, 415–22 (2003).
108. Holmes, C. *et al.* Long-term effects of A β 42 immunisation in Alzheimer's disease: follow-up of a randomised, placebo-controlled phase I trial. *Lancet (London, England)* **372**, 216–23 (2008).
109. Vellas, B. *et al.* Long-term follow-up of patients immunized with AN1792: reduced functional decline in antibody responders. *Curr. Alzheimer Res.* **6**, 144–51 (2009).
110. Pasquier, F. *et al.* Two phase 2 multiple ascending-dose studies of vanutide cridifcar (ACC-001) and QS-21 adjuvant in mild-to-moderate Alzheimer's Disease. *J. Alzheimers. Dis.* **51**, 1131–43 (2016).
111. Sperling, R. A. *et al.* Amyloid-related imaging abnormalities in amyloid-modifying therapeutic trials: recommendations from the Alzheimer's Association Research Roundtable Workgroup. *Alzheimers. Dement.* **7**, 367–85 (2011).
112. Bard, F. *et al.* Peripherally administered antibodies against amyloid β -peptide enter the central nervous system and reduce pathology in a mouse model of Alzheimer disease. *Nat. Med.* **6**, 916–9 (2000).
113. Wisniewski, T. & Goñi, F. Immunotherapeutic approaches for Alzheimer's disease. *Neuron* **85**, 1162–76 (2015).
114. van Dyck, C. H. Anti-Amyloid- β Monoclonal Antibodies for Alzheimer's Disease: Pitfalls and Promise. *Biol. Psychiatry* **83**, 311–319 (2018).
115. Roses, A. D. Apolipoprotein E alleles as risk factors in Alzheimer's disease. *Annu. Rev. Med.* **47**, 387–400 (1996).
116. Sperling, R. *et al.* Amyloid-related imaging abnormalities in patients with Alzheimer's disease treated with bapineuzumab: a retrospective analysis. *Lancet. Neurol.* **11**, 241–9 (2012).
117. Salloway, S. *et al.* A phase 2 multiple ascending dose trial of bapineuzumab in mild to moderate Alzheimer disease. *Neurology* **73**, 2061–70 (2009).
118. Delnomdedieu, M. *et al.* First-In-Human safety and long-term exposure data for AAB-003 (PF-05236812) and biomarkers after intravenous infusions of escalating doses in patients with mild to moderate Alzheimer's disease. *Alzheimers. Res. Ther.* **8**, 12 (2016).
119. Bohrmann, B. *et al.* Gantenerumab: a novel human anti-A β antibody demonstrates sustained cerebral amyloid- β binding and elicits cell-mediated removal of human amyloid- β . *J. Alzheimers. Dis.* **28**, 49–69 (2012).
120. Ostrowitzki, S. *et al.* Mechanism of amyloid removal in patients with Alzheimer disease treated with gantenerumab. *Arch. Neurol.* **69**, 198–207 (2012).

121. Lasser, R. *et al.* Efficacy and safety of gantenerumab in prodromal Alzheimer's disease: Results from scarlet road—a global, multicenter trial. *Alzheimer's Dement.* **11**, P331–P332 (2015).
122. Sevigny, J. *et al.* The antibody aducanumab reduces A β plaques in Alzheimer's disease. *Nature* **537**, 50–6 (2016).
123. Alves, R. P. S., Yang, M. J., Batista, M. T. & Ferreira, L. C. S. Alzheimer's disease: is a vaccine possible? *Brazilian J. Med. Biol. Res. = Rev. Bras. Pesqui. medicas e Biol.* **47**, 438–44 (2014).
124. Paradowska-Gorycka, A. & Jurkowska, M. Structure, expression pattern and biological activity of molecular complex TREM-2/DAP12. *Hum. Immunol.* **74**, 730–7 (2013).
125. Wang, Y. *et al.* TREM2 lipid sensing sustains the microglial response in an Alzheimer's disease model. *Cell* **160**, 1061–71 (2015).
126. Mazaheri, F. *et al.* TREM2 deficiency impairs chemotaxis and microglial responses to neuronal injury. *EMBO Rep.* **18**, 1186–1198 (2017).
127. Kleinberger, G. *et al.* TREM2 mutations implicated in neurodegeneration impair cell surface transport and phagocytosis. *Sci. Transl. Med.* **6**, 243ra86 (2014).
128. Jay, T. R. *et al.* TREM2 deficiency eliminates TREM2+ inflammatory macrophages and ameliorates pathology in Alzheimer's disease mouse models. *J. Exp. Med.* **212**, 287–95 (2015).
129. Turnbull, I. R. *et al.* Cutting edge: TREM-2 attenuates macrophage activation. *J. Immunol.* **177**, 3520–4 (2006).
130. Guerreiro, R. *et al.* TREM2 variants in Alzheimer's disease. *N. Engl. J. Med.* **368**, 117–27 (2013).
131. Jonsson, T. *et al.* Variant of TREM2 associated with the risk of Alzheimer's disease. *N. Engl. J. Med.* **368**, 107–16 (2013).
132. Klesney-Tait, J., Turnbull, I. R. & Colonna, M. The TREM receptor family and signal integration. *Nat. Immunol.* **7**, 1266–73 (2006).
133. Yeh, F. L., Hansen, D. V. & Sheng, M. TREM2, Microglia, and Neurodegenerative Diseases. *Trends Mol. Med.* **23**, 512–533 (2017).
134. Kleinberger, G. *et al.* The FTD-like syndrome causing TREM2 T66M mutation impairs microglia function, brain perfusion, and glucose metabolism. *EMBO J.* **36**, 1837–1853 (2017).
135. Wunderlich, P. *et al.* Sequential proteolytic processing of the triggering receptor expressed on myeloid cells-2 (TREM2) protein by ectodomain shedding and γ -secretase-dependent intramembranous cleavage. *J. Biol. Chem.* **288**, 33027–36 (2013).
136. Yeh, F. L., Wang, Y., Tom, I., Gonzalez, L. C. & Sheng, M. TREM2 binds to Apolipoproteins, including APOE and CLU/APOJ, and thereby facilitates uptake of amyloid- β by microglia. *Neuron* **91**, 328–40 (2016).
137. Atagi, Y. *et al.* Apolipoprotein E Is a ligand for Triggering Receptor Expressed on Myeloid Cells 2 (TREM2). *J. Biol. Chem.* **290**, 26043–50 (2015).

138. Zhao, Y. *et al.* TREM2 Is a Receptor for β -Amyloid that Mediates Microglial Function. *Neuron* **97**, 1023–1031.e7 (2018).
139. Wilson, M. J., Lindquist, J. A. & Trowsdale, J. DAP12 and KAP10 (DAP10)-novel transmembrane adapter proteins of the CD3zeta family. *Immunol. Res.* **22**, 21–42 (2000).
140. Call, M. E., Wucherpfennig, K. W. & Chou, J. J. The structural basis for intramembrane assembly of an activating immunoreceptor complex. *Nat. Immunol.* **11**, 1023–9 (2010).
141. Lanier, L. L., Corliss, B. C., Wu, J., Leong, C. & Phillips, J. H. Immunoreceptor DAP12 bearing a tyrosine-based activation motif is involved in activating NK cells. *Nature* **391**, 703–7 (1998).
142. N'Diaye, E.-N. *et al.* TREM-2 (triggering receptor expressed on myeloid cells 2) is a phagocytic receptor for bacteria. *J. Cell Biol.* **184**, 215–23 (2009).
143. Mazaheri, F. *et al.* TREM2 deficiency impairs chemotaxis and microglial responses to neuronal injury. *EMBO Rep.* **18**, 1186–1198 (2017).
144. Ulland, T. K. *et al.* TREM2 maintains microglial metabolic fitness in Alzheimer's Disease. *Cell* **170**, 649–663.e13 (2017).
145. Kleinberger, G. *et al.* The FTD-like syndrome causing TREM2 T66M mutation impairs microglia function, brain perfusion, and glucose metabolism. *EMBO J.* **36**, 1837–1853 (2017).
146. Piccio, L. *et al.* Identification of soluble TREM-2 in the cerebrospinal fluid and its association with multiple sclerosis and CNS inflammation. *Brain* **131**, 3081–91 (2008).
147. Piccio, L. *et al.* Cerebrospinal fluid soluble TREM2 is higher in Alzheimer disease and associated with mutation status. *Acta Neuropathol.* **131**, 925–33 (2016).
148. Heslegrave, A. *et al.* Increased cerebrospinal fluid soluble TREM2 concentration in Alzheimer's disease. *Mol. Neurodegener.* **11**, 3 (2016).
149. Suárez-Calvet, M. *et al.* sTREM2 cerebrospinal fluid levels are a potential biomarker for microglia activity in early-stage Alzheimer's disease and associate with neuronal injury markers. *EMBO Mol. Med.* **8**, 466–76 (2016).
150. Suárez-Calvet, M. *et al.* Early changes in CSF sTREM2 in dominantly inherited Alzheimer's disease occur after amyloid deposition and neuronal injury. *Sci. Transl. Med.* **8**, 369ra178 (2016).
151. Klünemann, H. H. *et al.* The genetic causes of basal ganglia calcification, dementia, and bone cysts: DAP12 and TREM2. *Neurology* **64**, 1502–7 (2005).
152. Borroni, B. *et al.* Heterozygous TREM2 mutations in frontotemporal dementia. *Neurobiol. Aging* **35**, 934.e7-10 (2014).
153. Cuyvers, E. *et al.* Investigating the role of rare heterozygous TREM2 variants in Alzheimer's disease and frontotemporal dementia. *Neurobiol. Aging* **35**, 726.e11-9 (2014).
154. Rayaprolu, S. *et al.* TREM2 in neurodegeneration: evidence for association of the p.R47H variant with frontotemporal dementia and Parkinson's disease. *Mol. Neurodegener.* **8**, 19 (2013).

155. Soragna, D. *et al.* An Italian family affected by Nasu-Hakola disease with a novel genetic mutation in the TREM2 gene. *J. Neurol. Neurosurg. Psychiatry* **74**, 825–6 (2003).
156. Kober, D. L. *et al.* Neurodegenerative disease mutations in TREM2 reveal a functional surface and distinct loss-of-function mechanisms. *Elife* **5**, 1–24 (2016).
157. Jin, S. C. *et al.* Coding variants in TREM2 increase risk for Alzheimer's disease. *Hum. Mol. Genet.* **23**, 5838–46 (2014).
158. Corder, E. . H. *et al.* Gene dose of apolipoprotein E type 4 allele and the risk of Alzheimer's disease in late onset families. *Science* **261**, 921–3 (1993).
159. Holtzman, D. M., Herz, J. & Bu, G. Apolipoprotein E and apolipoprotein E receptors: normal biology and roles in Alzheimer disease. *Cold Spring Harb. Perspect. Med.* **2**, a006312 (2012).
160. Sudom, A. *et al.* Molecular basis for the loss-of-function effects of the Alzheimer's disease-associated R47H variant of the immune receptor TREM2. *J. Biol. Chem.* **293**, 12634–12646 (2018).
161. Song, W. *et al.* Alzheimer's disease-associated TREM2 variants exhibit either decreased or increased ligand-dependent activation. *Alzheimers. Dement.* **13**, 381–387 (2017).
162. Song, W. M. *et al.* Humanized TREM2 mice reveal microglia-intrinsic and -extrinsic effects of R47H polymorphism. *J. Exp. Med.* **215**, 745–760 (2018).
163. Cheng-Hathaway, P. J. *et al.* The Trem2 R47H variant confers loss-of-function-like phenotypes in Alzheimer's disease. *Mol. Neurodegener.* **13**, 29 (2018).
164. Jay, T. R. *et al.* Disease progression-dependent effects of TREM2 deficiency in a mouse model of Alzheimer's Disease. *J. Neurosci.* **37**, 637–647 (2017).
165. Parhizkar, S. *et al.* Loss of TREM2 function increases amyloid seeding but reduces plaque-associated ApoE. *Nat. Neurosci.* **22**, 191–204 (2019).
166. Huynh, T.-P. V *et al.* Age-dependent effects of apoE reduction using antisense oligonucleotides in a model of β -amyloidosis. *Neuron* **96**, 1013–1023.e4 (2017).
167. Liu, C.-C. *et al.* ApoE4 accelerates early seeding of amyloid pathology. *Neuron* **96**, 1024–1032.e3 (2017).
168. Ma, J., Yee, A., Brewer, H. B., Das, S. & Potter, H. Amyloid-associated proteins α 1-antichymotrypsin and apolipoprotein E promote assembly of Alzheimer β -protein into filaments. *Nature* **372**, 92–4 (1994).
169. Cantoni, C. *et al.* TREM2 regulates microglial cell activation in response to demyelination in vivo. *Acta Neuropathol.* **129**, 429–47 (2015).
170. Guerreiro, R. J. *et al.* Using exome sequencing to reveal mutations in TREM2 presenting as a frontotemporal dementia-like syndrome without bone involvement. *JAMA Neurol.* **70**, 78–84 (2013).

Paper I: TREM2 deficiency reduces the efficacy of immunotherapeutic amyloid clearance (EMBO molecular medicine 2016)



Title page

TREM2 deficiency reduces the efficacy of immunotherapeutic amyloid clearance

Xianyuan Xiang^{1,2}, Georg Werner¹, Bernd Bohrmann³, Arthur Liesz^{4,6}, Fargol Mazaheri⁵, Anja Capell¹, Regina Feederle^{5,6,7}, Irene Knuesel³, Gernot Kleinberger^{1,6}, & Christian Haass^{1,5,6*}

¹Biomedical Center (BMC), Biochemistry, Ludwig-Maximilians- University Munich, 81377 Munich, Germany

²Graduate School of Systemic Neuroscience, Ludwig- Maximilians- University Munich, 82152 Munich, Germany

³Roche Pharmaceutical Research and Early Development NORD Discovery & Translational Area, Roche Innovation Center Basel, Basel, 4070, Switzerland

⁴Institute for Stroke and Dementia Research, Klinikum der Universität München, 81377 Munich, Germany

⁵German Center for Neurodegenerative Diseases (DZNE) Munich, 81377 Munich, Germany

⁶Munich Cluster for Systems Neurology (SyNergy), 81377 Munich, Germany

⁷Helmholtz Center Munich, German Research Center for Environmental Health, Institute for Diabetes and Obesity, Core Facility Monoclonal Antibody Development, 81377 Munich, Germany

*To whom correspondence should be addressed:
christian.haass@mail03.med.uni-muenchen.de

Running title: TREM2-dependent amyloid clearance
Character count: 39 743

Abstract

Immunotherapeutic approaches are currently the most advanced treatments for Alzheimer's disease (AD). Antibodies against amyloid β -peptide (A β) bind to amyloid plaques and induce their clearance by microglia via Fc receptor-mediated phagocytosis. Dysfunctions of microglia may play a pivotal role in AD pathogenesis and could result in reduced efficacy of antibody-mediated A β clearance. Recently, heterozygous mutations in the triggering receptor expressed on myeloid cells 2 (*TREM2*), a microglial gene involved in phagocytosis, were genetically linked to late onset AD. Loss of *TREM2* reduces the ability of microglia to engulf A β . We have now investigated if loss of *TREM2* affects the efficacy of immunotherapeutic approaches. We show that anti-A β antibodies stimulate A β uptake and amyloid plaque clearance in a dose-dependent manner in the presence or absence of *TREM2*. However, *TREM2*-deficient N9 microglial cell lines, macrophages as well as primary microglia showed significantly reduced uptake of antibody bound A β and as a consequence reduced clearance of amyloid plaques. Titration experiments revealed that reduced efficacy of amyloid plaque clearance by *TREM2* knockout cells can be compensated by elevating the concentration of therapeutic antibodies.

Keywords: Alzheimer's disease, immunotherapy, neurodegeneration, phagocytosis, *TREM2*.

Introduction

Alzheimer's disease (AD) is the most abundant neurodegenerative disorder and threatens our ageing society. Therapeutic treatment is desperately required to slow progression of dementia. The amyloid cascade¹ provides a number of opportunities to therapeutically interfere with disease onset and progression. Obvious targets are β - and γ -secretases, the two proteases, which generate the amyloid β -peptide ($A\beta$) from its precursor, the β -amyloid precursor protein (APP)². γ -secretase inhibition caused major side effects in a clinical trial, which were at least partially due to inhibition of its biological activity in Notch signaling³. Similarly, recent findings may also indicate that inhibition of β -secretase may be problematic due to the accumulation of alternative neurotoxic APP derived fragments⁴. Moreover, β -secretase has numerous brain specific substrates and their biological function may be disturbed upon inhibition of shedding⁵⁻⁷. In fact, neuregulin-1 signaling depends on biologically active β -secretase^{8,9}. Nevertheless, several β -secretase inhibitors are currently in late stage clinical development and if demonstrated to be safe may be of therapeutic value. The most advanced and very promising therapeutic approach is currently the anti- $A\beta$ immunotherapy¹⁰, a treatment strategy initiated after the pivotal report by Schenk *et al.*¹¹ demonstrating its efficacy in amyloid plaque removal and reduction of memory decline in an animal model¹². After crossing the blood brain barrier anti- $A\beta$ antibodies like 3D6 and others bind to amyloid plaques and trigger Fc-receptor mediated phagocytosis of plaques by microglia cells¹³. Indeed, 11C-PiB

positron emission tomography (PET) revealed a significant reduction of amyloid deposition in patients treated with anti-A β antibodies^{14,15}. Although initially there was no obvious beneficial effect on memory, data from two recent clinical trials now suggest that immunotherapy may significantly slow memory decline¹⁶. Moreover, a recent clinical trial using Aducanumab indicated that significant amyloid removal is required for clinical benefits suggesting a critical role of amyloid removal by microglia. Indeed, antibody-mediated clearance of amyloid plaques requires biologically active microglia cells¹³. Recently it was reported that heterozygous mutations in the triggering receptor expressed on myeloid cells 2 (*TREM2*) increase the risk for AD, Frontotemporal Lobar Degeneration, Amyotrophic Lateral Sclerosis, and Parkinson's disease¹⁷⁻²⁴. We have shown that certain mutations in *TREM2* such as p.T66M reduce the ability of microglia to phagocytose A β fibers, bacteria and beads due to impairment of *TREM2* maturation and cell surface transport²⁵. Furthermore, a complete knockout of *TREM2* also reduces the ability of primary microglia to phagocytose A β ²⁵. Similarly, in a cuprizone-model for acute demyelination *TREM2*-deficient mice showed reduced phagocytic removal of myelin debris²⁶. However, in mouse models for AD pathology *TREM2*-deficiency resulted in inconsistent findings. Jay *et al.* reported a detrimental role of *TREM2* in AD by demonstrating that its knockout leads to a reduction of the amyloid plaque load, inflammation, astrogliosis and tau phosphorylation²⁷. On the other hand, Wang *et al.* demonstrated that *TREM2*-deficiency enhanced amyloid plaque load²⁸. This discrepancy may be due to the use of different mouse models, but

also due to the fact that microglial function may be differentially compromised depending on the time point one investigates amyloid pathology²⁹.

It is well known that antibodies bound to amyloid plaques trigger Fc-receptors mediated A β clearance by microglia cells¹³. We were interested if antibody-mediated A β clearance may be influenced by TREM2 function. To avoid confounding effects of different mouse models, time points of analysis and differences in progression of disease pathology, which in aggressive APP/presenilin overexpressing mouse models may even override microglial amyloid plaque clearance, we choose several independent models to quantitatively investigate TREM2-dependent antibody-mediated A β clearance under controlled conditions. We used CRISPR/Cas9 modified N9 microglial cell lines as well as bone marrow derived macrophages (BMDM) and primary microglia cells from wild-type (wt) or *TREM2* knockout (ko) mice and investigated the potential of these cells for antibody-dependent phagocytosis of pre-formed A β fibrils or engulfment of antibody covered amyloid plaques from brain cryosections obtained from a mouse model for AD pathology.

Results

1. TREM2-deficiency reduces uptake efficacy of antibody-bound A β by phagocytic cells

To investigate a potential influence of TREM2-deficiency on antibody-mediated A β clearance, we first studied A β uptake in the microglial cell line N9³⁰. *TREM2* mutant cell lines were generated using the CRISPR/Cas9 technology³¹. We obtained a mutant cell line with a single nucleotide insertion (93_94insG) within the target site, which leads to a frameshift and an early stop codon that eliminates TREM2 expression (Fig. 1A). Immunoblotting confirmed the loss of full-length, membrane-bound TREM2 as well as soluble TREM2 (sTREM2) in *TREM2* mutant N9 cells (N9 mu) (Fig. 1B). In line with our previous findings²⁵, loss of TREM2 significantly reduced uptake of pre-aggregated HiLyte™ Fluor 488 labeled A β ₄₂ (fA β ₄₂) (Fig. 1C). Cytochalasin D, an inhibitor of actin polymerization, was used as negative control. Addition of 5 μ g/ml of antibody 2D8, an antibody raised to the N-terminus of the A β domain³², significantly stimulated A β uptake in both N9 wt and N9 mu, however phagocytosis remained less efficient in N9 mu (Fig. 1C). As a negative control we used antibody 6687 raised to the C-terminus of APP³³. Although this antibody interacts with APP it fails to increase A β uptake demonstrating that the specific interaction of 2D8 with A β is required to trigger the uptake (Fig. 1C).

To investigate antibody-stimulated A β clearance in primary phagocytic cells we first used BMDM derived from *TREM2* ko animals³⁴ or wt controls. Western blotting confirmed the absence of sTREM2 and full-length, membrane bound TREM2 in cells derived from *TREM2* ko mice (Fig. 1D). We then studied fA β ₄₂ uptake in the presence of 0, 1, 5, or 10 μ g/ml of antibody 2D8 or a non-binding control antibody 6687. BMDM readily internalized fA β ₄₂, which could be blocked entirely by addition of cytochalasin D (Fig. 1E). Consistent with our previous findings²⁵, BMDM derived from *TREM2* ko mice showed a significantly reduced phagocytic activity compared to BMDM derived from wt mice (Fig. 1E). Phagocytosis of fA β ₄₂ in wt BMDM could be intensively stimulated by antibody 2D8 with a maximum stimulation at 5 μ g/ml. Antibody 6687 even at a high concentration of 10 μ g/ml had only a very minor effect (Fig. 1E). Although antibody 2D8 significantly stimulated uptake of fA β ₄₂ even in *TREM2* ko BMDM, phagocytosis was less efficient compared to wt at all antibody concentrations used (Fig. 1E). These findings suggest that fA β ₄₂ uptake is greatly stimulated upon antibody binding in both wt and *TREM2* ko BMDM, however the overall uptake capacity is reduced in *TREM2* ko BMDM. In line with that there was no significant change in the relative increase of antibody-stimulated uptake in both genotypes (Fig. 1F) suggesting that antibody-stimulated uptake *per se* is not reduced due to TREM2 deficiency.

Next, we used the monoclonal antibody mAb11, a murine IgG2a antibody, which has similar amyloid binding properties like the therapeutically used human IgG1 anti-A β antibody Gantenerumab^{35,36} and performed titration experiments in the fA β ₄₂ uptake assay using BMDM derived from wt or *TREM2*

ko mice. mAb11 but not an IgG2a isotype control (50 µg/ml) strongly stimulated phagocytosis of fAβ₄₂ (Fig. 1G). Interestingly, even very low concentrations of 0.1 µg/ml, which may be reached in the brain by peripheral antibody administration, were sufficient to trigger fAβ₄₂ uptake. Uptake plateaued at 20 µg/ml and could not be further enhanced by using antibody concentrations up to 50 µg/ml (Fig. 1G). In line with the data shown in Fig. 1C & E, fAβ₄₂ uptake by BMDM derived from *TREM2* ko mice could be efficiently stimulated by increasing the amounts of mAb11 (Fig. 1G & H). However, again the phagocytic capacity never reached the level of wt BMDM even at the highest antibody concentration used (Fig. 1G). Thus, a monoclonal antibody with efficient target engagement similar to the therapeutically used Gantenerumab stimulates both TREM2 dependent and independent engulfment of fAβ₄₂.

To investigate if sTREM2 could rescue reduced fAβ₄₂ uptake of BMDM derived from *TREM2* ko mice in a non-cell autonomous manner we supplemented the culture media of wt and ko cells with increasing amounts of recombinant mouse sTREM2. sTREM2 even added at a 10-fold higher concentration as compared to its physiological concentration in plasma of mice (approximately 10 ng/ml) did not rescue fAβ₄₂ uptake efficacy of *TREM2* ko cells in the presence or absence of mAb11 (Fig. 1I). Thus, receptor mediated signaling in a cell autonomous manner appears to trigger fAβ₄₂ uptake.

Finally, we further confirmed our findings in primary microglia derived from wt or *TREM2* ko mice. Western blotting confirmed the absence of sTREM2 and full-length, membrane bound TREM2 in primary microglia from *TREM2* ko mice (Fig. 1J). In line with our previous findings ²⁵, microglia from *TREM2* ko mice showed significantly less uptake of $\text{fA}\beta_{42}$ (Fig. 1K). Again, phagocytosis was similarly stimulated by mAb11 in a concentration-dependent manner in both, microglia derived from wt and from *TREM2* ko mice (Fig. 1K & L). In line with the above data derived from N9 cells and BMDM (Fig. 1C, E and G), total uptake capacity was reduced at each antibody concentration in *TREM2* ko microglia (Fig. 1K).

2. Increased Fc γ -receptors expression and enhanced Syk phosphorylation in *TREM2*-deficient BMDM

To investigate if reduced phagocytic capacity but similar increases of antibody-stimulated uptake in the absence of TREM2 may be due to compensatory mechanisms, we first investigated expression of Fc γ -receptors (Fc γ R), which are of central importance for antibody-mediated phagocytosis. Compared to wt BMDM, cell surface Fc γ RI, Fc γ RIIB and (or) Fc γ RIII were significantly increased in *TREM2* ko cells (Fig. 2A & B). Correspondingly, mRNA levels of the respective Fc γ R (I, IIB, III) were all significantly increased in *TREM2* ko cells (Fig. 2C). mRNA level of Fc γ RIV was also increased but it did not result in enhanced cell surface protein level (Fig. 2A-C). To further

validate the compensatory mechanisms, downstream signaling was studied. It is well known that upon stimulation of TREM2 as well as Fcγ-receptors, Syk gets phosphorylated and activates a variety of downstream signaling cascades^{23,37,38}. As expected, Syk phosphorylation strongly increases upon incubation of wt BMDM with 2D8-bound Aβ which was not the case when using an isotype-control antibody together with Aβ (Fig. 2D & E). Interestingly, phosphorylation of Syk is further increased upon stimulation with antibody-bound Aβ in the absence of TREM2 (Fig. 2D & E).

Together with increased levels of FcγR this may suggest a compensatory increase of TREM2 independent antibody/antigen uptake pathways probably explaining why TREM2 ko cells still respond to increasing concentrations of anti-Aβ antibodies.

3. TREM2-deficiency reduces antibody-mediated amyloid plaque clearance

Next we used an *ex vivo* model (Fig. 3A), which would allow monitoring antibody-dependent amyloid plaque clearance under controlled and comparable conditions¹³. We used cryosections of whole brains from APP/PS1 mice¹⁶ at 6-months of age, a time point where these mice are known to exhibit a high amyloid plaque burden within the brain¹⁶. mAb11, but not the isotype control, binds selectively to the methoxy-X04 positive amyloid plaques (Fig. 3B). When wt BMDM (Fig. 3C) or primary microglia (Fig. 3D) were added

to brain sections pre-incubated with mAb11, we observed a clustering of CD68 positive cells around methoxy-X04 labeled amyloid plaques. Moreover, cells clustering around amyloid plaques engulfed A β fibers, as shown by the intracellular methoxy-X04 staining, which partially co-localized with the lysosomal protein CD68 (Fig. 3C & D).

We next used the *ex vivo* assay to investigate TREM2-dependent antibody-stimulated amyloid plaque clearance. When cryosections of APP/PS1 mice were incubated with BMDM derived from wt or *TREM2* ko mice, a significant TREM2-dependent reduction of amyloid plaque clearance was observed (Fig. 4A & B). Upon pre-incubation of cryosections with mAb11 (1 μ g/ml), amyloid plaque clearance by wt BMDM was significantly stimulated (Fig. 4A & B). In line with the results in Fig. 1, TREM2-deficient BMDM were significantly less efficient in clearing amyloid plaques than wt BMDM under the same experimental conditions (Fig. 4A & B). Cell densities in the different experiments were similar, as assessed by CD68 staining on consecutive slices (Fig. 4C & D). Reduced amyloid plaque clearance by BMDM derived from the *TREM2* ko animals upon antibody stimulation was confirmed by western blotting of total protein lysates generated from cryosections after termination of the experiment. In line with the experiments in Fig. 4A & B, mAb11 caused a stronger reduction of A β signals on western blots in the presence than in the absence of TREM2. However, even in the absence of TREM2, a reduction of A β was observed with mAb11 pre-incubation as compared to the no-antibody control (Fig. 4E).

4. Improvement of amyloid plaque clearance by elevated antibody concentrations

We next titrated mAb11 with the aim to compare the efficacy of antibody-mediated TREM2-dependent amyloid plaque clearance. Cryosections from brains of APP/PS1 mice were pre-incubated with increasing concentrations of mAb11 from 0.001 $\mu\text{g/ml}$ to 5 $\mu\text{g/ml}$ before incubation with BMDM derived from wt or *TREM2* ko mice. In line with the $\text{fA}\beta_{42}$ uptake assays described in Fig. 1, this revealed a concentration dependent clearance of amyloid plaques (Fig. 5A & B). Comparison of the extend of methoxy-X04 positive amyloid labeling after clearance by BMDM derived from wt or *TREM2* ko mice demonstrates that antibody-mediated clearance can occur in the absence of TREM2 (Fig. 5A & B), similar to the uptake of $\text{fA}\beta_{42}$ shown in Fig. 1. However, the total capacity to engulf amyloid plaques is reduced in *TREM2* ko BMDM (Fig. 5A & B). Of note, a statistically significant effect on amyloid plaque clearance is observed in *TREM2* ko BMDM at 0.1 $\mu\text{g/ml}$, a concentration which is therapeutically reachable in brain by appropriate dose adjustment ^{35,36}. Taken together, our finding suggests that patients with compromised TREM2 function may require a higher dose of the therapeutic antibody to achieve efficient $\text{A}\beta$ clearance.

Discussion

A pivotal role of microglia and inflammatory mechanisms in AD and other neurodegenerative disorders, which was already emphasized early during AD research³⁹, was recently strongly supported by genetic evidence²⁴. Specifically, rare heterozygous mutations in *TREM2*, which within the brain is exclusively expressed in microglia cells, dramatically increase the risk for late onset AD in a magnitude similar to *ApoE ε4*^{20,21}. Although *TREM2* is well known to be involved in phagocytosis and removal of apoptotic neurons^{40–42} the pathological consequences of a *TREM2* loss-of-function in the context of AD pathogenesis is highly controversial. While $A\beta$ was shown to be engulfed at least to some extent in a *TREM2*-dependent manner in cultured cells²⁵, experiments on mouse models for AD pathology reached surprising and opposite results. On the one hand, reduction of *TREM2* ameliorated several aspects of AD pathology, including inflammation, astrogliosis and amyloid plaque burden²⁷ while on the other hand, *TREM2*-deficiency leads to exacerbated disease pathology including increased amyloid plaque burden²⁸. However, attenuated $A\beta$ engulfment by microglia was thought to be due to reduced migration and survival and thus not directly associated with phagocytic activity of microglial cells²⁸. Our findings may now provide direct evidence that *TREM2* is required at least partially for $A\beta$ engulfment and clearance. Even in the absence of antibody stimulation we consistently find reduced $A\beta$ uptake and amyloid plaque clearance in all model systems used. Potential survival deficits in *TREM2* ko cells do not impact our results, since

uptake was measured after 2 hours of incubation in the phagocytosis assay. Moreover, equal amounts of cells were used in the *ex vivo* plaque clearance assay and cell density was assessed after termination of experiments ruling out differences due to survival or the total number of phagocytic cells.

After antibody binding to A β , uptake and amyloid plaque clearance increase in a concentration-dependent manner in the presence or absence of functional TREM2, although the total uptake capacity of cells lacking TREM2 is reduced. This indicates that TREM2-independent Fc γ -receptor-mediated pathways are intact and used in addition to TREM2-dependent uptake mechanisms. Indeed, it has been shown previously that Syk phosphorylation is an important signaling event upon Fc γ -receptors activation in macrophage phagocytosis^{37,43}. Higher levels of Fc γ R and upregulated phosphorylated Syk in *TREM2* ko BMDM upon stimulation with A β -2D8 immune complexes may therefore suggest a compensatory upregulation of TREM2-independent phagocytosis.

Our findings might also indicate that direct effects of TREM2 on amyloid plaque clearance are difficult to assess *in vivo* since in the absence of an antibody stimulus A β uptake is 4-5 fold lower and probably difficult to quantify. In addition, the mouse models used to study the effects of TREM2 on amyloid plaque clearance not only highly overexpress APP but also express rather aggressive familial AD associated mutations, which may override modulatory effects of TREM2. Moreover, since TREM2 affects survival of microglial cells^{28,44}, the age as well as the specific mouse model used for the investigation

must be carefully considered. In that regard, it is interesting to note that at very early time points of amyloid plaque deposition A β accumulation was similar in wt and *TREM2* ko mice, but *TREM2* ko mice showed reduced microglia accumulations around amyloid plaques ⁴⁵.

Finally, our findings may be valid for future immunotherapeutic approaches. Anti A β immunotherapy is currently a promising and clinically advanced approach ¹⁰. It not only lowers the amyloid plaque load, but also prevents *de novo* deposition of plaques and stabilized memory deficits at least to some extent in two recently reported clinical trials ⁴⁶. We now demonstrate that mAb11, a murine IgG2a antibody, which has similar amyloid binding properties like Gantenerumab ³⁶ which is currently explored in clinical trials ³⁵, significantly stimulates A β engulfment even in the absence of TREM2. For successful immunotherapy, knowledge on microglial activity and survival in individual patients may be crucial for optimal outcome of the treatment. In that regard we recently demonstrated that in AD patients, sTREM2 levels significantly increase very early before onset of AD and tend to decrease in later phases of the disease ⁴⁷. In addition to CSF biomarkers, microglial PET imaging may be required similar to amyloid PET imaging used in the clinic to select patients for enrollment into clinical trials and to *in vivo* prove the effects of treatment on amyloid plaque load. If microglial function and survival are reduced during ageing in a TREM2-dependent manner, one may also speculate to modulate TREM2 activity. Moreover, in case of attenuated TREM2 function an increased dose of therapeutic antibodies may be required to compensate impaired plaque clearance.

Materials and Methods

1. Mice

All animal experiments were performed in accordance to local animal handling laws. APP/PS1 and *TREM2* knockout mice (*TREM2* ko)³⁴ were maintained on a C57BL/6J background. For bone marrow extraction, adult mice (from 2-months old to 12-months old, mixed gender) were euthanized by CO₂ then sacrificed by cervical dislocation. For primary microglia culture, postnatal day P0-2 mice (mixed gender) were sacrificed by decapitation.

2. CRISPR/Cas9-mediated genome engineering in N9

The murine microglia cell line N9³⁰ was maintained in Dulbecco's modified Eagle's medium (DMEM) + GlutaMAXTM (Life Technologies) with 10% (v/v) fetal calf serum (FCS; Sigma-Aldrich) and 100 U/ml penicillin, 100 µg/ml streptomycin. All cells were mycoplasmas free. N9 cells were transfected with pSpCas9(BB)-2A-Puro V2.0 (PX459; gift from Feng Zhang; Addgene plasmid # 62988) using the NucleofectorTM SF-Kit for 4D-NucleofectorTM (Lonza) according to manufacturer's recommendations. 24 h post transfection, cells were selected with 4 µg/ml puromycin for 2 days. Single cell clones were then cultured with normal culture medium, followed by screening for genetic modifications in *TREM2* by PCR amplification and missense detection using

T7 Endonuclease I (NEB). Mutations were confirmed by direct sequencing (GATC-Biotech).

3. Bone marrow derived macrophages culture

Bone marrow derived macrophages (BMDM) were prepared essentially as described before ⁴⁸. Briefly, mice femurs and tibias were dissected and sterilized with 70% ethanol. The bones were flushed with a syringe filled with advanced RPMI 1640 (Life Technologies) to extrude bone marrow. Cell suspensions were filtered through a 100 µm cell strainer and incubated for 2 min in ACK lysis solution (Thermo Fisher Scientific) to lyse red blood cells. The bone marrow cells were cultured and differentiated in advanced RPMI 1640 supplemented with 2mM L-Glutamine, 10% (v/v) FCS, 100 U/ml penicillin, 100 µg/ml streptomycin and 50 ng/ml murine M-CSF (R&D System) using non-tissue culture treated Petri dishes (BD Biosciences). Three days after seeding fresh murine M-CSF (final concentration of M-CSF 50 ng/ml) was added and media was changed at day 5 of culture. BMDM were used for experiments at day 7 *in vitro*. Immunostaining with CD68 (Fig. 3C and Fig. 4C) as well as flow cytometry (see below) using anti-CD11b antibody (Fig. EV1A) were used to confirm the identity of these cells.

4. Primary microglial culture

Primary murine microglial murine cell cultures were prepared as previously described. Briefly, mixed glial cultures were prepared from the whole brain devoid meninges and cerebellum of P0-2 mice and cultured in DMEM with Glutamax I (Life Technologies), supplemented with 10% (v/v) FCS, 100 U/ml penicillin and 100 µg/ml streptomycin. 50% of the medium was replaced every other day and 10 ng/ml murine M-CSF (R&D System) was supplemented at day 7 in culture. After 10 days in culture, cells were shaken at 200 rpm for 30 min to isolate microglia. The medium containing microglia was pelleted at 200 g for 8 min and reseeded to corresponding plates for experiments. Cell identity was confirmed using anti-CD68 (Fig. 3D) and anti-CD11b (Fig. EV1B) antibodies.

5. Flow Cytometry

BMDM or primary microglial cells were suspended in FACS buffer (Hank's Balanced Salt Solution, no calcium, no magnesium; 0.2% bovine serum albumin; Thermo Fisher Scientific). Samples were labeled with anti-CD11b antibodies (M1/70), APC-Cy7® conjugated (1:100; Life Technologies) for 30 min at 4 °C. Data were acquired using MACSQuant® VYB (Miltenyi Biotec) and analyzed by FlowJo software.

To quantify absolute expression levels for the different cell surface Fcγ-receptors (FcγR), BMDM were labeled with PE anti- FcγRII/III (1:100; BD Bioscience), PE anti- FcγRI (1:100; R&D System) or PE anti-FcγRIV (1:100; BD Bioscience) at 4 °C for 30 min. Data were acquired on a FACSVerse flow cytometer (BD, USA) and analyzed using FACSuite software (BD, USA). Absolute numbers of PE anti-FcγR molecules per cell were determined using QuantiBRITE (BD Bioscience) PE calibration beads following the analysis strategy according to the manufacturer's protocol. Gates were set according to unlabeled and isotope controls. Absolute PE anti-FcγR molecules counts were performed per individual sample and normalized to the mean of the wt control group.

6. Cell lysis and immunoblotting

Western blot analysis of membrane bound TREM2 was performed as previously described²⁵. For western blot analysis of Aβ, lysates were prepared with 8 M urea lysis buffer (8M Urea, 50mM Tris-HCL pH 7.4) freshly supplemented with a protease inhibitor cocktail (Sigma-Aldrich) and incubated on ice for 30 min. The lysate was mixed with Laemmli sample buffer supplemented with beta mercaptoethanol, and equal amounts of protein were separated by SDS-PAGE. After transfer onto polyvinylidene difluoride membranes (Amersham Hybond P 0.45 PVDF, GE Healthcare Life Science) or nitrocellulose membranes (GE Healthcare Life Science), blots were blocked

for 1 h with I-BlockTM (Thermo Fisher Scientific) and exposed to 5F4 for TREM2 and sTREM2 or 2D8³² for A β . Signals were visualized with HRP-conjugated secondary antibodies using ECL kit (Thermo Fisher Scientific).

7. Antibodies

For *in vitro* and *ex vivo* phagocytosis assay the following antibodies were used: rat monoclonal antibody 2D8 against A β ₁₋₁₆³², rabbit polyclonal antibody 6687 against cytosolic domain of APP³³, mouse IgG2a isotype control (Sigma-Aldrich), mouse monoclonal mAb11 (IgG2a;^{35,36}. mAb11 is a closely related clone to the clinically used anti-A β antibody Gantenerumab that binds preferentially to A β 40/42 aggregates, namely A β fibrils and oligomers via a conformational epitope comprising N-terminal and central epitopes (more details on epitopes in^{35,36}. Affinity parameters were determined before for both antibodies by surface plasmon resonance (Biacore) and revealed equilibrium dissociation constant (KD) values for mAb11 between 0.14–0.67 nM, which were determined for A β 40 and A β 42, which is similar to Gantenerumab with a KD of 0.6 nM^{35,36}. Binding and stability of bound antibody to soluble A β monomers is substantially lower. We measured a KD of 18 nM for Gantenerumab binding to A β monomers with a notably kinetically instable complex with monomers showing a rapid off-rate. In more details, the kinetically most stable complex formation with Gantenerumab was observed

for A β fibrils (kd 2.8×10^{-4} 1/s) and A β oligomers (kd 4.9×10^{-4} 1/s), whereas for monomeric A β a higher dissociation rate was observed (kd 1.2×10^{-2} 1/s) suggesting rapid exchange of antibody-bound monomeric A β . Thus, mAb11 binding parameters can be considered almost identical to Gantenerumab. Selective binding to aggregated A β 40/42 is in agreement with demonstrated amyloid plaque binding measured by immuno-fluorescence *in vitro* and *in vivo*. Selective and sensitive binding to amyloid plaques in human AD and transgenic mouse brain tissues is again very comparable for Gantenerumab and mAb11 with positive immunodecoration detectable at low concentration of 10 ng/mL and plaque binding *in vivo* in transgenic mice^{35,36}.

For immunofluorescence staining of BMDM and primary microglia, staining was performed using rat anti-CD68 (1:500; AbD Serotec) and goat anti rat Alexa Fluor 555 (1:200; Thermo Fisher Scientific).

For western blotting of TREM2, we raised a rat monoclonal antibody (clone 5F4; 1:50) against the extracellular domain of murine TREM2 (Creative Biomart; TREM2-3276M). Further used antibodies were rat antibody 2D8 (1:100)³² against A β , rabbit-anti calnexin (1:3000; Enzo Life Sciences), secondary antibodies HRP-conjugated goat anti-rat (1:5,000; Santa Cruz Biotechnology) and goat anti-rabbit IgG (1:10,000; Promega).

8. *In vitro* A β phagocytosis assay

Phagocytosis assays with N9, BMDM and primary microglia were performed as described²⁵ with minor adjustments. Briefly, HiLyte™ Fluor 488 A β ₁₋₄₂ (Anaspec) was aggregated overnight at 37°C with agitation. 3×10⁴ N9 cells, BMDM, or 2×10⁴ primary microglia were plated in poly-D-lysine coated black-walled 96 well plates (Greiner bio-one). Pre-aggregated HiLyte™ Fluor 488 A β ₁₋₄₂ (fA β ₄₂) was incubated with antibodies for 1 h at 37°C. Fibril A β ₄₂ or antibody-fA β ₄₂ complexes were added to a final concentration 1 μ M and incubated for 2 h. As negative control, 10 mM cytochalasin D was added 30 min before addition of fA β ₄₂ or antibody-fA β ₄₂. Before measurement, medium was removed and extracellular fA β ₄₂ was quenched with 100 μ l 0.2% trypan blue in phosphate buffered saline (PBS), pH 4.4 for 1 min. After aspiration fluorescence signals were measured at 485 nm excitation/538 nm emission using a Fluoroskan Ascent™ Microplate Fluorometer (Lab Systems).

For the experiment shown in Fig. 11, BMDM were incubated with recombinant mouse sTREM2 (Creative Biomart) overnight before adding fA β ₄₂ or antibody-fA β ₄₂ complexes.

9. *Ex vivo* plaque clearance assay

Ex vivo plaque clearance assays were performed as previously described¹³ with the following slight modifications. 6-months old APP/PS1 transgenic

mice (mixed gender) were perfused with PBS. Brains were separated into two hemispheres and snap-frozen using dry ice powder. Frozen brains were sectioned into 10 μm sagittal sections using a cryostat (Leica) and collect onto poly-D-lysine-coated round glass coverslips (15 mm). Sections were dried at room temperature for 2 h followed by incubation with antibodies (isotype control (IC) or anti-A β) in culture medium for 1 h at 37°C. BMDM or primary microglia cells were seeded at densities of 3×10^5 cells per well in 12 well plates and incubated at 37 °C with 5% CO₂ for 24 h. After incubation, cultures were fixed with 4% paraformaldehyde for 15 min and stained with methoxy-X04 (2 $\mu\text{g}/\text{ml}$; Tocris Bioscience). In the indicated experiments, the fixed cultures were permeabilized with 0.1% Triton-X100 for 3 min and stained with rat anti-CD68 antibody overnight at 4°C followed by methoxy-X04 staining.

Images were acquired on a LSM700 confocal microscope with Z stacks and tile scan to cover the entire sagittal sections using the Zen 2009 imaging software (Zeiss). Maximum intensity projection from each sagittal sections was then analyzed by ImageJ⁴⁹ to obtain methoxy-x04 signal intensities. In Fig. 4A & B, four consecutive slices were set as a group, and signals from slices incubated with no cell were set as base line. Methoxy-X04 signal intensities from slices either incubated with wt or *TREM2* ko BMDM were compared to base line. In Fig. 5 A & B eight consecutive slices (#1 - 8) were used as a group and signal intensities from slices #1 and 8 were set as base line. Signals from slices #2 to 6, which were incubated with increasing concentrations of mAb11 (0 – 5 $\mu\text{g}/\text{ml}$) in the presence of BMDM were compared to base line.

10. Quantitative real-time PCR analysis

Total RNA was isolated from BMDM using the RNeasy Mini Kit (Qiagen) according to the manufacturer's instructions. The concentration and purity of RNA were determined using the NanoPhotometer (Implen). Equal amounts of RNA were reverse transcribed into cDNA using High-capacity cDNA Reverse Transcription kit (Thermo Fisher). The expression level of Fcγ-receptors (I, IIB, III, IV) were analyzed by Taqman[®] real-time PCR assay. Probes target to FcγRI (Mm00438874_m1, Thermo Fisher Scientific), or FcγRIIB (Mm00438875_m1, Thermo Fisher Scientific), or FcγIIIR (Mm00438882_m1, Thermo Fisher Scientific), or FcγRIV (Mm00519988_m1, Thermo Fisher Scientific) were mixed with 1:5 diluted cDNA, added to the Taqman[®] master mix (Thermo Fisher Scientific) and amplified with the 7500 fast real-time PCR system (Applied Biosystems). Geometric mean of two housekeeping genes, Gusb (Mm01197698_m1, Thermo Fisher Scientific) and Hsp90ab1 (Mm00833431_g1, Thermo Fisher Scientific), which highly correlate with each other, were used as endogenous controls. Fold change of mRNA in TREM2 ko BMDM was calculated using wt BMDM as reference sample.

11. Statistics

All statistical analysis were performed using Prism 6 (GraphPad). Data are presented as mean +/- SEM with biological repeats. Data from the phagocytosis assays were analyzed by 2 way ANOVA with Bonferroni correction for multiple comparison. Cell surface FcγR relative levels were analyzed by student t-test. Fold change of mRNA was analyzed by one sample t-test of its log₂ value. Western blot quantification in Fig 2C was analyzed by 2 way ANOVA with Bonferroni correction for multiple comparison. Methoxy-X04 signal intensity presented in Fig 4B and Fig 5B were analyzed by 2 way ANOVA, with Tukey's and Fisher's least significant difference (LSD) post-hoc tests for pair-wise comparisons respectively. All tests were 2-tailed, with a significant level of ≤ 0.05 .

Acknowledgements

This work was supported by the Deutsche Forschungsgemeinschaft (DFG) within the framework of the Munich Cluster for Systems Neurology (EXC 1010 SyNergy), the European Research Council under the European Union's Seventh Framework Program (FP7/2007–2013)/ERC Grant Agreement No. 321366-Amyloid, the general legacy of Mrs. Ammer, the MetLife award, and the Cure Alzheimer's fund. We would like to thank Dr. Feng Zhang (Broad Institute) for providing PX459 V2.0. We thank Dr. Marco Colonna for providing *TREM2* knockout mice. We thank Samira Parhizkar for screening antibodies against TREM2 and Dr. Marc Suárez-Calvet for critically reading the manuscript.

Author contributions

X.X. G.K. and C.H. designed the study and interpreted the results. X.X. performed all experiments except generating mutant N9 cells, which was performed by G.W. and A.C., the quantification of cell surface Fcγ-receptors expression level was done by A.L.; B.B. and I.K. provided antibodies. R.F. generated monoclonal antibody against TREM2 (clone 5F4). F.M. and G.K. provided bone marrow cells. C.H. wrote the manuscript with input of all co-authors.

Conflict of interest

C.H. is an advisor of F. Hoffmann - La Roche. I.K. and B.B. are full-time employees at Roche. All other authors declare that they have no conflict of interest.

References

1. Hardy, J. & Selkoe, D. J. The amyloid hypothesis of Alzheimer's disease: progress and problems on the road to therapeutics. *Science* **297**, 353–6 (2002).
2. Haass, C. Take five--BACE and the γ -secretase quartet conduct Alzheimer's amyloid β -peptide generation. *EMBO J.* **23**, 483–8 (2004).
3. Doody, R. S. *et al.* A phase 3 trial of semagacestat for treatment of Alzheimer's disease. *N. Engl. J. Med.* **369**, 341–50 (2013).
4. Willem, M. *et al.* η -Secretase processing of APP inhibits neuronal activity in the hippocampus. *Nature* **526**, 443–7 (2015).
5. Kuhn, P.-H. *et al.* Secretome protein enrichment identifies physiological BACE1 protease substrates in neurons. *EMBO J.* **31**, 3157–68 (2012).
6. Barão, S., Moechars, D., Lichtenthaler, S. F. & De Strooper, B. BACE1 physiological functions may limit its use as therapeutic target for Alzheimer's Disease. *Trends Neurosci.* **39**, 158–169 (2016).
7. Zhou, L. *et al.* The neural cell adhesion molecules L1 and CHL1 are cleaved by BACE1 protease in vivo. *J. Biol. Chem.* **287**, 25927–40 (2012).
8. Cheret, C. *et al.* Bace1 and Neuregulin-1 cooperate to control formation and maintenance of muscle spindles. *EMBO J.* **32**, 2015–28 (2013).
9. Willem, M. *et al.* Control of peripheral nerve myelination by the β -secretase BACE1. *Science* **314**, 664–6 (2006).
10. Wisniewski, T. & Goñi, F. Immunotherapeutic approaches for Alzheimer's disease. *Neuron* **85**, 1162–76 (2015).
11. Schenk, D. *et al.* Immunization with amyloid- β attenuates Alzheimer-disease-like pathology in the PDAPP mouse. *Nature* **400**, 173–7 (1999).
12. Morgan, D. *et al.* A β peptide vaccination prevents memory loss in an animal model of Alzheimer's disease. *Nature* **408**, 982–5 (2000).
13. Bard, F. *et al.* Peripherally administered antibodies against amyloid β -peptide enter the central nervous system and reduce pathology in a mouse model of Alzheimer disease. *Nat. Med.* **6**, 916–9 (2000).
14. Ostrowitzki, S. *et al.* Mechanism of amyloid removal in patients with Alzheimer disease treated with gantenerumab. *Arch. Neurol.* **69**, 198–207 (2012).
15. Rinne, J. O. *et al.* 11C-PiB PET assessment of change in fibrillar amyloid- β load in patients with Alzheimer's disease treated with bapineuzumab: a phase 2, double-blind, placebo-controlled, ascending-dose study. *Lancet. Neurol.* **9**, 363–72 (2010).
16. Radde, R. *et al.* A β 42-driven cerebral amyloidosis in transgenic mice reveals early and robust pathology. *EMBO Rep.* **7**, 940–6 (2006).

17. Borroni, B. *et al.* Heterozygous TREM2 mutations in frontotemporal dementia. *Neurobiol. Aging* **35**, 934.e7-10 (2014).
18. Cady, J. *et al.* TREM2 variant p.R47H as a risk factor for sporadic amyotrophic lateral sclerosis. *JAMA Neurol.* **71**, 449–53 (2014).
19. Colonna, M. & Wang, Y. TREM2 variants: new keys to decipher Alzheimer disease pathogenesis. *Nat. Rev. Neurosci.* **17**, 201–7 (2016).
20. Guerreiro, R. *et al.* TREM2 variants in Alzheimer's disease. *N. Engl. J. Med.* **368**, 117–27 (2013).
21. Jonsson, T. *et al.* Variant of TREM2 associated with the risk of Alzheimer's disease. *N. Engl. J. Med.* **368**, 107–16 (2013).
22. Rayaprolu, S. *et al.* TREM2 in neurodegeneration: evidence for association of the p.R47H variant with frontotemporal dementia and Parkinson's disease. *Mol. Neurodegener.* **8**, 19 (2013).
23. Ulrich, J. D. & Holtzman, D. M. TREM2 Function in Alzheimer's Disease and Neurodegeneration. *ACS Chem. Neurosci.* **7**, 420–7 (2016).
24. Villegas-Llerena, C., Phillips, A., Garcia-Reitboeck, P., Hardy, J. & Pocock, J. M. Microglial genes regulating neuroinflammation in the progression of Alzheimer's disease. *Curr. Opin. Neurobiol.* **36**, 74–81 (2016).
25. Kleinberger, G. *et al.* TREM2 mutations implicated in neurodegeneration impair cell surface transport and phagocytosis. *Sci. Transl. Med.* **6**, 243ra86 (2014).
26. Cantoni, C. *et al.* TREM2 regulates microglial cell activation in response to demyelination in vivo. *Acta Neuropathol.* **129**, 429–47 (2015).
27. Jay, T. R. *et al.* TREM2 deficiency eliminates TREM2+ inflammatory macrophages and ameliorates pathology in Alzheimer's disease mouse models. *J. Exp. Med.* **212**, 287–95 (2015).
28. Wang, Y. *et al.* TREM2 lipid sensing sustains the microglial response in an Alzheimer's disease model. *Cell* **160**, 1061–71 (2015).
29. Tanzi, R. E. TREM2 and risk of Alzheimer's Disease--friend or foe? *N. Engl. J. Med.* **372**, 2564–5 (2015).
30. Sessa, G. *et al.* Distribution and signaling of TREM2/DAP12, the receptor system mutated in human polycystic lipomembraneous osteodysplasia with sclerosing leukoencephalopathy dementia. *Eur. J. Neurosci.* **20**, 2617–28 (2004).
31. Ran, F. A. *et al.* Genome engineering using the CRISPR-Cas9 system. *Nat. Protoc.* **8**, 2281–2308 (2013).
32. Shirotani, K., Tomioka, M., Kremmer, E., Haass, C. & Steiner, H. Pathological activity of familial Alzheimer's disease-associated mutant presenilin can be executed by six different γ -secretase complexes. *Neurobiol. Dis.* **27**, 102–7 (2007).
33. Capell, A. *et al.* Presenilin-1 differentially facilitates endoproteolysis of the β -amyloid precursor protein and Notch. *Nat. Cell Biol.* **2**, 205–11 (2000).

34. Turnbull, I. R. *et al.* Cutting edge: TREM-2 attenuates macrophage activation. *J. Immunol.* **177**, 3520–4 (2006).
35. Bohrmann, B. *et al.* Gantenerumab: a novel human anti-A β antibody demonstrates sustained cerebral amyloid- β binding and elicits cell-mediated removal of human amyloid- β . *J. Alzheimers. Dis.* **28**, 49–69 (2012).
36. Lathuilière, A. *et al.* A subcutaneous cellular implant for passive immunization against amyloid- β reduces brain amyloid and tau pathologies. *Brain* **139**, 1587–604 (2016).
37. Crowley, M. T. *et al.* A critical role for Syk in signal transduction and phagocytosis mediated by Fc γ receptors on macrophages. *J. Exp. Med.* **186**, 1027–39 (1997).
38. Paradowska-Gorycka, A. & Jurkowska, M. Structure, expression pattern and biological activity of molecular complex TREM-2/DAP12. *Hum. Immunol.* **74**, 730–7 (2013).
39. McGeer, P. L. & Rogers, J. Anti-inflammatory agents as a therapeutic approach to Alzheimer's disease. *Neurology* **42**, 447–9 (1992).
40. Colonna, M., Turnbull, I. & Klesney-Tait, J. The enigmatic function of TREM-2 in osteoclastogenesis. *Adv. Exp. Med. Biol.* **602**, 97–105 (2007).
41. Hsieh, C. L. *et al.* A role for TREM2 ligands in the phagocytosis of apoptotic neuronal cells by microglia. *J. Neurochem.* **109**, 1144–56 (2009).
42. Takahashi, K., Rochford, C. D. P. & Neumann, H. Clearance of apoptotic neurons without inflammation by microglial triggering receptor expressed on myeloid cells-2. *J. Exp. Med.* **201**, 647–57 (2005).
43. Greenberg, S., Chang, P. & Silverstein, S. C. Tyrosine phosphorylation of the γ subunit of Fc γ receptors, p72syk, and paxillin during Fc receptor-mediated phagocytosis in macrophages. *J. Biol. Chem.* **269**, 3897–902 (1994).
44. Wu, K. *et al.* TREM-2 promotes macrophage survival and lung disease after respiratory viral infection. *J. Exp. Med.* **212**, 681–97 (2015).
45. Wang, Y. *et al.* TREM2-mediated early microglial response limits diffusion and toxicity of amyloid plaques. *J. Exp. Med.* **213**, 667–75 (2016).
46. Reardon, S. Antibody drugs for Alzheimer's show glimmers of promise. *Nature* **523**, 509–10 (2015).
47. Suárez-Calvet, M. *et al.* sTREM2 cerebrospinal fluid levels are a potential biomarker for microglia activity in early-stage Alzheimer's disease and associate with neuronal injury markers. *EMBO Mol. Med.* **8**, 466–76 (2016).
48. Marim, F. M., Silveira, T. N., Lima, D. S. & Zamboni, D. S. A method for generation of bone marrow-derived macrophages from cryopreserved mouse bone marrow cells. *PLoS One* **5**, e15263 (2010).
49. Schneider, C. A., Rasband, W. S. & Eliceiri, K. W. NIH Image to ImageJ: 25 years of image analysis. *Nat. Methods* **9**, 671–5 (2012).

Figure legends

Fig. 1 TREM2-deficiency reduces efficacy of antibody-stimulated A β uptake by phagocytic cells.

(A) Schematic of the mouse *TREM2* locus and the TREM2 protein. Sequence alignment of wild-type N9 (N9 wt) and TREM2 mutant N9 (N9 mu) surrounding the gRNA target site. The gRNA sequence is in cyan and protospacer-adjacent motif (PAM) is marked with a line. The single nucleotide insertion is labeled in red. Schematic representation of wild-type TREM2 (NP_112544.1) and CRISPR/Cas9 modified TREM2 (N9 mu). TM, trans-membrane domain; SP, signal peptide.

(B) Westernblot analysis of lysates and media from wt and mutant N9 cells (N9 wt /mu) using antibody anti-murine TREM2 (clone 5F4), which is raised against the murine TREM2 extracellular domain. sTREM2, soluble TREM2

* Indicate unspecific bands. Anti-calnexin antibody was used as loading control.

(C) Phagocytosis of 1 μ M HiLyte™ Fluor 488 A β ₁₋₄₂ (fA β ₄₂) by N9 wt and N9 mu in the presence or absence of antibody 2D8 or the non-binding antibody 6687. Cytochalasin D (CytoD, 10 mM) was used as control to verify phagocytic uptake. (n = 4, +/- SEM; 2-way ANOVA, interaction P=0.61, genotype P<0.0001, treatment P=0.0001; post hoc tests wt vs. mu for the following conditions: fA β ₄₂ P=0.0043, fA β ₄₂-2D8 P=0.0436).

(D) Westernblot of BMDM derived from wt and *TREM2* knockout (ko) animals using antibody 5F4.

(E) Phagocytosis of fA β ₄₂ by BMDM from wt and *TREM2* ko animals in the presence or absence of 2D8, or the non-binding control antibody 6687. (n = 3,

+/- SEM; 2 way ANOVA, interaction $P=0.0005$, genotype $P<0.0001$, treatment $P<0.0001$; post hoc tests wt vs. ko for the following conditions: $fA\beta_{42}$ $P=0.0021$, $fA\beta_{42}$ -2D8 1 $\mu\text{g/ml}$ $P<0.0001$, $fA\beta_{42}$ -2D8 5 $\mu\text{g/ml}$ $P<0.0001$, $fA\beta_{42}$ -2D8 10 $\mu\text{g/ml}$ $P<0.0001$, $fA\beta_{42}$ /6687 10 $\mu\text{g/ml}$ $P=0.0007$)

(F) Quantification of relative $fA\beta_{42}$ uptake to lowest antibody concentration used.

(G) Phagocytosis of $fA\beta_{42}$ by BMDM from wt and *TREM2* ko animals in the presence or absence of mAb11, or an isotype control antibody (IC). (n = 4, +/- SEM; 2 way ANOVA, interaction $P=0.0223$, genotype $P<0.0001$, treatment $P<0.0001$; post hoc tests wt vs. ko for the following conditions: $fA\beta_{42}$ -mAb11 1 $\mu\text{g/ml}$ $P=0.0391$, $fA\beta_{42}$ -mAb11 5 $\mu\text{g/ml}$ $P=0.0069$, $fA\beta_{42}$ -mAb11 10 $\mu\text{g/ml}$ $P<0.0001$, $fA\beta_{42}$ -mAb11 20 $\mu\text{g/ml}$ $P=0.0001$, $fA\beta_{42}$ -mAb11 50 $\mu\text{g/ml}$ $P<0.0001$).

(H) Quantification of relative $fA\beta_{42}$ uptake to lowest antibody concentration used.

(I) Recombinant mouse sTREM2 does not rescue $fA\beta_{42}$ uptake in *TREM2*-deficient BMDM. Increasing amounts of sTREM2 were added to the media of wt or *TREM2* ko BMDM in the presence or absence of mAb11 (10 $\mu\text{g/ml}$).

(J) Westernblot of primary microglia from wt or *TREM2* ko animals using antibody 5F4.

(K) Phagocytosis of $fA\beta_{42}$ by primary microglia from wt and *TREM2* ko animals in the presence or absence of mAb11, or an isotype control antibody (IC). (n = 5, +/- SEM; 2 way ANOVA, interaction $P=0.4797$, genotype $P<0.0001$, treatment $P<0.0001$; post hoc tests wt vs. ko for the following conditions: $fA\beta_{42}$ -mAb11 5 $\mu\text{g/ml}$ $P=0.0449$, $fA\beta_{42}$ -mAb11 10 $\mu\text{g/ml}$ $P=0.0370$, $fA\beta_{42}$ -mAb11 20 $\mu\text{g/ml}$ $P=0.0299$, $fA\beta_{42}$ -mAb11 50 $\mu\text{g/ml}$ $P=0.0120$).

(L) Quantification of relative $fA\beta_{42}$ uptake to lowest antibody concentration used.

(C, E, G, K) Quantification of internalized $fA\beta_{42}$ was normalized to wt without antibody. Bonferroni-corrected pair-wise post hoc tests were used.

Fig. 2 Increased Fc γ -receptors expression and enhanced Syk phosphorylation in TREM2-deficient BMDM

(A) Representative histograms for Fc γ -receptors-PE (Fc γ R-PE) expression levels as used for quantification. Stacked histograms for log PE fluorescence intensity of wt and *TREM2* ko BMDM are shown for the respective Fc γ R (I, IIB/III and IV).

(B) Relative quantification of cell surface levels of Fc γ R molecules. Absolute number of cell surface Fc γ R-PE molecules was determined by the BD QuantiBRITE® method (see methods section for details) and normalized to expression levels of the respective wt control. (n=4, +/- SEM, t test, two-tailed; wt vs. ko: Fc γ RI-PE P=0.0008, Fc γ RIIB/III-PE P=0.0033, Fc γ RIV-PE P=0.7001).

(C) mRNA levels of Fc γ R are increased in *TREM2* ko BMDM. Fold changes of the respective Fc γ R (I, IIB, III, IV) mRNA levels in *TREM2* ko BMDM were determined by quantitative real-time PCR. (n=6, +/- SEM; one-sample t test, two-tailed; wt vs. ko: Fc γ RI P=0.0118, Fc γ RIIB P=0.0006, Fc γ RIII P=0.0004, Fc γ RIV P=0.0284)

(D) Phosphorylated Syk (P-Syk) and total Syk (T-Syk) levels were determined by western blotting in lysates from wt and *TREM2* ko BMDM after 1 h treatment with $A\beta$ alone, together with antibody 2D8 ($A\beta$ -2D8), or an isotype control ($A\beta$ -IC). Actin was used as a loading control.

(E) Quantification of P-Syk normalized to T-Syk. (n = 4, +/- SEM; 2-way ANOVA, interaction P=0.0490, genotype P=0.0898, treatment P<0.0001. Bonferroni-corrected pair-wise post hoc tests, ** P =0.0075 vs. wt).

Fig. 3 Engulfment of fibrillar A β by BMDM and primary microglia

(A) A schematic show 10 μ m cryosections of unfixed brain cryosections from 6-months old APP/PS1 mice, which show a high amyloid plaque burden (right panel with methoxy-X04 staining), were incubated with antibody for 1 h, followed by adding BMDM or primary microglia on top of the sections. After 24 h incubation, sections were analyzed by immunostaining or immunoblotting.

(B) mAb11 but not the IC co-localized with methoxy-X04.

BMDM (C) or primary microglia (D) were cultured on cryosections pre-incubated with mAb11 (1 μ g/ml). After 24 h, sections were processed for immunostaining using antibody against CD68 to identify myeloid cells and methoxy-X04 staining to visualize A β . Note that both cell types internalize A β into intracellular vesicles (right panels show enlargement of insets). Scale bar: 10 μ m.

Fig. 4 TREM2-deficiency reduces antibody-mediated amyloid plaque clearance

(A) BMDM from wt or *TREM2* ko mice were cultured on APP/PS1 mice brain cryosections incubated with or without mAb11 (1 μ g/ml) or an isotype control (IC; 1 μ g/ml) for 24 h. Sections were then probed with methoxy-X04. Scale bar, 500 μ m.

(B) The amyloid plaque load was quantified from the entire sagittal section. Sections incubated with medium (no cell) were set as baseline. (n = 6, +/- SEM;

2 way ANOVA, interaction $P < 0.0001$, genotype $P < 0.0001$, treatment $P < 0.0001$; Tukey's multiple comparisons tests; wt vs. ko for the following conditions: no antibody $P = 0.0304$, IC $P = 0.0049$, mAb11 $P = 0.0212$; wt : IC vs. wt : mAb11 $P = 0.0008$; ko : IC vs. ko : mAb11 $P = 0.0001$).

(C, D) Equal numbers of wt and *TREM2* ko BMDM were added and cell numbers were analyzed after termination of experiments by quantifying the CD68 positive cells on top of the sections. (n = 4, +/-SEM; t-test; n.s., nonsignificant, $P = 0.5004$). Scale bar, 200 μm .

(E) A β was extracted by urea buffer from replicate slices of the experiment shown in (A) and total A β was identified by western blotting.

Fig. 5 Compensation of reduced amyloid plaque clearance by elevated antibody dose

(A) Cryosections from unfixed brain of 6-months old APP/PS1 mice were pre-incubated with increasing concentrations of mAb11 (0.001, 0.01, 0.1, 1, 5 $\mu\text{g/ml}$). BMDM from wt or *TREM2* ko mice were added for 24 h. Sections were stained with methoxy-X04. Scale bar, 500 μm .

(B) Methoxy-X04 signals were quantified from the entire sagittal section. (n = 5, +/- SEM; 2 way ANOVA, interaction $P = 0.0082$, genotype $P < 0.0001$, treatment $P < 0.0001$. Fisher's LSD post hoc comparisons; * show statistics between wt and ko under the same experimental condition. # in black show wt compares to no antibody stimulation; # in grey show ko compares to no antibody stimulation; wt vs. ko for the following conditions: no antibody $P = 0.0053$, mAb11 0.001 $\mu\text{g/ml}$ $P = 0.0003$, mAb11 0.01 $\mu\text{g/ml}$ $P < 0.0001$, mAb11 0.1 $\mu\text{g/ml}$ $P = 0.0001$, mAb11 1 $\mu\text{g/ml}$ $P = 0.0007$, mAb11 5 $\mu\text{g/ml}$ $P = 0.0011$; Following conditions compare to wt / no antibody: wt / mAb11 0.01 $\mu\text{g/ml}$ $P = 0.0166$, wt / mAb11 0.1 $\mu\text{g/ml}$ $P = 0.0002$, wt / mAb11 1 $\mu\text{g/ml}$ $P < 0.0001$, wt / mAb11 5 $\mu\text{g/ml}$ $P < 0.0001$; Following conditions compare to ko /

no antibody: ko / mAb11 0.1 $\mu\text{g/ml}$ $P=0.0099$, ko / mAb11 1 $\mu\text{g/ml}$ $P<0.0001$,
ko / mAb11 5 $\mu\text{g/ml}$ $P<0.0001$.

Expanded View Figure legends

Fig. EV1 BMDM and primary microglia are positive for CD11b

Surface staining of CD11b was analyzed using flow cytometry. (A) 97.1% bone marrow derived macrophages (BMDM) were positive for CD11b. (B) Primary microglia from mixed glial culture were 90.4% positive for CD11b.

Figures

Figure 1

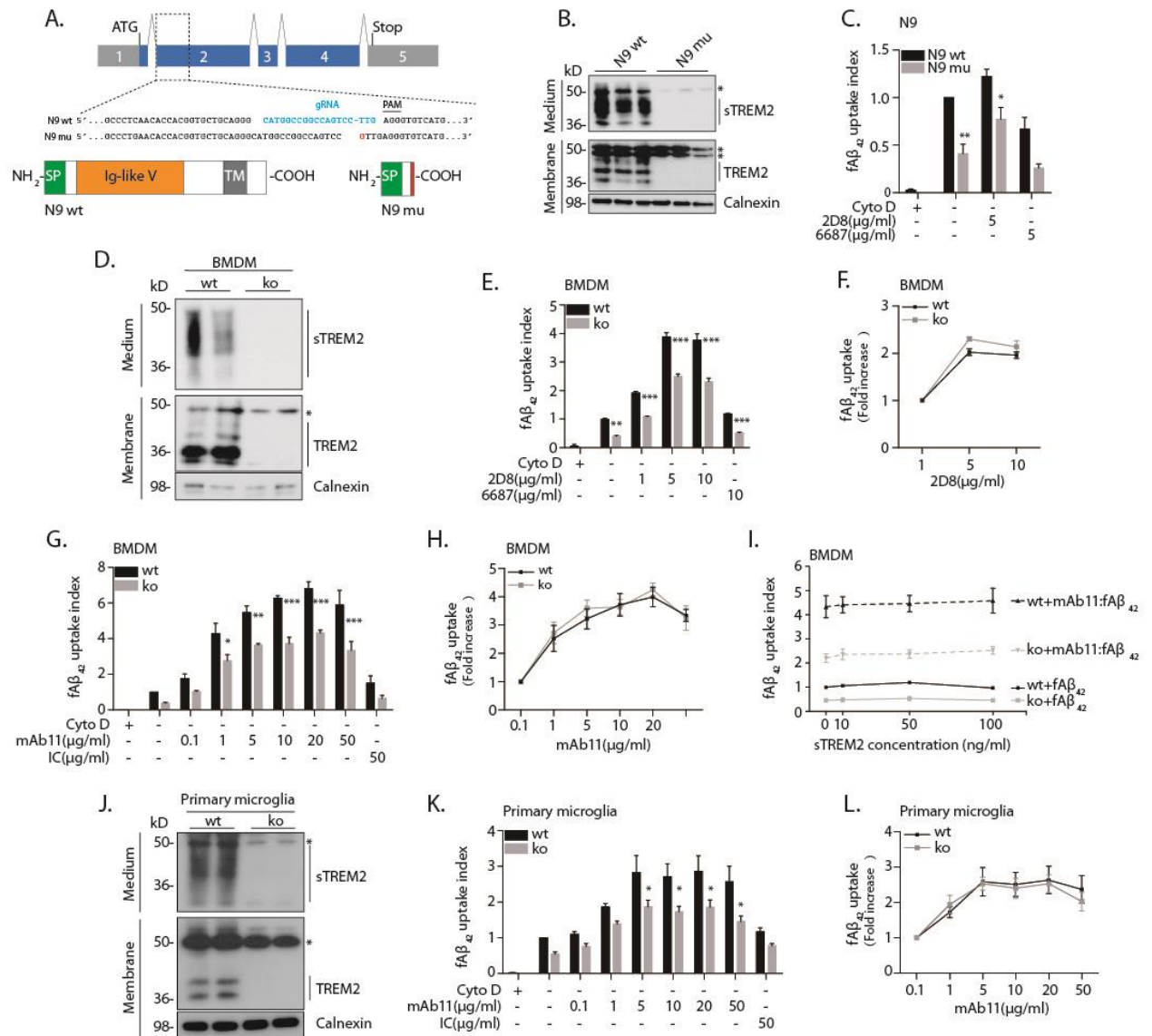


Figure 2

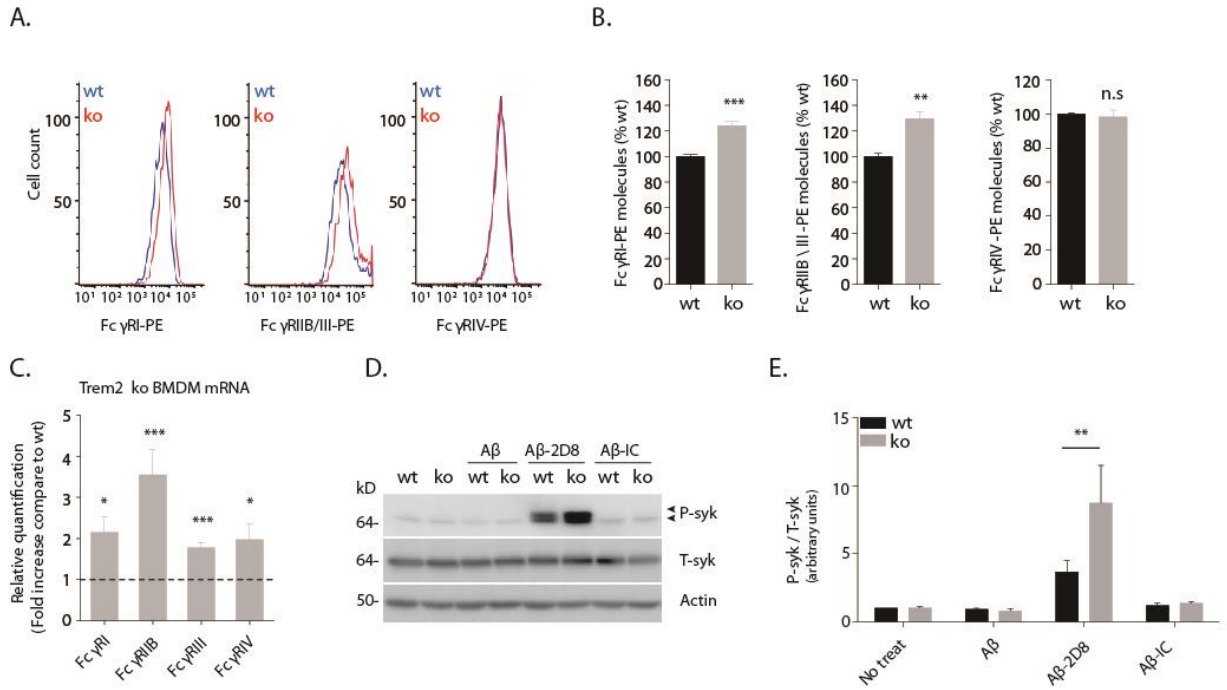


Figure 3

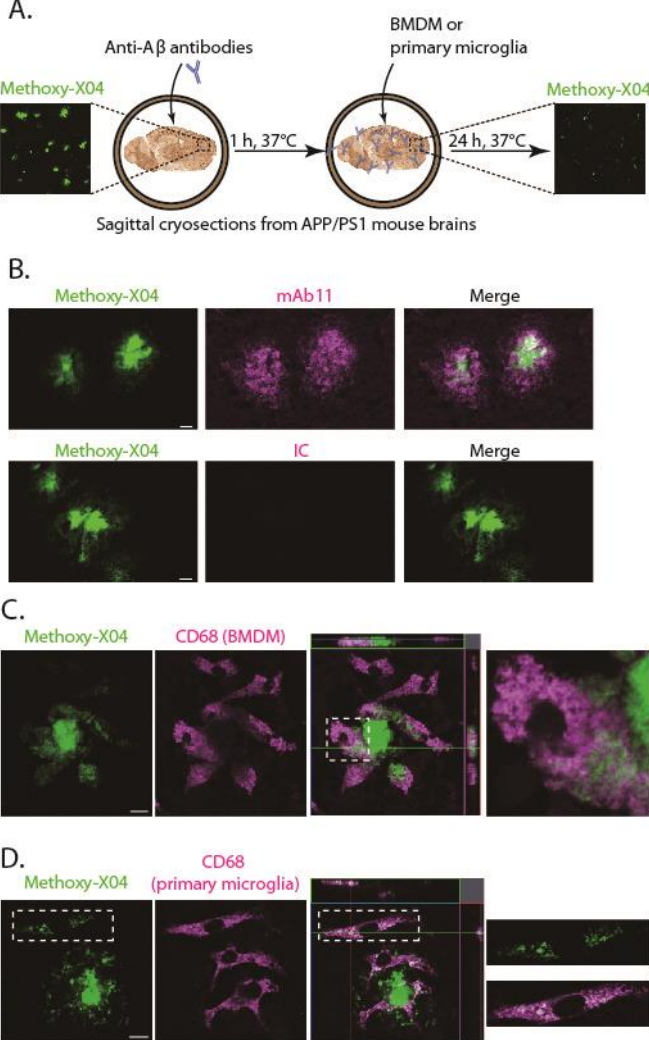


Figure 4

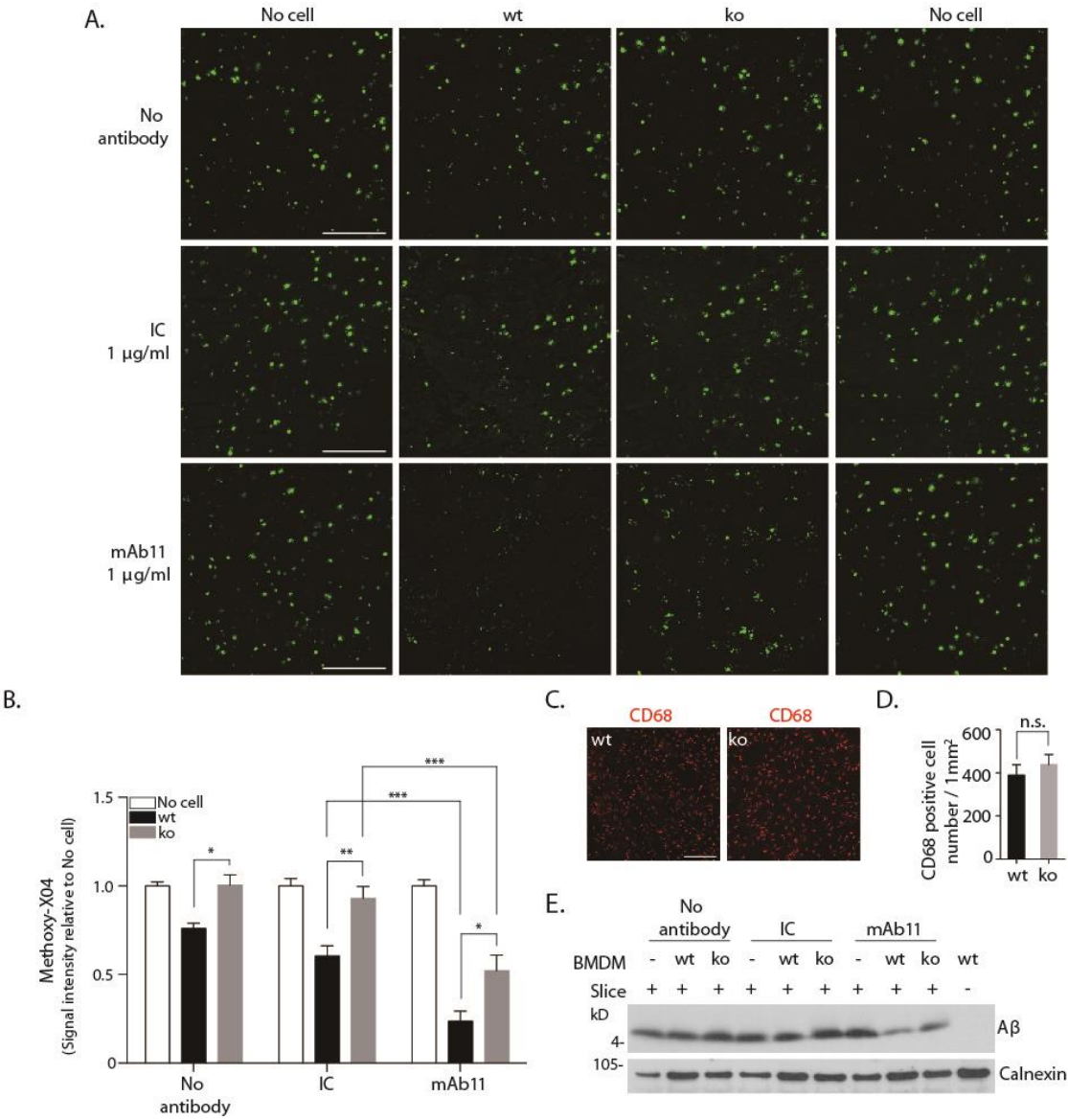
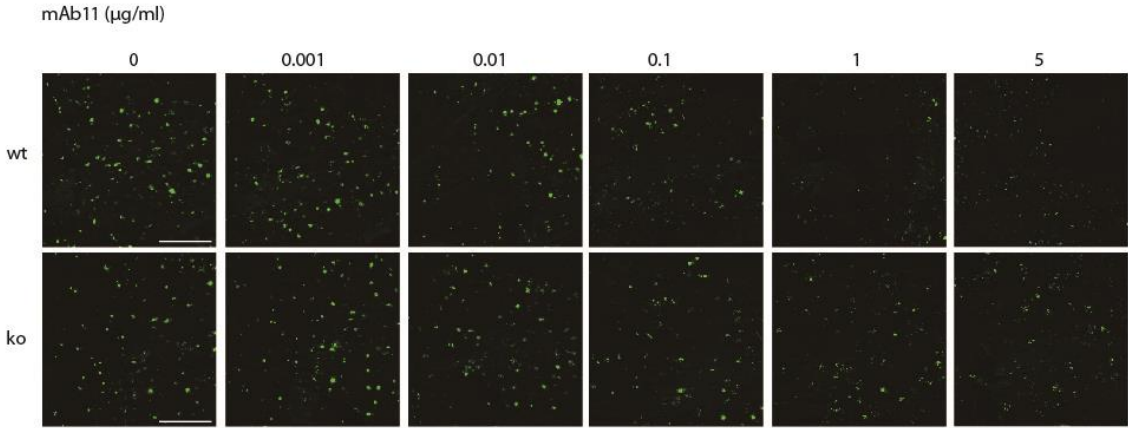
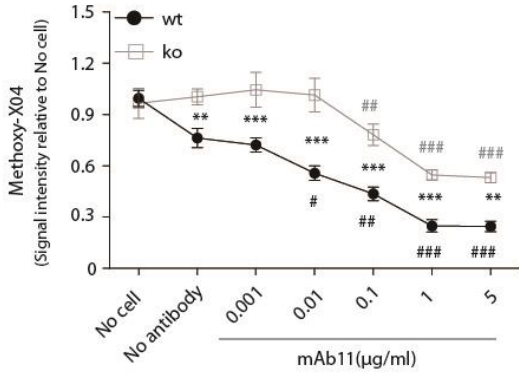


Figure 5

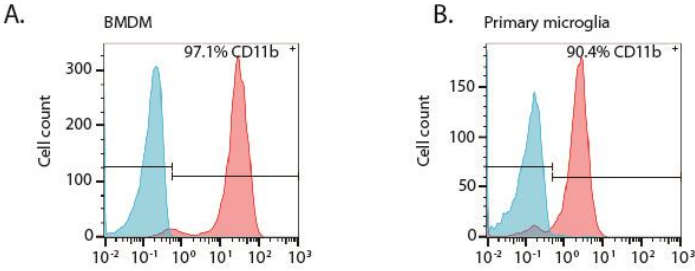
A.



B.



Expanded View Figure 1



Paper II: The TREM2 R47H Alzheimer's risk variant impairs splicing and reduces TREM2 mRNA and protein in mice but not in humans (Molecular neurodegeneration 2018)

Title Page

The TREM2 R47H Alzheimer's risk variant impairs splicing and reduces TREM2 mRNA and protein in mice but not in humans

Xianyuan Xiang^{1,2}, Thomas M Piers⁹, Benedikt Wefers^{3,5}, Kaichuan Zhu^{3,4}, Anna Mallach⁹,
Bettina Brunner³, Gernot Kleinberger^{1,4}, Wilbur Song⁷, Marco Colonna^{7,8}, Jochen Herms³,
Wolfgang Wurst^{3,4,5,6}, Jennifer M Pocock⁹ & Christian Haass^{1,3,4*}

¹Metabolic Biochemistry, Biomedical Center (BMC), Faculty of Medicine, Ludwig-Maximilians-Universität München, 81377 Munich, Germany

²Graduate School of Systemic Neuroscience, Ludwig-Maximilians-University Munich, 82152 Munich, Germany

³German Center for Neurodegenerative Diseases (DZNE) Munich, 81377 Munich, Germany

⁴Munich Cluster for Systems Neurology (SyNergy), 81377 Munich, Germany

⁵Institute of Developmental Genetics, Helmholtz Zentrum München, German Research Center for Environmental Health, Neuherberg, Germany

⁶Technische Universität München-Weihenstephan, 85764 Neuherberg/Munich, Germany

⁷Department of Immunology and Pathology, Washington University in St. Louis, St. Louis, MO, USA

⁸Department of Medicine, Division of Gastroenterology and Hepatology, Shinshu University School of Medicine, Matsumoto, Japan

⁹Cell Signalling Lab, Department of Neuroinflammation, University College London Institute of Neurology, London WC1N 1PJ, UK

*To whom correspondence should be addressed:

christian.haass@mail03.med.uni-muenchen.de

Abstract

Background: The R47H variant of the Triggering Receptor Expressed on Myeloid cells 2 (TREM2) significantly increases the risk for late onset Alzheimer's disease. Mouse models accurately reproducing phenotypes observed in Alzheimer' disease patients carrying the R47H coding variant are required to understand the TREM2 related dysfunctions responsible for the enhanced risk for late onset Alzheimer's disease.

Methods: A CRISPR/Cas9-assisted gene targeting strategy was used to generate TREM2 R47H knock-in mice. TREM2 mRNA and protein levels as well as TREM2 splicing patterns were assessed in these mice, in iPSC derived human microglia-like cells, and in human brains from Alzheimer's patients carrying the TREM2 R47H risk factor.

Results: Two independent TREM2 R47H knock-in mouse models show reduced TREM2 mRNA and protein production. In both mouse models TREM2 haploinsufficiency was due to atypical splicing of mouse TREM2 R47H, which introduced a premature stop codon. Cellular splicing assays using minigene constructs demonstrate that the R47H variant induced abnormal splicing only occurs in mice but not in humans. TREM2 mRNA levels and splicing patterns were both normal in iPSC induced human microglia-like cells and patient brains with the TREM2 R47H variant.

Conclusions: The TREM2 R47H variant activates a cryptic splice site that generates miss-spliced transcripts leading to TREM2 haploinsufficiency

only in mice but not in humans. Since TREM2 R47H related phenotypes are mouse specific and do not occur in humans, humanized TREM2 R47H knock-in mice should be generated to study the cellular consequences caused by the human TREM2 R47H coding variant. Currently described phenotypes of TREM2 R47H knock-in mice can therefore not be translated to humans.

Keywords: Alzheimer's disease; microglia; neurodegeneration; TREM2; pre-mRNA splicing; human microglia

Background

Microgliosis has long been thought to play a central role in the initiation and progression of Alzheimer's disease (AD) pathology. Indeed, genetic analyses recently revealed risk variants in a number of genes exclusively or at least preferentially expressed in microglia¹⁻⁵. Among these, the gene encoding the triggering receptor expressed on myeloid cells 2 (TREM2) plays a pivotal role in regulating microglial activity⁶⁻⁹. As part of the disease associated signature of microglia (DAM; also called MGnD (microglia neurodegenerative disease)), TREM2 is one of the most upregulated genes when microglia encounter acute injuries within the brain or respond to neurodegenerative disorders such as AD and amyotrophic lateral sclerosis^{6,10}. Moreover, absence of functional TREM2 caused by a gene knockout or certain disease associated sequence variants, which missfold TREM2 and retain the protein within the endoplasmic reticulum, lock microglia in a homeostatic state and prevent their activation *in vivo*^{7,11}. As a consequence cellular defense mechanisms such as chemotaxis, prominently visible by the lack of clustering around amyloid plaques, proliferation, phagocytosis of dead cells and amyloid fibrils are all reduced^{8,12,13}. Furthermore, overexpression of wt human TREM2 in a TREM2 knockout mouse corrects loss-of-function phenotypes¹⁴. Thus TREM2 is believed to have protective functions. In line with that, TREM2 is upregulated early during disease development. In a study on patients with dominantly inherited AD (DIAN), soluble TREM2 was found to be increased five years before onset of clinical symptoms, which may also be interpreted as

a protective response ¹⁵. Consistent with this conclusion, lack of functional TREM2 affects amyloid plaque morphology and increases plaque associated neuritic dystrophies ^{13,16}. Furthermore, in models of acute neuronal injury such as the cuprizone model, TREM2 activity facilitates clearance of cellular debris and recovery ^{11,17,18}. For tauopathies there are, however, opposing results indicating either protective or detrimental functions ^{19,20}. In line with findings in mouse models for AD pathology, this may be due to stage specific functions of TREM2.

Mouse models and cellular systems greatly helped to understand the consequences of loss-of-function mutations / haploinsufficiency of TREM2. However, the most important disease variant, namely R47H, which has been shown to increase the risk for late onset AD to a similar extent as the Apo lipoprotein E (ApoE) ε4 allele ^{3,4}, has been much less investigated. In cultured cells TREM2 R47H reduces ligand binding ²¹⁻²³. Consistent with a pivotal role in ligand binding, structural analyses revealed that arginine 47 is required to stabilize a conformation, which is capable to interact with ligands such as ApoE, and phosphatidylserine ²⁴. Furthermore maturation of the R47H variant within the secretory pathway may also be delayed ²⁵. In line with these findings, expression of human TREM2 R47H in TREM2 knockout mice failed to rescue their phenotypes ¹⁴. These findings may therefore be indicative for a loss-of-function. In fact, very recently CRISPR/Cas9 generated mouse models expressing the R47H variant within the endogenous TREM2 mouse locus revealed a significant loss-of function ^{26,27}. TREM2 R47H mice exhibited reduced TREM2 upregulation in microglia, reduced microgliosis, reduced

clustering around amyloid plaques and an overall reduction of TREM2 protein²⁶. Haploinsufficiency of TREM2 was confirmed by a significant reduction of TREM2 mRNA derived from the mutant allele²⁶. Thus, heterozygous TREM2 R47H mice appear to phenocopy a heterozygous knockout of TREM2.

We also independently generated TREM2 R47H knock-in mice using the CRISPR/Cas9 technology and reproduced haploinsufficiency of TREM2 in this model. Moreover, we could demonstrate that reduced mRNA stability due to a splicing error leads to a severe reduction of TREM2 mRNA. However, aberrant splicing was mouse specific and could not be observed in humans. Thus phenotypes associated with the R47H variant inserted into the endogenous mouse locus may not allow conclusions on the cellular mechanism affected in humans.

Materials and Methods

1. Mice

Animal handling and animal experiments were performed in accordance to local animal laws and housed in standard cages in a specific pathogen-free facility on a 12-h light/dark cycle with *ad libitum* access to food and water.

Jax TREM2 R47H ki mice were purchased from Jackson laboratory. In-house TREM2 R47H mice were generated using CRISPR/Cas9 technology in C57BL/6N background. Both strains were housed and bred in the same animal facility. To extract bone marrow, mice were first euthanized by CO₂ followed by cervical dislocation.

2. Generation of TREM2 R47H knock-in mice

TREM2 R47H knock-in mice (R47H ki mice) were generated by CRISPR/Cas9-assisted gene targeting in zygotes as described previously^{28,29}. Briefly, pronuclear stage zygotes were obtained by mating C57BL/6N males with superovulated C57BL/6N females (Charles River). Embryos were then microinjected into the male pronucleus with an injection mix containing 25 ng/μl Cas9 mRNA, 12.5 ng/μl TREM2-specific sgRNA, and 25 ng/μl single-stranded oligodeoxynucleotide (ssODN). Cas9 mRNA was prepared from XbaI-lineralized pCAG-Cas9v2-162A by in vitro transcription using the

mMESSAGE mMACHINE™ T7 ULTRA Transcription Kit (Thermo Fisher Scientific, #AM1345) and purified using the MEGAclean™ Transcription Clean-Up Kit (Thermo Fisher Scientific, #AM1908). TREM2-specific sgRNA (protospacer: GAAGCACTGGGGGAGACGCA) was prepared by IVT from pBS-T7-sgTREM2 using the MEGAscript™ T7 Transcription Kit (Thermo Fisher Scientific, #AM1354) and purified with the MEGAclean™ Transcription Clean-Up Kit. The 130nt ssODN targeting molecule ssTREM2 R47H (5'-GGGCATGGCCGGCCAGTCCTTGAGGGTGTTCATGTACTTATGACGCCTTG AAGCACTGGGGT**CGACA**CAAAGCCTGGTGT**CGGC**AGCTGGGTGAGGAG GGCCATGCCAGCGTGTGGT**GAGCACAC**CGGT -3'), comprising the G>A substitution (underlined) and three additional silent mutations (bold), was synthesized by Metabion. After microinjection, zygotes were cultured in KSOM medium until they were transferred into pseudopregnant CD-1 foster animals.

3. Off target analysis of TREM2 R47H mice

To identify putative off target sites of the TREM2-specific sgRNA, the online tool CRISPOR (<http://crispor.tefor.net/>)³⁰ was used. Predicted sites with a CFD score >0.5 and an MIT score >0.6 were chosen for off-target analysis. For analysis, genomic DNA of wildtype and heterozygous mutant TREM2 R47H mice was isolated and the loci were PCR amplified with primers flanking the putative cut sites. PCR amplicons were subsequently Sanger sequenced

using PCR amplification primers and the traces compared to a reference sequence.

4. Bone marrow derived macrophages culture

Bone marrow derived macrophages (BMDM) were prepared as previously described^{31,32}. Briefly, the bone marrow cells were flushed out using advanced RPMI 1640 (Life Technologies). Cells were differentiated using advanced RPMI 1640 supplemented with 2mM L-Glutamine, 10% (v/v) fetal calf serum (FCS), 100 U/ml penicillin, 100 µg/ml streptomycin and 50 ng/ml murine M-CSF (R&D System) for 7 days in non-cell culture treated dishes.

5. Microglia isolation

Microglia were isolated as previously described with some modification³³. Wild type and TREM2 R47H ki mice were perfused with cold phosphate buffered saline (PBS). Whole brain without the cerebellum was cut into small pieces and gently homogenized by mechanical dissociation in homogenization buffer (HBSS no calcium, no magnesium, with phenol red; 15 mM HEPES, 0.6% glucose). Homogenized cell suspensions were passed through a 100 µm cell strainer. Cells were pelleted at 300 g for 10 min and the supernatant discarded. To remove myelin, the cell pellets were re-suspended in 22% percoll (GE Healthcare) and centrifuged for 20 min at 900 g (acceleration 4, deceleration 0). Microglia were purified from the pellet using MACS CD11b magnetic beads

according to manufacturer's instructions. Briefly, 20 μ l CD11b microbeads (Miltenyi) were incubated with cell suspension for 15 min. After incubation, 500 μ l MACS buffer were added and cells were passed over a pre-rinsed Miltenyi LS column attached to a magnetic field. The column was washed three times with 500 μ l MACS buffer, removed from the magnetic field and CD11b positive cells were washed out in 5 ml of MACS buffer.

6. Cell lysis and immunoblotting

To detect membrane bound TREM2, membrane fractions were collected as previously described³². Briefly, cells were lysed in hypotonic buffer (100 mM Tris-HCl, pH 7.4, 1mM EDTA, 1 mM EGTA, pH 7.4) freshly supplemented with a protease inhibitors cocktail (Sigma-Aldrich). Membrane fractions were pelleted by centrifugation for 45 min at 16,000 g at 4 °C. Membranes were lysed in STEN lysis buffer (150 mM NaCl, 50 mM Tris-HCl, pH 7.6, 2 mM EDTA, 1% Triton-X 100) on ice for 20 min. Equal amounts of protein were mixed with Laemmli sample buffer supplemented with beta mercaptoethanol followed by protein separation by SDS-PAGE. Proteins were transferred onto polyvinylidene difluoride membranes (Amersham Hybond P 0.45 PVDF, GE Healthcare Life Science) and blocked in 10% I-BlockTM (Thermo Fisher Scientific) for 1 hour. Monoclonal antibody 5F4 (dilution 1:100)³² was used to detect TREM2.

7. iPSC generation

Ethical permission for this study was obtained from the National Hospital for Neurology and Neurosurgery and the Institute of Neurology joint research ethics committee (study reference 09/H0716/64). R47H heterozygous fibroblasts were acquired with a material transfer agreement between University College London and University of California Irvine Alzheimer's Disease Research Center (UCI ADRC; M Blurton-Jones). Fibroblast reprogramming was performed by episomal plasmid nucleofection (Lonza) as previously described ³⁴, using plasmids obtained from Addgene (#27077, #27078 and #27080). Nucleofected cultures were transferred to Essential 8 medium (Life Technologies) after 7 days in vitro (DIV) and individual colonies were picked after 25-30 DIV. All iPSCs were maintained and routinely passaged in Essential 8 medium. Karyotype analysis was performed by The Doctors Laboratory (London, UK). Control iPSC lines used in this study are as follows: CTRL1 (kindly provided by Dr Selina Wray, UCL Institute of Neurology); CTRL2 (SBAD03, Stembancc); CTRL3 (SFC840, Stembancc); CTRL4 (BIONi010-C, EBiSC).

8. iPSC-derived microglia (iMG)

Using previously described protocols, iPSC-microglia (iMG) were generated ^{35,36}.

Day 0: iPSC lines were cultured to 60% confluency in E8 medium on vitronectin-coated 6-well plates. Cells were washed with PBS (w/o Ca²⁺/Mg²⁺), followed by trypLE digestion (1ml/well; 4 min at 37°C). The solution was added to 4 volumes of PBS (w/o Ca²⁺/Mg²⁺), and triturated to a single cell suspension. The suspension was centrifuged for 3 minutes at 300g and the cell pellet resuspended in 1 ml EB differentiation medium (Adapted from ³⁶; EBdiff; Essential 8, 50ng/ml BMP-4, 50ng/ml VEGF, 20ng/ml SCF, and 10µM Y-27632). Cells were counted, and resuspended in EBDiff medium to a density of 10⁵ cells/ml. To generate embryoid bodies (EBs), 100 µl of the suspension was added to 96 well ultra-low attachment round bottom tissue culture plates (Corning), centrifuged at 115g for 3 min, and transferred to a tissue culture incubator at 37°C with 5% CO₂.

Day 2: 50 µl of EBDiff medium was added to each well.

Day 3: Dense EBs were formed and collected with a P1000 Gilson pipette into a sterile 15 ml tube, and left to settle. The spent EBDiff medium was discarded and 10 ml of myeloid differentiation medium (Mdiff; X-VIVO 15 medium (Lonza), 1X Glutamax (Life Technologies), 100U Penicillin/Streptomycin (Life Technologies), 50 µM β-mercaptoethanol (Life Technologies), 100 ng/ml MCSF (Peprotech), and 25 ng/ml IL-3 (Cell Guidance Systems)) added. Approximately 150 embryoid bodies (1.5 x96 well plates) were transferred to a 175 cm² flask containing a further 20 ml of Mdiff medium.

Day 9-11: Mdiff medium (30ml) was added, to avoid acidosis, being careful not to disturb the EBs

Day 26: Cells were collected from the medium for myeloid marker analysis.

Day 33: Once a week, 1/2 of the Mdiff medium/flask containing budded myeloid cells was collected through a 40 µm cell strainer (Falcon, Corning), replacing the collected medium with fresh Mdiff. The myeloid cell suspension was centrifuged for 3 minutes at 300g and the cell pellet resuspended in 1 ml microglial differentiation medium (Adapted from ³⁵; MGdiff; DMEM/F12 HEPES no phenol red, 2% ITS-G (Life Technologies), 1% N2 supplement (Life Technologies), 200 µM monothioglycerol (Sigma), 1X Glutamax, 1X NEAA (Life Technologies), 5µg/ml Insulin (Sigma), 100 ng/ml IL34 (Peprotech), 25 ng/ml MCSF and 5 ng/ml TGFβ1 (Peprotech), filtered through a 0.22 µm syringe filter. Cells were counted and plated in MGdiff, and medium replaced every 3-4 days.

Day 46: MGdiff medium was replaced with microglial maturation medium (MGmat: MGdiff + 100ng/ml CD200 (Generon), and 100ng/ml CX3CL1 (Peprotech)) for 4 days to generate iMG.

9. Isolation of human blood derived-monocytes

Monocytes were obtained from blood through centrifugation with Histopaque (Sigma) to isolate peripheral blood mononuclear cells followed by separation and purification with CD14-conjugated magnetic beads (Miltenyi). Peripheral blood monocytes (PBM) were matured into monocyte-derived macrophages (hMacs) in X-VIVO 15 medium with 1% Glutamax, 100U Penicillin/Streptomycin, and 100ng/ml MCSF for 7 days.

10. Microglia signature gene array

A custom gene array based on published microglial expression data ^{35,37–39} was used to confirm a microglial signature in our iMG cultures (TaqMan Array Plate 32 plus Candidate Endogenous Control Genes; Thermo Fisher Scientific). Complementary DNA was generated from iMG, iPSC-derived microglial like cells ³⁶, and human monocyte-derived macrophage (hMacs) RNA samples using the High-Capacity RNA-cDNA kit (Life Technologies), according to the manufacturer's instructions. Human primary microglia cDNA was also analyzed as a control sample (ScienCell). Quantitative PCR were conducted on the Mx3000p qPCR system with MxPro qPCR software (Stratagene) using TaqMan Gene Expression Mastermix (Thermo Fisher Scientific). Heat maps were generated with the gplots ⁴⁰ and d3heatmap ⁴¹ packages in R.

Microglial gene signature primer details:

Gene name	Primer ID
18s rRNA	Hs99999901_s1
GAPDH	Hs99999905_m1
HPRT	Hs99999909_m1
GUSB	Hs99999908_m1
APOE	Hs00171168_m1
C1QA	Hs00706358_s1
C1QB	Hs00608019_m1
ITGAM	Hs00167304_m1
CSF1R	Hs00911250_m1
CX3CR1	Hs01922583_s1
GAS6	Hs01090305_m1
GPR34	Hs00271105_s1
AIF1	Hs00610419_g1
MERTK	Hs01031979_m1
OLFML3	Hs01113293_g1
PROS1	Hs00165590_m1
SALL1	Hs01548765_m1
SLCO2B1	Hs01030343_m1
TGFBR1	Hs00610320_m1
TMEM119	Hs01938722_u1
TREM2	Hs00219132_m1
BIN1	Hs00184913_m1
CD33	Hs01076282_g1
SPI1	Hs02786711_m1
HEXB	Hs01077594_m1
ITM2B	Hs00222753_m1
C3	Hs00163811_m1
A2M	Hs00929971_m1
C1QC	Hs00757779_m1
RGS1	Hs01023772_m1
FTL	Hs00830226_gH
P2RY12	Hs01881698_s1

11. Immunocytochemistry

Cells were fixed in 4% PFA/sucrose in PBS for 20 minutes at room temperature (RT), quenched with 50 mM NH₄Cl in PBS for 10 min at RT, and permeabilised with 0.2% Triton X-100 in PBS for 5 min at RT. Blocking was performed with 5% normal goat serum (NGS) in PBS for 30 min. Primary antibodies were diluted in 5% NGS/PBS and incubated at RT for 2 hours, followed by PBS washes and incubation with corresponding secondary antibodies for 1 hour at RT in the dark, with gentle rocking. Nuclei were counterstained during mounting using Vectorshield with DAPI (4', 6-diamidino-2-phenylindol; Vector Labs). Fluorescence microscopy was performed on a Zeiss Axioskop 2 microscope and Axiovision software (Zeiss, v4.8). Confocal microscopy was performed on a Zeiss LSM 710 confocal microscope using Zen software (Zeiss, Version 2012), and all images were processed with Image J1.51K (www.imagej.nih.gov/ij). The following antibodies were used: mouse anti-CD68 (1:100, DAKO), rabbit-anti-P2YR12 (1:200, Atlas Antibodies), mouse-anti- β -Actin (1:500, Sigma), mouse-anti-EZR (1:250, Atlas Antibodies), goat anti-rabbit Alexafluor488 (1:500, Life Technologies), goat-anti-mouse Alexafluor568 (1:500, Life Technologies).

12. Cellular splicing assay

Human and mouse TREM2 genomic fragments encoding exon 1, intron 1, exon 2, and a FLAG tag were synthesized by Integrated DNA Technologies. The following primer sets were used for vector cloning: EcoRV-Hs TREM2-Fw (GGATATCCGGGCAGCGCCTGACATGCCTG) and NotI-Hs TREM2-Rv (ATGCGGCCGCTTAGGATTACAAGGATGACGACGATAAG); HindIII-Mm TREM2 Fw (CCCAAGCTTGGGGCGCCTACCCTAGTCC) and XhoI-Mm TREM2-Rv (CCGCTCGAGCGGCTACTTGTCGTCATCG). The amplified fragments were digested by EcoRV/NotI or HindIII/XhoI and the digested fragments were inserted into pcDNA3.1 (+) (Invitrogen). The mutations were introduced in the human and mouse minigene using the Quikchange™ site-directed mutagenesis kit (Agilent). The following mutants were generated:

- (1) R47H is the G>A variant alone encoding arginine;
- (2) R47H^{TCA} is corresponding to sequence variants expressed by the in-house generated TREM2 R47H ki mice (GA>TC, G>A, G>A; also see Fig. 4B);
- (3) R47H^{AA} represents the TREM2 R47H ki mice generated by Jackson Laboratory (G>A, G>A, C>A; also see Fig. 4B);
- (4) TC are the silent mutations in in-house generated TREM2 R47H ki mice (GA>TC)
- (5) AA are the silent mutations in Jax R47H ki mice (G>A, C>A).
- (6) R47H^T represents TREM2 R47H ki mice generated by Cheng Hathaway et al.²⁶

For the cellular splicing assay 8×10^5 HEK293 cells were seeded in 6-well plates with Dulbecco's Modified Eagle Medium (Life Technologies)

supplemented with GlutaMAX™, 10% (v/v) FCS, 100 U/ml penicillin, 100 µg/ml streptomycin and cultured overnight. Cells were transfected with 3 µg of plasmids to express human or mouse TREM2 minigenes using 6 µl lipofectamine 2000 according the manufacturer's instructions (Thermo Fisher Scientific). Transfected cells were cultured in normal medium for 48 hours and collected for RNA extraction using RNeasy Mini Kit (Qiagen) according the manufacturer's instructions. The RNA was used for Reverse transcription polymerase chain reaction (RT-PCR).

13. Reverse transcription polymerase chain reaction

1 µg of total RNA was transcribed into cDNA using SuperScript IV reverse transcriptase and oligo dT (Thermo Fisher Scientific). 2 µl of cDNA was used as template and amplified by polymerase chain reaction (PCR) with GoTaq DNA polymerase (Promega) according the manufacturer's instructions. The reaction condition and primer sequences are listed in Table 1. The PCR products were loaded into 2% agarose gel with GelRed™ (Biotium) for DNA visualization.

Table 1 Primers and PCR conditions used for detecting splice pattern (Forward: Fwd; Reverse: Rev).

Name	Sequence	Reaction condition
MmTREM 2 Fwd	GCTCAATCCAGGAGCACAG T	95°C 1min; (95°C 30sec, 65°C 15sec,

MmTREM 2 Rev	C	TCTGACACTGGTAGAGGCC	72°C 1min) *35 cycle; 72°C 10min
HsTREM 2 Fwd	C	GCCTGACATGCCTGATCCT	95°C 1min; (95°C 30sec, 65°C 15sec, 72°C 1min) *35 cycle; 72°C 10min
HsTREM 2 Rev	C	AGGACCTTCCTGAGGGTGT	72°C 1min) *35 cycle; 72°C 10min

14. Quantitative real-time polymerase chain reaction

RNeasy Mini Kit (Qiagen) was used for total RNA isolation according the manufacturer's instructions. 1 µg of total RNA was transcribed into cDNA using SuperScript IV reverse transcriptase and oligo dT (Thermo Fisher Scientific). RNA levels of human and mouse TREM2 and Tyrobp were analyzed by Taqman® real-time PCR using the 7500 Fast real-time PCR system (Applied Biosystems). For endogenous controls Gusb (Mm01197698_m1, Thermo Fisher Scientific) and Hsp90ab1 (Mm00833431_g1, Thermo Fisher Scientific) or GUSB (Hs00939627_m1, Thermo Fisher Scientific) and HSPAB1 (Hs03043878_g1, Thermo Fisher Scientific) were used. Probes that target mouse TREM2 and Tyrobp are Mm04209424_g1, Mm04209423_g1, Mm01273682_g1, Mm00449152_m1 (Thermo Fisher Scientific). Probes that target human TREM2 and TYROBP are Hs01010721_m1, Hs01003899_m1, Hs00182426_m1 (Thermo Fisher Scientific). For allele specific mRNA expression custom made primers and probes were designed. The primer pair for mouse TREM2 is: CCTTGAGGGTGTTCATGTACTTAT and TCCATTCCGCTTCTTCAG. The probes for the mouse wild-type allele and R47H allele are /5HEX/CCTT+G+C+GT+CT+CC/3IABkFQ/ (+, lock nucleic

acid) and /56-FAM/CTT+T+G+T+GT+C+GA+C/3IABkFQ/, respectively (Integrated DNA Technologies). The primer pair for human TREM2 is ACAAGTTGTGCGTGCTGA and ATGACTCCATGAAGCACTGG. The probes for the human wild-type allele and the R47H allele are /5HEX/CTT+G+C+GCCT+CC/3IABkFQ/ and /56-FAM/TT+G+T+GC+CT+CC/3IABkFQ/, respectively (Integrated DNA Technologies). The probes and primers were mixed in 1:2 ratios for quantitative PCR reaction.

cDNAs were diluted 1:5 with H₂O and 9 µl of diluted cDNA together with 1 µl of primer probe mix, 10 µl of Taqman® master mix (Thermo Fisher Scientific) were used in one 20µl reaction.

Results

1. Reduced mRNA and protein level in TREM2 R47H knock-in mice

The rare TREM2 variant rs75932628-T encodes a histidine instead of arginine at position 47 (R47H) and increases the risk for AD around three fold^{3,4}. The DNA and amino acid sequence around arginine at position 47 is highly conserved across different mammalian species (Fig. 1a & b). To study the impact of this variant on TREM2 function in microglia *in vivo* we generated TREM2 R47H knock-in mice (R47H ki mice) by introducing a G>A mutation using the CRISPR/Cas9 technology (Fig. 1c). Two silent mutations were additionally introduced (GA>TC) to create a Sall restriction site for genotyping (Fig. 1c). In addition, a silent G>A mutation was generated to block the protospacer-adjacent motif (PAM) to allow higher gene editing efficiency (Fig. 1c). The predicted potential off-target sites were analyzed. An off-target event with a Δ 10-Indel mutation was identified at an intragenic region on chromosome 11 (Additional file 1: Fig. 1, putative off-target #2). The founder mouse was back-crossed to C57BL/6N, and off-spring with positive TREM2 R47H ki but negative off-target #2 (i.e ID-7-1; ID-7-2; ID-7-4) were used for establishing the mouse line. Expression of total TREM2 mRNA as well as both TREM2 mRNA transcripts (NM_031254.3 and NM_001272078.1), encoding either membrane bound TREM2 or a truncated soluble version was validated in brain. Interestingly, total TREM2 mRNA including both TREM2 transcripts

was significantly reduced in a gene dose-dependent manner, whereas mRNA expression of Tyrobp (NM_011662), the adaptor protein of TREM2⁴², remained unchanged (Fig. 1d). Using allele specific qPCR we confirmed that expression of the R47H allele is selectively reduced compared to the wt allele in heterozygous R47H ki mice (Fig. 1e & Additional file 4: Table S1).

To confirm decreased TREM2 expression on protein level, we purified microglia from wild-type (wt), heterozygous (het), and homozygous (hom) R47H ki mice and performed western blotting of membrane fractions. Membrane-bound TREM2 showed a gene dose-dependent reduction (Fig. 1f).

Reduced TREM2 R47H mRNA and protein expression was further confirmed in bone marrow derived macrophages (BMDM). Consistent with our findings in brain and microglia, mRNA of both TREM2 transcripts decreased in a gene dose-dependent manner whereas mRNA of Tyrobp remained unchanged (Fig. 1g). Furthermore, immature and mature TREM2 as well as soluble TREM2 (sTREM2) were also reduced in a gene dose dependent manner (Fig. 1h).

To exclude that reduced TREM2 mRNA and protein expression is artificially caused by the introduction of the three silent mutations, we analyzed TREM2 R47H knock-in mice generated by Jackson laboratory (Jax R47H ki mice). In addition to the target variant R47H, these mice harbor two silent mutations (Fig. 2a). One of the silent mutations is a G>A exchange to block the PAM sequence exactly like in the mice generated within our laboratory. The second silent mutation C>A is only present in the Jax R47H ki mice (Fig. 2a).

We investigated TREM2 mRNA and protein levels using homozygous Jax R47H ki mice and their wt counterparts. Again, mRNA from total TREM2 as well as from both transcripts of TREM2 decreased in brains of homozygous ki mice whereas mRNA expression of Tyrobp remained unchanged (Fig. 2b). Western blotting of membrane fractions from BMDM from the Jax R47H ki mice also confirmed a significant reduction of membrane bound and soluble TREM2 (Fig. 2c). Thus reduction of mRNA and protein levels in TREM2 R47H ki mouse was confirmed in two independent mouse models.

2. Aberrant splicing of exon1/2 in TREM2 R47H knock-in mice

Next, we searched for the cellular mechanism responsible for the substantial reduction of the TREM2 R47H mRNA in the two mouse models. Since nonfunctional mRNAs are rapidly removed by mRNA surveillance systems⁴³, we studied splicing of the first intron which separates exon 2 containing the R47H variant from exon 1 harboring the translation initiation site and upstream untranslated sequences. Using RT-PCR with primer pairs against the 5' end of exon 1 and the 3' end of exon 2, we compared the splicing patterns of TREM2 in R47H ki and wt mice (Fig. 3a). A single splicing product of the expected length (465 base pairs) was obtained from wt TREM2 mRNA (Fig. 3b). Surprisingly, an additional smaller splicing product (346 base pairs) was observed in TREM2 R47H heterozygous mice, which was even

more abundant in TREM2 R47H homozygous mice (Fig. 3b) while at the same time the larger splicing product was reduced in a gene dose dependent manner (Fig. 3b). This suggests aberrant splicing of TREM2 pre-mRNA derived from the mutant allele. To independently confirm aberrant splicing, we investigated the Jax R47H ki mice described in Fig. 2. Again, we found an additional smaller RT-PCR product in mutant but not wt mice (Fig. 3c). Furthermore, the larger splicing product was reduced in homozygous ki mice (Fig. 3c). Thus aberrant splicing of R47H pre-mRNA occurs in two independent mouse models. DNA sequencing of the splicing products revealed correct splicing of exon 1 and exon 2 in wt mice and to a lesser extent also in the ki mice (Fig. 3d). However, DNA sequencing of the additional shorter RT-PCR product of both mutant mice revealed that 119 base pairs were deleted at the 5' end of exon 2 (Fig. 3d & Additional file 2: Fig. 2). The deletion leads to a frame shift and a premature stop codon in exon2 (Fig. 3d), which may lead to nonsense mediated mRNA decay and thus explain the consistent reduction of the mutant mRNA in both mouse models.

3. The R47H variant does not affect splicing and mRNA levels in humans

To directly compare the splicing pattern of mouse and human TREM2 R47H, we expressed mouse or human TREM2 minigenes containing exon 1, intron 1, and exon2 in human embryonic kidney 293 cells (HEK 293) (Fig. 4a).

To separately investigate the disease causing TREM2 R47H variant and the silent mutations, we introduced the corresponding sequence variants either alone or together (Fig. 4b). Upon expression of the minigene encoding the mouse TREM2 sequence, we observed miss-splicing induced by the R47H variant alone (R47H) (Fig. 4c). Similar aberrant splicing was observed when the two silent mutations of the Jax R47H ki mice were expressed in addition to the R47H variant (R47H^{AA}), whereas introduction of the two silent mutations alone (AA) did not affect splicing (Fig. 4c). Moreover, when the three silent mutations used to generate our in-house mouse model were combined with the R47H (R47H^{TCA}), a striking increase of aberrant splicing was observed. When we only introduced the unique TC mutations used to generate our mouse model (TC) we also observed impaired splicing (Fig. 4c), suggesting that R47H and TC together display synergistic effects on aberrant splicing. This demonstrates that the R47H variant by itself is sufficient to induce aberrant splicing, but enhanced miss-splicing upon the addition of silent mutations implies that this genomic region is very sensitive for splicing errors induced by minor changes within the pre-mRNA sequence. Finally, we also investigated if the mutations introduced into the mouse genome by Cheng-hathaway et al.²⁶ affect pre-mRNA splicing of TREM2. Very similar to our R47H ki mice and those generated by the Jackson Laboratories, the mutations introduced by Cheng-hathaway and colleagues (R47H^T) caused aberrant splicing (Fig. 4c), which is consistent with the haploinsufficiency also observed in this model²⁶.

To prove if this is also true for human TREM2, we investigated the same TREM2 variants in human minigene constructs (Fig. 4a, b & d). Surprisingly, our results demonstrate that neither the R47H variant alone or in combination with the silent mutations used to generate the ki mouse models affected correct exon1/2 splicing (Fig. 4d). This suggests that only the mouse gene locus is vulnerable for aberrant splicing upon introduction of these sequence variants and implies that the R47H mutation does not affect splicing and mRNA levels in humans.

To provide direct evidence for this prediction, we investigated exon 1/2 splicing in humanized TREM2 mice generated by ectopic expression of the human wt or R47H mutant TREM2 locus in TREM2^{-/-} mice¹⁴. Using the same RT-PCR strategy as described above (Fig. 3a), we could only detect the correctly spliced exon 1 and 2 but no aberrantly spliced additional products (Fig. 5a).

Similarly, in human induced pluripotent stem cell (iPSC) derived microglia (iMG) with the wt TREM2 allele or heterozygous for the TREM2 R47H variant (Additional file 3: Fig.3) we also detected only the correctly spliced exon 1 and 2 (Fig. 5b). Furthermore, no aberrant splicing was detected in AD cases carrying one R47H mutant allele (Fig. 5c). Direct sequencing demonstrated correct exon1/2 splicing in human iMG and in AD cases. Lack of aberrant splicing of human TREM2 R47H is consistent with no reduction of total TREM2 mRNA in iMG with one R47H allele (Fig. 5d). In addition, using allele specific qPCR we confirmed that the expression of the R47H allele is comparable to wt

in iMG (Fig. 5e & Additional file 5: Table S2), and in human brain (Fig. 5f & Additional file 5: Table S2). Taken together, aberrant splicing of R47H mutant pre-mRNA is not observed in humans and consequently no haploinsufficiency of TREM2 could be detected.

Discussion

Most functional studies of TREM2 have so far been performed with either total loss-of-function models or by studying the TREM2 T66M mutation^{7,8,11-13,19,20,44,45}, which is associated with an FTD-like syndrome. Homozygous mice expressing the TREM2 T66M variant phenocopy a number of functional deficits also observed upon total loss of the TREM2 encoding gene¹¹. These include delayed resolution of inflammation upon lipopolysaccharide stimulation, reduced phagocytic activity, reduced microglial activation during physiological ageing and neurological insults, reduced cerebral blood flow, reduced cerebral brain glucose metabolism, impaired chemotaxis and clustering of microglia around amyloid plaques¹¹. However, much less is known about the functional impact of the TREM2 R47H variant, which is associated with a high risk for AD similar to that caused by the ApoE ϵ 4 allele^{3,4,46}. *In vitro* studies suggested reduced binding of A β oligomers, ApoE, and phosphatidylserine due to structural alterations in TREM2^{8,21-24}. Furthermore maturation of the R47H variant within the secretory pathway may also be delayed²⁵. Expression of human TREM2 R47H in TREM2 knockout mice failed to rescue the knockout phenotypes again supporting the notion that TREM2 is protective and that TREM2 variants associated with neurodegenerative diseases may cause a loss-of-function¹⁴. TREM2 R47H knock-in mice expressing this variant under physiological conditions resulted in phenotypes that were compatible with a loss-of function²⁶. Cheng-Hathaway et al. reported that TREM2 R47H heterozygous mice showed reduced TREM2 expression in microglia close to

amyloid plaques, reduced microglial proliferation, reduced dense core plaques and increased neuritic dystrophy²⁶. These phenotypes were associated with reduced TREM2 mRNA expression²⁶. Similarly, Sodom et al. reported reduced TREM2 protein expression in brain as well as reduced sTREM2 in plasma from R47H knock-in mice²⁴. All together, this suggests that the AD-associated TREM2 R47H variant is also associated with a loss-of-function. However, whereas the T66M mutation causes a loss-of-function due to retention of the misfolded mutant protein within the endoplasmic reticulum^{11,25}, the R47H mutation appears to cause haploinsufficiency due to reduced mRNA levels²⁶. We generated a similar mouse model using the CRISPR/Cas9 technology. Consistent with published findings, our mouse model also showed reduced TREM2 mRNA and protein levels. Furthermore, similar findings were made using an independent mouse generated by Jackson Laboratories. We therefore searched for a joined cellular mechanism, which may be involved in the significant reduction of TREM2 mRNA and protein in both mouse models. Surprisingly, we found that the introduction of the R47H variant by itself but even more so the introduction of additional silent mutations caused aberrant splicing. Direct sequencing of the aberrant splicing product revealed that it lacks 119 base pairs. Close inspection of the sequence of the alternative splice product revealed that a cryptic splice acceptor site within the exon 2 was activated. This leads to the elimination of parts of exon 2 resulting in a splicing product containing a premature stop codon. It is well known that such aberrant mRNAs are rapidly degraded by nonsense-mediated mRNA decay⁴⁷. Note that the TaqMan probes used for detecting TREM2

mRNA were either bound to exon 3/4 or exon 4/5 boundary (Fig. 1d) thus they detect both the full length functional TREM2 mRNA and the aberrantly spliced shorter variant. Therefore, the apparent degree of reduction for TREM2 mRNA and protein is not equal (Fig. 1d & f). In addition however, we cannot fully exclude the possibility that the R47H variant may also affect mouse TREM2 protein stability.

The mRNA reductions caused by aberrant splicing, which were consistent in two independent mouse models, led us to investigate if aberrant exon 2 splicing in humans also leads to TREM2 haploinsufficiency. We found that TREM2 mRNA levels and splicing patterns were both normal in iPSC derived human microglia-like cells and in patient brain with the TREM2 R47H variant. Furthermore, cellular splicing assays using minigene constructs demonstrate that the R47H variant induced abnormal splicing only occurs in mice but not in humans. Thus, both the R47H variant as well as additionally introduced silent variants cause a mouse specific reduction of the TREM2 mRNA. Therefore, these findings cannot be translated to humans calling for novel humanized R47H mouse models.

Conclusions

The AD-associated TREM2 R47H variant in combination with silent mutations introduced by the CRISPR/Cas9 technology causes mouse specific aberrant splicing of exon 2, which leads to an alternative TREM2 mRNA

containing a premature stop codon. The observed significant reduction of TREM2 mRNA and protein in R47H ki mice are most likely the consequence of nonsense-mediated mRNA decay of the aberrant transcript and it is not observed in human systems. Thus, functional data derived from TREM2 R47H knock-in mice cannot be translated to humans.

Abbreviations

AD: Alzheimer's disease; A β : amyloid β -peptide; TREM2: Triggering receptor expressed on myeloid cell 2; sTREM2: soluble TREM2; knock-in: ki; PAM: Protospacer-adjacent motif; WT: Wild-type; Het: heterozygous; Hom: Homozygous; BMDM: Bone marrow derived macrophages; RT-PCR: Reverse transcriptase polymerase chain reaction; qPCR: Quantitative polymerase chain reaction; iPSC: Induced pluripotent stem cell; iMG: iPSC derived microglia-like cells; HEK293: Human embryonic kidney 293.

Declarations

1. Ethics approval

All mice were handled according to institutional guidelines approved by the animal welfare and use committee of the government of Upper Bavaria.

Ethics committee from Ludwig-Maximilians- University and University College London approved this research project using human tissue.

2. Consent for publication

Consent for publication on using human tissue in this study is detailed in the Material Transfer Agreement (MTA) between organizations.

3. Availability of data and materials

The datasets used and/or analyzed during the current study are available from the corresponding author on reasonable request.

4. Competing interests

C.H. collaborates with DENALI Therapeutics and received a speaker honorarium from Novartis and Roche. The other authors declare that they have no competing interests.

5. Funding

This work was supported by the Deutsche Forschungsgemeinschaft (DFG) within the framework of the Munich Cluster for Systems Neurology (EXC 1010 SyNergy) and the Koselleck Project HA1737/16-1 (to C.H.) This work was funded by the German Federal Ministry of Education and Research (BMBF) through the Joint Project HIT-Tau (High Throughput Approaches for the Individualized Therapy of Tau-Related Diseases TP2: Grant 01EK1605C to W. W.). This work was supported by the Biotechnology and Biological Sciences Research Council (grant number BB/M009513/1) to A.M. and by funding from the Innovative Medicines Initiative 2 Joint Undertaking under grant agreement No 115976 (for T.P to J.P). This Joint Undertaking receives support from the European Union's Horizon 2020 research and innovation programme and EFPIA. This work was funded by NIH grant RF1 AG051485 to M.C.

6. Authors' contributions

XX designed and conceived the study. XX and CH interpreted the results. CH and XX wrote the manuscript with input from all co-authors. BW and WW generated the TREM2 R47H knock-in mice. GK and BW analyzed potential off-targets. XX, KZ and JH prepared bone marrow and isolated microglia from mice. XX and BB performed RNA analyses and immunoblotting. XX performed RT-PCR, allele specific qPCR and cellular splicing analysis. TP, AM and JP

generated the iPSC derived microglia-like cells and performed qPCR on these cells. MC and WS provided the mouse brain samples from humanized TREM2 mice.

7. Acknowledgements

The authors thank the Queen Square Brain Bank for access to tissue: this resource is funded in part by the Weston Foundation and the MRC.

Publisher's Note

Springer Nature remains neutral with regard to jurisdictional claims in published maps and institutional affiliations.

References

1. Sims, R. *et al.* Rare coding variants in PLCG2, ABI3, and TREM2 implicate microglial-mediated innate immunity in Alzheimer's disease. *Nat. Genet.* **49**, 1373–1384 (2017).
2. Jiang, T. *et al.* A rare coding variant in TREM2 increases risk for Alzheimer's disease in Han Chinese. *Neurobiol. Aging* **42**, 217.e1-3 (2016).
3. Jonsson, T. *et al.* Variant of TREM2 associated with the risk of Alzheimer's disease. *N. Engl. J. Med.* **368**, 107–16 (2013).
4. Guerreiro, R. *et al.* TREM2 variants in Alzheimer's disease. *N. Engl. J. Med.* **368**, 117–27 (2013).
5. Chan, G. *et al.* CD33 modulates TREM2: convergence of Alzheimer loci. *Nat. Neurosci.* **18**, 1556–8 (2015).
6. Krasemann, S. *et al.* The TREM2-APOE pathway drives the transcriptional phenotype of dysfunctional microglia in neurodegenerative diseases. *Immunity* **47**, 566–581.e9 (2017).
7. Mazaheri, F. *et al.* TREM2 deficiency impairs chemotaxis and microglial responses to neuronal injury. *EMBO Rep.* **18**, 1186–1198 (2017).
8. Wang, Y. *et al.* TREM2 lipid sensing sustains the microglial response in an Alzheimer's disease model. *Cell* **160**, 1061–71 (2015).
9. Ulland, T. K. *et al.* TREM2 maintains microglial metabolic fitness in Alzheimer's Disease. *Cell* **170**, 649–663.e13 (2017).
10. Keren-Shaul, H. *et al.* A unique microglia type associated with restricting development of Alzheimer's Disease. *Cell* **169**, 1276–1290.e17 (2017).
11. Kleinberger, G. *et al.* The FTD-like syndrome causing TREM2 T66M mutation impairs microglia function, brain perfusion, and glucose metabolism. *EMBO J.* **36**, 1837–1853 (2017).
12. Jay, T. R. *et al.* TREM2 deficiency eliminates TREM2+ inflammatory macrophages and ameliorates pathology in Alzheimer's disease mouse models. *J. Exp. Med.* **212**, 287–95 (2015).
13. Yuan, P. *et al.* TREM2 haploinsufficiency in mice and humans impairs the microglia barrier function leading to decreased amyloid compaction and severe axonal dystrophy. *Neuron* **92**, 252–264 (2016).
14. Song, W. M. *et al.* Humanized TREM2 mice reveal microglia-intrinsic and -extrinsic effects of R47H polymorphism. *J. Exp. Med.* **215**, 745–760 (2018).
15. Suárez-Calvet, M. *et al.* Early changes in CSF sTREM2 in dominantly inherited Alzheimer's disease occur after amyloid deposition and neuronal injury. *Sci. Transl. Med.* **8**, 369ra178 (2016).
16. Wang, Y. *et al.* TREM2-mediated early microglial response limits diffusion and toxicity of amyloid plaques. *J. Exp. Med.* **213**, 667–75 (2016).

17. Cantoni, C. *et al.* TREM2 regulates microglial cell activation in response to demyelination in vivo. *Acta Neuropathol.* **129**, 429–47 (2015).
18. Poliani, P. L. *et al.* TREM2 sustains microglial expansion during aging and response to demyelination. *J. Clin. Invest.* **125**, 2161–70 (2015).
19. Bemiller, S. M. *et al.* TREM2 deficiency exacerbates tau pathology through dysregulated kinase signaling in a mouse model of tauopathy. *Mol. Neurodegener.* **12**, 74 (2017).
20. Leyns, C. E. G. *et al.* TREM2 deficiency attenuates neuroinflammation and protects against neurodegeneration in a mouse model of tauopathy. *Proc. Natl. Acad. Sci. U. S. A.* **114**, 11524–11529 (2017).
21. Atagi, Y. *et al.* Apolipoprotein E is a ligand for Triggering Receptor Expressed on Myeloid Cells 2 (TREM2). *J. Biol. Chem.* **290**, 26043–50 (2015).
22. Zhao, Y. *et al.* TREM2 is a receptor for β -amyloid that mediates microglial function. *Neuron* **97**, 1023–1031.e7 (2018).
23. Yeh, F. L., Wang, Y., Tom, I., Gonzalez, L. C. & Sheng, M. TREM2 binds to Apolipoproteins, including APOE and CLU/APOJ, and thereby facilitates uptake of Amyloid- β by microglia. *Neuron* **91**, 328–40 (2016).
24. Sudom, A. *et al.* Molecular basis for the loss-of-function effects of the Alzheimer's disease-associated R47H variant of the immune receptor TREM2. *J. Biol. Chem.* **293**, 12634–12646 (2018).
25. Kleinberger, G. *et al.* TREM2 mutations implicated in neurodegeneration impair cell surface transport and phagocytosis. *Sci. Transl. Med.* **6**, 243ra86 (2014).
26. Cheng-Hathaway, P. J. *et al.* The Trem2 R47H variant confers loss-of-function-like phenotypes in Alzheimer's disease. *Mol. Neurodegener.* **13**, 29 (2018).
27. Cheng, Q. *et al.* TREM2-activating antibodies abrogate the negative pleiotropic effects of the Alzheimer's disease variant Trem2R47H on murine myeloid cell function. *J. Biol. Chem.* **293**, 12620–12633 (2018).
28. Brandl, C. *et al.* Creation of targeted genomic deletions using TALEN or CRISPR/Cas nuclease pairs in one-cell mouse embryos. *FEBS Open Bio* **5**, 26–35 (2015).
29. Wefers, B., Bashir, S., Rossius, J., Wurst, W. & Kühn, R. Gene editing in mouse zygotes using the CRISPR/Cas9 system. *Methods* **121–122**, 55–67 (2017).
30. Haeussler, M. *et al.* Evaluation of off-target and on-target scoring algorithms and integration into the guide RNA selection tool CRISPOR. *Genome Biol.* **17**, 148 (2016).
31. Marim, F. M., Silveira, T. N., Lima, D. S. & Zamboni, D. S. A method for generation of bone marrow-derived macrophages from cryopreserved mouse bone marrow cells. *PLoS One* **5**, e15263 (2010).
32. Xiang, X. *et al.* TREM2 deficiency reduces the efficacy of immunotherapeutic amyloid clearance. *EMBO Mol. Med.* **8**, 992–1004 (2016).
33. Galatro, T. F., Vainchtein, I. D., Brouwer, N., Boddeke, E. W. G. M. & Eggen, B. J. L. Isolation of microglia and immune infiltrates from mouse and primate central nervous system. *Methods Mol. Biol.* **1559**, 333–342 (2017).

34. Okita, K. *et al.* A more efficient method to generate integration-free human iPSC cells. *Nat. Methods* **8**, 409–12 (2011).
35. Abud, E. M. *et al.* iPSC-derived human microglia-like cells to study neurological diseases. *Neuron* **94**, 278–293.e9 (2017).
36. van Wilgenburg, B., Browne, C., Vowles, J. & Cowley, S. A. Efficient, long term production of monocyte-derived macrophages from human pluripotent stem cells under partly-defined and fully-defined conditions. *PLoS One* **8**, e71098 (2013).
37. Butovsky, O. *et al.* Identification of a unique TGF- β -dependent molecular and functional signature in microglia. *Nat. Neurosci.* **17**, 131–43 (2014).
38. Muffat, J. *et al.* Efficient derivation of microglia-like cells from human pluripotent stem cells. *Nat. Med.* **22**, 1358–1367 (2016).
39. Haenseler, W. *et al.* A highly efficient human pluripotent stem cell microglia model displays a neuronal-co-culture-specific expression profile and inflammatory response. *Stem cell reports* **8**, 1727–1742 (2017).
40. CRAN - Package gplots.
41. Interactive Heat Maps Using 'htmlwidgets' and 'D3.js' [R package d3heatmap version 0.6.1.2].
42. Bouchon, A., Hernández-Munain, C., Cella, M. & Colonna, M. A DAP12-mediated pathway regulates expression of CC chemokine receptor 7 and maturation of human dendritic cells. *J. Exp. Med.* **194**, 1111–22 (2001).
43. Isken, O. & Maquat, L. E. Quality control of eukaryotic mRNA: safeguarding cells from abnormal mRNA function. *Genes Dev.* **21**, 1833–56 (2007).
44. Jay, T. R. *et al.* Disease progression-dependent effects of TREM2 deficiency in a mouse model of Alzheimer's Disease. *J. Neurosci.* **37**, 637–647 (2017).
45. Wang, Y. *et al.* TREM2-mediated early microglial response limits diffusion and toxicity of amyloid plaques. *J. Exp. Med.* **213**, 667–75 (2016).
46. Colonna, M. & Wang, Y. TREM2 variants: new keys to decipher Alzheimer disease pathogenesis. *Nat. Rev. Neurosci.* **17**, 201–7 (2016).
47. Maquat, L. E. Nonsense-mediated mRNA decay in mammals. *J. Cell Sci.* **118**, 1773–6 (2005).

Figure legends

Figure 1 Trem2 mRNA and protein are reduced in a novel Trem2 R47H knock-in mouse model

a & b Evolutionary conservation of TREM2 at the DNA (**a**) and protein (**b**) level. **c** Strategy to generate Trem2 R47H knock-in (R47H ki) mice indicating the protospacer region (green), protospacer adjacent region (PAM, purple), and the introduced nucleotide changes (orange or red). The restriction site for Sall is underlined. **d** Trem2 and Tyrobp mRNA levels in brains from R47H ki mice. TaqMan probes for the exon 4/5 boundary were used to detect total Trem2 mRNA. TaqMan probes for the Trem2 exon 3/4 boundary were used for isoform discrimination. (N=3, +/-SEM, one way ANOVA, Bonferroni-corrected pair-wise post hoc tests, total Trem2 WT vs. Het P=0.0002, WT vs. Hom P<0.0001; Trem2 isoform 1 WT vs. Het P=0.0029, WT vs. Hom P<0.0001; Trem2 isoform 2 WT vs. Het P=0.0031, WT vs. Hom P=0.0002. n.s. Non-significant.). **e** Allele specific Trem2 mRNA expression in heterozygous R47H ki mice. Customized probes were against Trem2 R47H and its neighbor region (see also Materials and Methods). (N=3, +/-SEM, unpaired t test, P<0.0001). **f** Trem2 protein expression in microglia isolated from Trem2 wt or R47H ki mice. (N=3,+/-SEM, one way ANOVA, P<0.0001, Bonferroni-corrected pair-wise post hoc tests, WT vs. Het P=0.0005, WT vs. Hom P<0.0001). **g** Trem2 and Tyrobp mRNA levels in bone marrow derived macrophages (BMDM) isolated from Trem2 wt and R47H ki mice. (N=3, +/-SEM, one way ANOVA, Bonferroni-corrected pair-wise *post hoc* tests,

Trem2 WT vs. Het P=0.0002, WT vs. Hom P<0.0001; Trem2 isoform 1 WT vs. Het P<0.0001, WT vs. Hom P<0.0001; Trem2 isoform 2 WT vs. Het P=0.0008, WT vs. Hom P<0.0001. n.s. Non-significant.) **h** Expression levels of membrane bound and soluble Trem2 (sTrem2) protein in bone marrow derived macrophages (BMDM) isolated from Trem2 wt or R47H ki mice. (N=3, +/-SEM, one way ANOVA, Trem2 P=0.0003, Bonferroni-corrected pair-wise *post hoc* tests, WT vs. Het P=0.0026, WT vs. Hom P=0.0002, sTrem2 P=0.0007, WT vs. Het P=0.0469, WT vs. Hom P=0.0005).

Figure 2 Trem2 haploinsufficiency in an independent R47H knock-in mouse model provided by Jackson laboratories

a DNA sequence comparison of in-house made Trem2 R47H ki mice (R47H ki mice) and Jax Trem2 R47H ki mice (Jax R47H ki mice). **b** Trem2 and Tyrobp mRNA levels in brains of wt or Jax R47H ki mice. (N=3, +/-SEM, unpaired t test, Trem2 isoform1 P=0.0002; Trem2 isoform2 P=0.0001. n.s. Non-significant.). **c** Expression levels of membrane bound and soluble Trem2 (sTrem2) protein in bone marrow derived macrophages (BMDM) isolated from Trem2 wt or Jax R47H ki mice (N=3, +/-SEM, unpaired t test, Trem2 P=0.0016, sTrem2 P=0.0433)

Figure 3 Aberrant splicing of exon1/2 in two independent Trem2 R47H knock-in mice

a Schematic representation of exon/intron boundaries of Trem2 and the strategy used to investigate exon 1/2 splicing. **b** RT-PCR mediated amplification of splicing products generated by R47H ki mice. **c** RT-PCR mediated amplification of splicing products generated by Jax R47H ki mice. **d** DNA and amino acid sequence of the two splice products identified.

Figure 4 Aberrant splicing of Trem2 variants containing the R47H mutation with and without additional mutations used to create three different R47H ki mice

a The minigene construct used to investigate exon1/2 splicing of the Trem2 variants shown in **(b)**. **b** Sequence alignment of Trem2 variants investigated for aberrant splicing. **c** Exon 1/2 splicing of mouse Trem2 variants described in **(b)**. **d** Exon 1/2 splicing of human TREM2 variants described in **(b)**. Note that only mouse transcripts undergo aberrant splicing. EV: empty vector.

Figure 5 Normal exon 1/2 splicing of human TREM2 pre-mRNA encoding the R47H variant

a Normal splicing of human TREM2 upon ectopic expression of the human wt or R47H mutant TREM2 locus in Trem2^{-/-} mice. **b** Normal exon 1/2 splicing of Trem2 in human induced pluripotent stem cell (iPSC) derived

microglia (iMG) with the wt TREM2 allele or heterozygous for the TREM2 R47H variant. **c** No aberrant splicing of the R47H variant in an AD case carrying one R47H mutant allele. **d** No reduction of total TREM2 mRNA in iMG with one R47H allele. (N=4, +/-SEM, unpaired t test, non-significant.) **e** Allele specific qPCR demonstrates that the expression of the R47H allele is comparable to the wt allele in iMG. (N=7, +/-SEM) **f** Allele specific qPCR demonstrates that the expression of the R47H allele is comparable to wt allele in human brain derived from a R47H carrier. (N=2). Customized probes were against Trem2 R47H and its neighbor region (see also Materials and Methods).

Additional file 1: Figure 1 Off-target analysis of in-house made Trem2 R47H knock-in mice

a Sanger-sequencing chromatogram of the Trem2 on-target site and the six putative off target sites of animal Trem2 R47H ki ID-7. Mixed peaks in the Trem2 locus show the correct R47H substitution (CGC>CAC) and the three silent mutations for genotyping purposes. Mixed peaks in traces of site #2 reveal a Δ 10-Indel mutation at the putative cut site, indicating a true off target event. Underlined: Protospacer; arrow head: putative cut site; green letters: PAM site on shown strand; red letters: PAM site on complementary strand; yellow: Δ 10-Indel mutation. **b** Sanger sequencing results of Trem2 R47H positive off-springs of male ID-7, which was crossed with a C57BL/6N female.

The $\Delta 10$ -Indel allele was inherited to animals ID-7-3 und ID-7-12 that were excluded from any further breedings and experiments.

Additional file 2: Figure 2 Sequence of the aberrantly spliced murine Trem2 mRNA

Trem2 gene sequence. Exon in black; intron in green; // indicates splicing sites.

Additional file 3: Figure 3 iMG differentiation and validation

a Schematic of the in vitro differentiation of iPSC-derived microglia (iMG). (i): Human iPSCs are grown in feeder free conditions with no spontaneous differentiation. Scale bar: 250 μm . (ii): Embryoid bodies are formed in the presence of 3 factors SCF, BMP4, and VEGF; Scale bar: 750 μm . (iii): Myeloid cells are generated after culturing with IL3 and MCSF growth factors for 3-4 weeks, then stained for classic myeloid/macrophage markers CD68. Scale bar: 50 μm . (iv): Further differentiation to microglia-like cells that positive for microglial markers P2RY12. Scale bar: 20 μm . (v): Addition of the two final factors (CD200 and CX3CL1) matures the iMG. Scale bar: 20 μm . **b** Heat map showing mRNA expression of a microglial gene signature in iMG, human monocyte-derived macrophages (hMac), human primary microglia (hMG), and iPSC samples. Clear clustering is observed between iMG and hMG.

**Additional files 4: Table S1 Allele specific quantitative PCR for Trem2
R47H knock-in mice**

**Additional files 5: Table S2 Allele specific quantitative PCR for iMG
and patient brains**

Figures

Figure 1

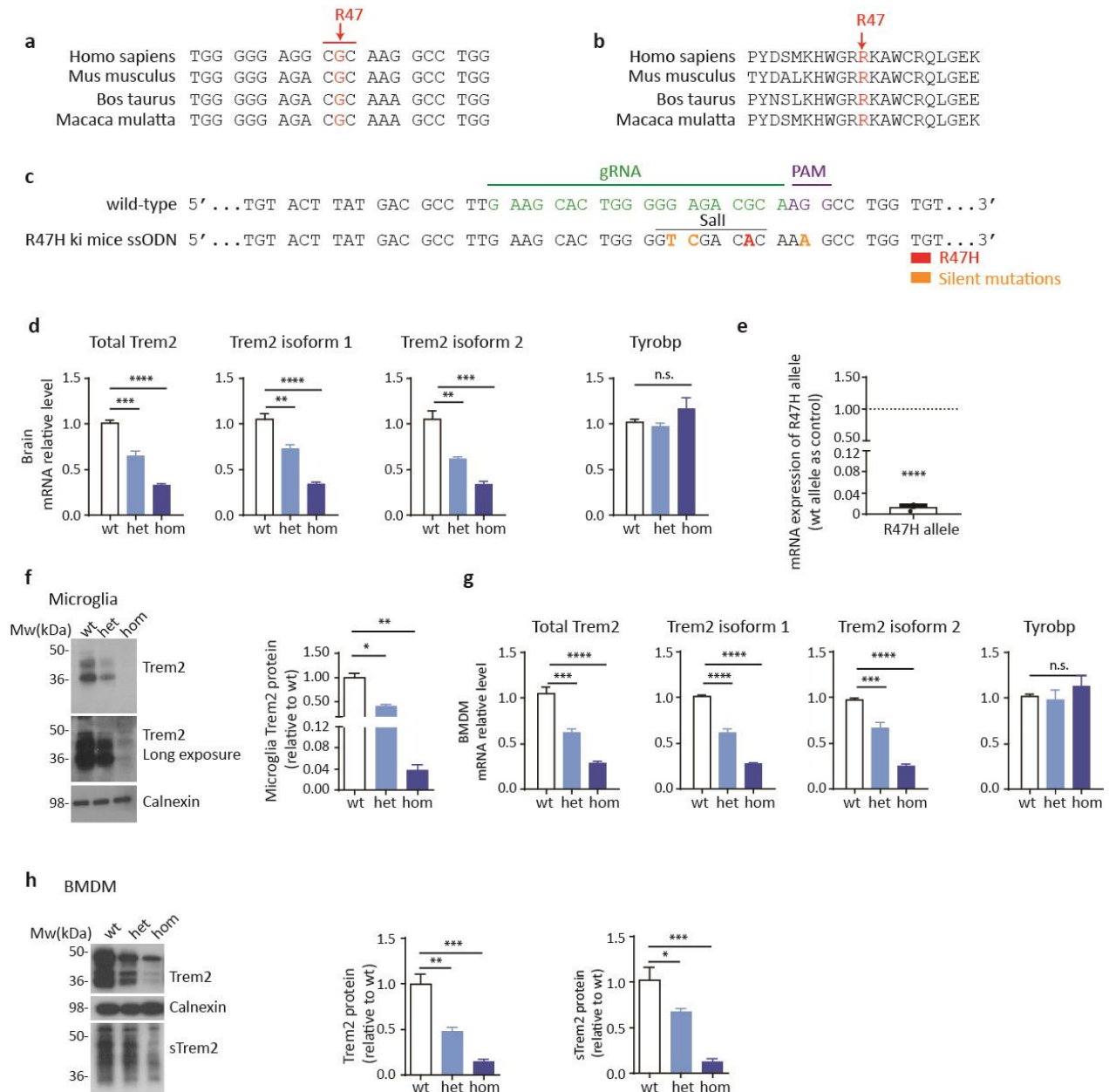


Figure 2

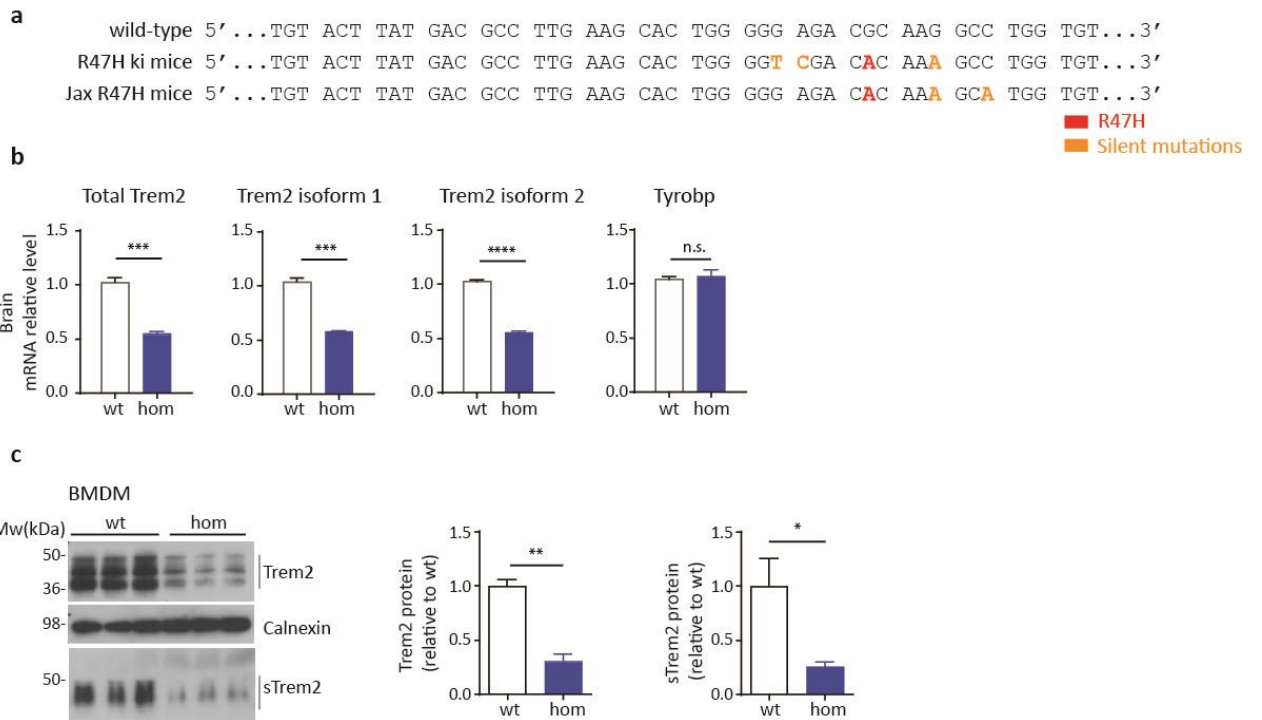


Figure 3

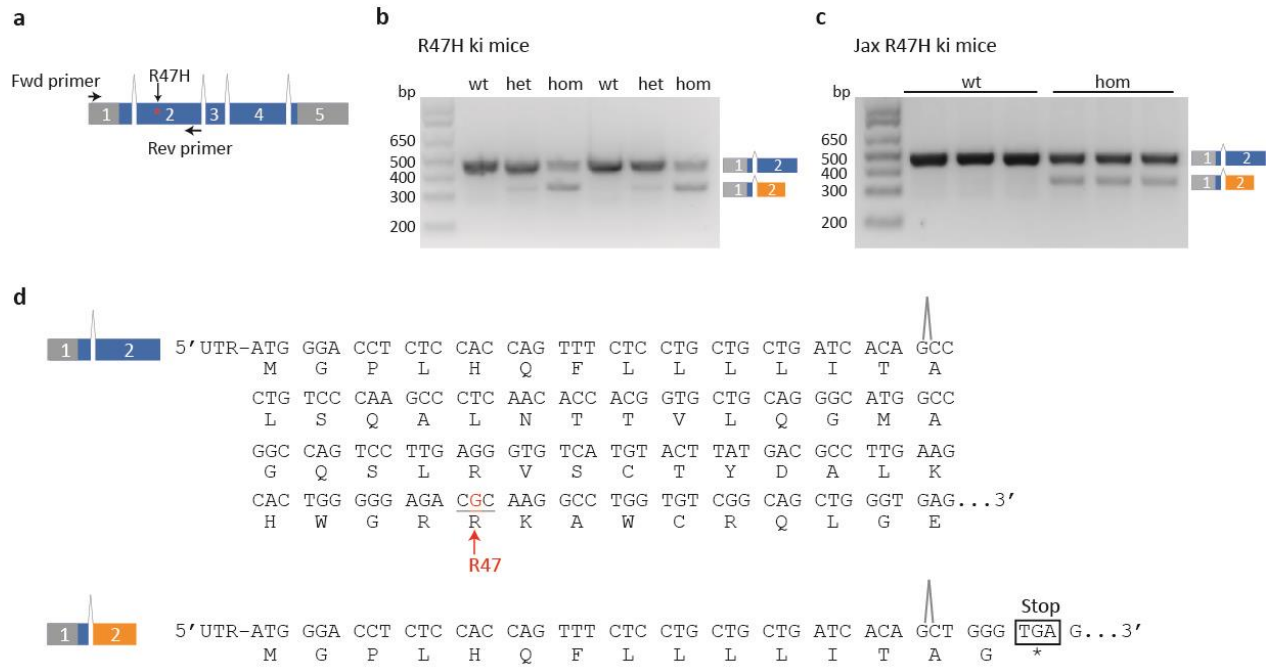
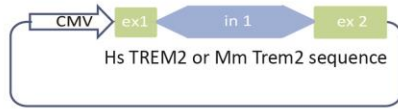


Figure 4

a



b

Mouse Trem2 sequence

wt	5'...TTG AAG CAC TGG GGG AGA CGC AAG GCC TGG...3'	Mouse Trem2 wild-type
R47H	5'...TTG AAG CAC TGG GGG AGA CAC AAG GCC TGG...3'	
R47H ^{TC}	5'...TTG AAG CAC TGG GGT CGA CAC AAA GCC TGG...3'	R47H ki mice
TC	5'...TTG AAG CAC TGG GGT CGA CGC AAG GCC TGG...3'	
R47H ^{AA}	5'...TTG AAG CAC TGG GGG AGA CAC AAA GCA TGG...3'	Jax R47H ki mice
AA	5'...TTG AAG CAC TGG GGG AGA CGC AAA GCA TGG...3'	
R47H ^T	5'...TTG AAG CAC TGG GGG AGA CAC AAG GCT TGG...3'	Cheng-Hathaway et al ki mice

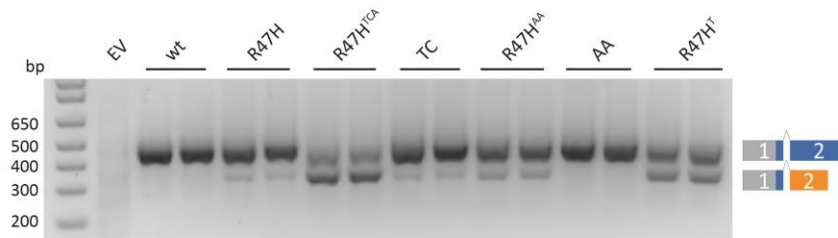
Human Trem2 sequence

wt	5'...ATG AAG CAC TGG GGG AGG CGC AAG GCC TGG...3'
R47H	5'...ATG AAG CAC TGG GGG AGG CAC AAG GCC TGG...3'
R47H ^{TC}	5'...ATG AAG CAC TGG GGT CGG CAC AAA GCC TGG...3'
TC	5'...ATG AAG CAC TGG GGT CGG CGC AAG GCC TGG...3'
R47H ^{AA}	5'...ATG AAG CAC TGG GGG AGG CAC AAA GCA TGG...3'
AA	5'...ATG AAG CAC TGG GGG AGG CGC AAA GCA TGG...3'
R47H ^T	5'...ATG AAG CAC TGG GGG AGG CAC AAG GCT TGG...3'

■ R47H
■ Silent mutations

c

HEK293 / Mouse Trem2 minigene



d

HEK293 / Human TREM2 minigene

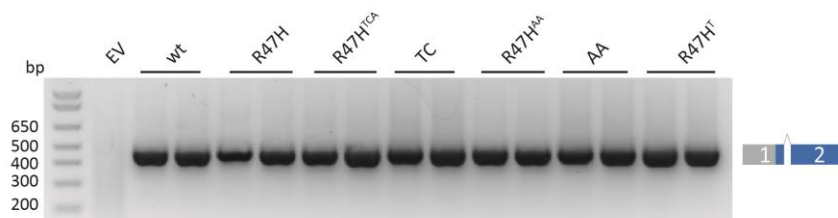
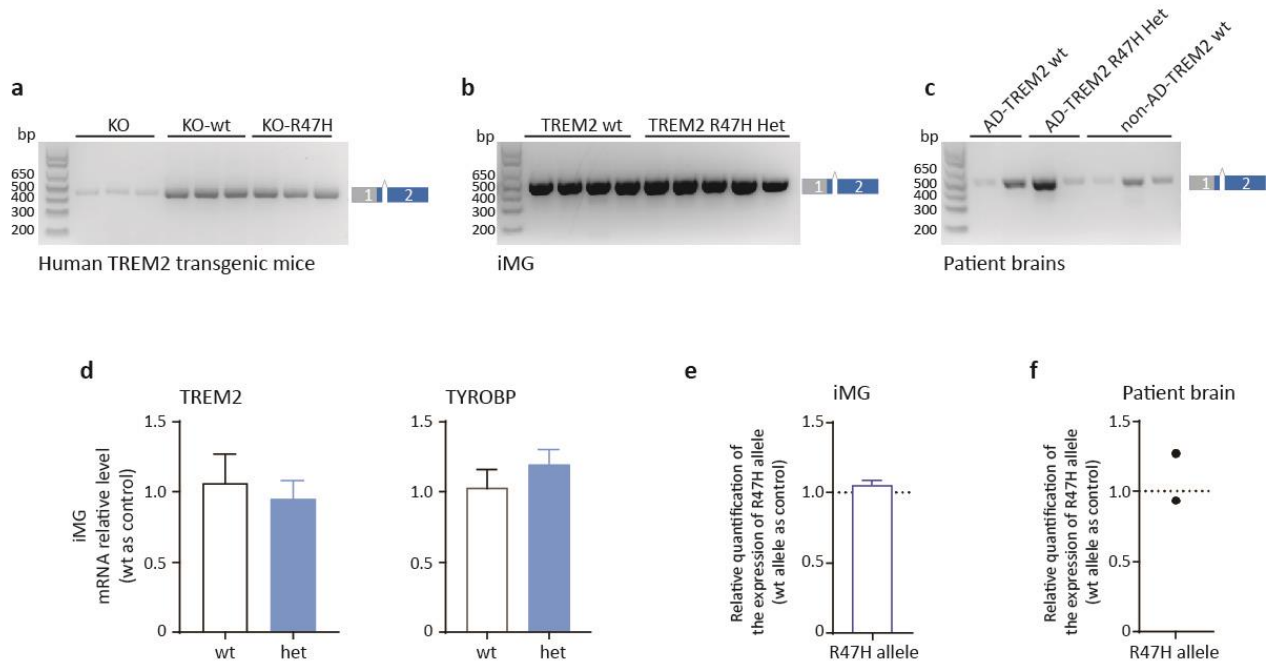
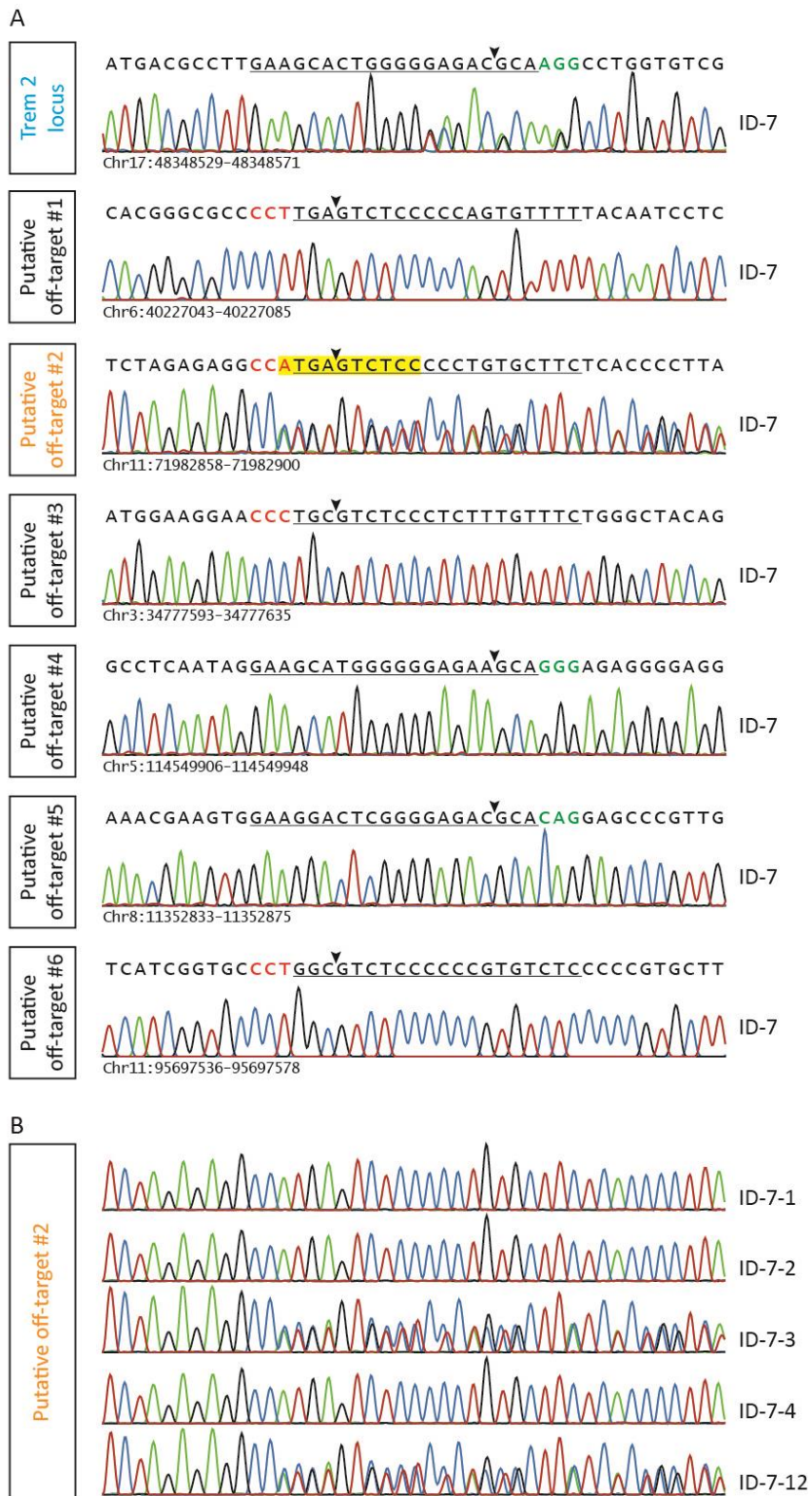


Figure 5



Supplement Figure 1



Supplement Figure 2

a

Normal splicing of Trem2 exon 1 and 2

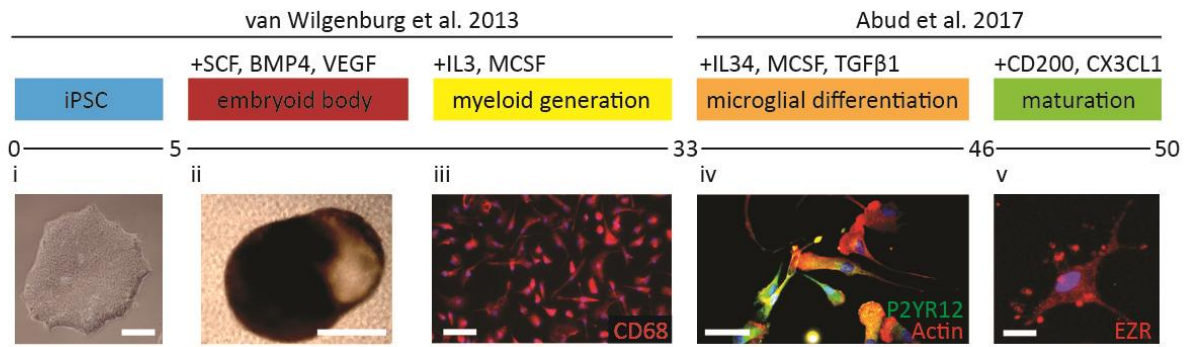
5' UTR-ATGGGACCTCTCCACCAGTTTCTCCTGCTGCTGATCACAG//**GTGGGACCACAGGAGGGAC**
CTA...TGTCTCCTCTGCAG//CCCTGTCCCAAGCCCTCAACACCACGGTGCTGCAGGGCATGGCCGG
CCAGTCCTTGAGGGTGTTCATGTACTTATGACGCCTTGAAGCACTGGGGGAGACGCAAGGCCTGGTGTC
GGCAGCTGGGTGAGGAGGGCCCATGCCAGCGTGTGGTGAGCACACACGGTGTGTGGCTGCTGGCCTTC
CTGA...

Aberrant splicing of Trem2 exon 1 and 2

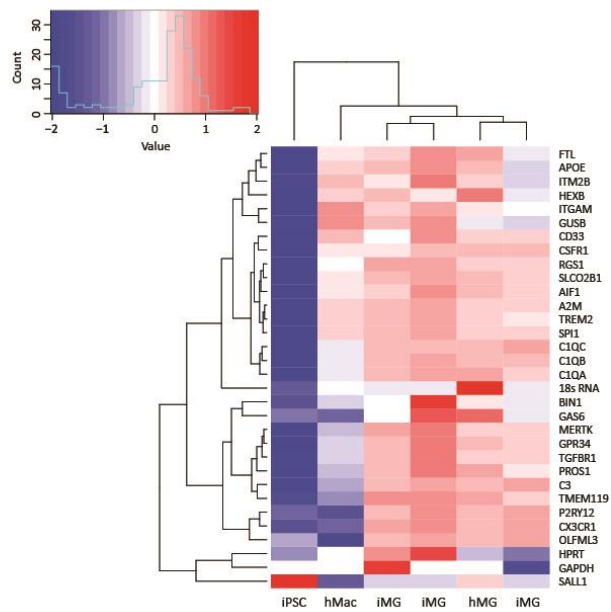
5' UTR-ATGGGACCTCTCCACCAGTTTCTCCTGCTGCTGATCACAG//**GTGGGACCACAGGAGGGAC**
CTA...TGTCTCCTCTGCAGCCCTGTCCCAAGCCCTCAACACCACGGTGCTGCAGGGCATGGCCGGCC
AGTCCTTGAGGGTGTTCATGTACTTATGACGCCTTGAAGCACTGGGGGAGACGCAAGGCCTGGTGTCGG
CAG//CTGGGTGA**GGAGGGCCCATGCCAGCGTGTGGTGAGCACACACGGTGTGTGGCTGCTGGCCTTC**
CTGA... **Stop**

Supplement Figure 3

a



b



Supplement Table 1

Table S1. Allele specific quantitative PCR for Trem2 R47H knock-in mice

Ct mean			
	WT allele	R47H allele	RQ
WT	16,00	Undetermined	-
	15,98	Undetermined	-
	16,12	Undetermined	-
R47H hom	Undetermined	19,92	-
	Undetermined	19,64	-
	Undetermined	19,24	-
R47H het	17,22	24,68	0,0057
	17,43	23,20	0,0183
	17,02	23,00	0,0159

Supplement Table 2

Table S2. Allele specific quantitative PCR for human TREM2 materials

	Ct Mean		
	WT allele	R47H allele	RQ
iMG TREM2 wt	19,922	Undetermined	-
	19,122	Undetermined	-
	26,041	Undetermined	-
	19,616	Undetermined	-
BAC mice TREM2 wt	19,005	Undetermined	-
	19,199	Undetermined	-
BAC mice TREM2 R47H Hom	Undetermined	17,296	-
	Undetermined	17,628	-
iMG TREM2 R47H Het	20,790	20,737	1,038
	20,074	20,061	1,009
	20,674	20,589	1,061
	19,804	19,905	0,932
	21,68	21,63	1,034
	20,89	20,65	1,177
	21,68	21,63	1,034
TREM2 R47H Het patient brain	26,99	27,09	0,934
	31,20	30,86	1,270

Summary and general Discussion

TREM2 contributes to antibody-mediated uptake

My findings indicate that TREM2 deficiency impairs anti-A β antibody-mediated amyloid clearance. In line with the well described phagocytic defects in TREM2 ko cells ¹⁻⁶, showed that microglia and macrophages lacking functional TREM2 engulf less fibrillar A β . This is in contrast to some studies that show wt and TREM2-deficient microglia engulfed similar amount of A β fibrils in *in vitro* assay ^{7,8}. The discrepancy may be explained by differences of A β fibril preparation and/or differences in microglia preparation and cultivation conditions. One of the limitations of *in vitro* phagocytosis assays is the use of synthetic A β fibrils for phagocytosis, which may not represent amyloid plaque clearance. With this limitation in mind, I used an *ex vivo* slice assay to monitor the clearance of physiologically-formed amyloid plaques. Microglia with or without functional TREM2 were cultured on top of consecutive cryosection slices from aged APP/PS1 mice with amyloid plaque pathology. In line with the phagocytosis of fibrillar A β , TREM2-deficient microglia clear fewer physiologically-formed amyloid plaques. This finding suggests that TREM2 loss-of-function reduces amyloid plaque clearance. This clearance defect suggests that TREM2 regulates A β phagocytosis as well as A β degradation, which is supported by the finding that TREM2 regulates the degradation of A β oligomers ⁷. The reduced plaque clearance capacity in microglia lacking functional TREM2 is further supported by the recent finding

that TREM2-dependent activity may promote A β clearance to limit the growth of newly seeded plaques ⁹. *In vivo* TREM2-dependent activities include many aspects of microglial functions, for example, phagocytosis, migration, proliferation and ApoE-secretion. TREM2 deficiency impairs microglial survival in mice with AD pathology ⁸. In the *ex vivo* slice assay, cell survival was controlled by measuring cell density before and after incubation. No cell death was detected during the incubation period. This may be due to the short incubation period or to the fact that the cells were in an activated stage since they were in close contact with brain slices. TREM2 deficiency also reduces microglial migration towards stimuli ¹⁰. This migration defect might contribute to the observed reduction in plaque clearance in TREM2 loss-of-function cells; therefore, a high density of microglia was used in this study to limit the migration requirements.

To study the anti-A β antibody-mediated uptake, Anti-A β antibody mAb11 was used to mimic the clinical situation as the binding properties of mAb11 is similar to the clinically used gantenerumab ^{11,12}. mAb11 strongly boosted A β and amyloid plaque engulfment in a concentration-dependent manner in the presence or absence of functional TREM2. However, TREM2-deficiency significantly reduced the uptake of antibody-bound fibrillar A β and the clearance of antibody-covered plaques in all conditions tested, indicating that the phagocytic machinery is impaired. Surprisingly, the fold increase of uptake in response to increasing antibody concentration was similar between TREM2 ko phagocytes and their wt counterpart. This indicates that although the

TREM2-dependent machinery is impaired, a TREM2-independent pathway might contribute to the antibody-mediated uptake.

The uptake of antibody-bound immune complexes are mainly mediated by the Fc gamma receptors (FcγR) ^{13,14}. FcγR mediated pathway might compensate the phagocytic defects in TREM2 deficient cells. The mRNA level of the main Fc gamma receptors, FcγRI, FcγRIIB, FcγRIII and FcγRIV, were increased in macrophages from TREM2 deficient animals, and this mRNA upregulation is translated into increased cell surface protein expression of FcγRI, FcγRIIB, FcγRIII. The functional consequence of the increased cell surface FcγRs was that the phosphorylation of Syk, the common downstream signal for TREM2 and FcγR activation ¹⁵⁻¹⁷, was much stronger in TREM2-deficient cells upon Aβ-antibody complex stimulation. This demonstrates that increased cell surface FcγRs induced stronger downstream signaling. Furthermore, the increased FcγRs signaling might compensate for the TREM2-dependent phagocytic defects, explaining why antibody treatment can promote Aβ and amyloid plaque clearance in a concentration-dependent manner in the absence of functional TREM2. In addition to phagocytosis, activation of FcγRs results in pro-inflammatory response including the release of TNFα and IL-1β, which may negatively affect neurons ^{18,19}. Therefore, the observed increase in FcγRs activation in TREM2 loss-of-function microglia may lead to stronger antibody-induced side effects. To finally address this question, it will be important to study TREM2-dependent antibody effector functions *in vivo*.

Antibody-mediated amyloid plaque clearance is normally time- and dose-dependent^{11,20}. Titration experiments were used to study the efficacy of antibody-mediated uptake. An obvious concentration-dependent clearance was observed in both genotypes. Again, at all conditions used, TREM2-deficient macrophages cleared less amyloid deposits. The *ex vivo* assay indicates that TREM2-deficiency impairs the amyloid clearance capacity; however, it can be promoted with increasing antibody concentration due to the enhanced FcγR signaling.

A limitation of my study is that it is lacking *in vivo* validation. In future *in vivo* studies, the experimental subjects should be carefully chosen (e.g. age and models), since the impact of TREM2 on plaque load is biphasic, with attenuation of plaque growth at the early but not late stage⁹. Most mouse models with plaque pathology have strong overexpression of APP and PS1 with disease-causing mutations, and this may easily override the modulation effects mediated by TREM2.

The *in vitro* and *ex vivo* assays are controlled systems that were used for investigation of TREM2-dependent antibody-mediated phagocytosis. Thus, my finding that the phagocytic deficiency is partially compensated for by enhanced FcγRs signaling in TREM2 loss-of-functions microglia is relevant for clinical studies as microglia-mediated plaque clearance is important for the outcome of amyloid-based AD therapies. My data also suggest that higher antibody dosage should be considered in TREM2 deficient patients. TREM2-dependent phagocytosis is important for both amyloid and antibody-bound amyloid

clearance, and thus microglia activation via TREM2-modulation may boost amyloid clearance to achieve optimal therapeutic outcome.

The TREM2 R47H variant impairs TREM2 splicing in mice but not in humans

The TREM2 R47H variant, encoded by rs75932628-T, is one of the strongest risk factors for LOAD ^{21,22}. Studies utilizing TREM2-deficient mice and cells reveal that TREM2 is crucial for microglial functions, for example, microglia activation during normal aging, phagocytosis of cellular debris and protein aggregates, and migration ^{1,3,23–25}. *In vitro* studies indicate that the R47H variant impairs TREM2 binding to lipids, ApoE and A β oligomers ^{7,8,26,27}, suggesting that the R47H variant weakens TREM2 functions. In addition, structural analysis of TREM2 shows that R47 is important for structure stabilization of TREM2 ²⁸. However, it is unclear how the R47H variant modulates disease progression *in vivo*. Overexpression of human TREM2 R47H in *TREM2*^{-/-} : 5xFAD mice failed to rescue TREM2 loss-of-function phenotypes, including reduced microgliosis and microglia activation ²⁹. This data suggests that the AD-associated variant R47H causes loss-of-function phenotypes and that TREM2 is protective against disease progression. The potential functions of sTREM2 might also be impaired by the R47H mutation. sTREM2 binds to neurons and amyloid plaques, and the R47H variant impairs this binding ²⁹. Consistent with the loss-of-function hypothesis, Parhizkar and colleagues reported that microgliosis and plaque-associated ApoE both are reduced in AD patients with the TREM2 R47H variant ⁹. A very recent study using TREM2 R47H ki mouse model with endogenous TREM2 expression shows that the TREM2 R47H heterozygous mice exhibited reduced plaque

associated microglia, reduced proliferation and increased plaque-associated neuritic dystrophy³⁰. The R47H variant reduces the TREM2 mRNA level, and this was thought to be the reason for the TREM2 loss-of-function phenotypes, at least in mice³⁰.

Together with B. Wefer, I also independently generated TREM2 R47H ki mice (R47H ki mice) using the CRISPR/Cas9 technology. Of note, all the available TREM2 R47H ki mice, including the one generated in-house, the one reported by Cheng-Hathaway et al³⁰ and the one generated by Jackson laboratory (Jax R47H mice), harbor the R47H mutation as well as silent mutations facilitating genome editing. In line with the published findings³⁰, TREM2 mRNA and protein were reduced in the in-house R47H ki mice in a dose-dependent manner. Furthermore, TREM2 mRNA and protein are also decreased in Jax R47H mice. The observed TREM2 mRNA and protein reduction from three different TREM2 R47H ki mice is most likely caused by the R47H variant.

It is known that the quality of mRNA is tightly controlled by mRNA surveillance systems³¹. Surprisingly, an aberrant splicing was detected in two TREM2 R47H ki mouse models (in-house generated R47H ki mice and Jax R47H mice). A cryptic acceptor site within the exon 2 was activated, leading to a deletion of nucleotides 1-119 at the 5' end of exon 2 and also to a frame shift and a premature stop codon in exon 2. mRNA with a premature stop codon is quickly degraded by the mRNA surveillance system called nonsense-mediated mRNA decay³². It is likely that the aberrantly spliced TREM2 mRNA with the

premature stop codon was degraded by the nonsense-mediated mRNA decay pathway, hence less TREM2 mRNA was detected in TREM2 R47H ki mice. Thus, aberrant splicing-induced mRNA decay leads to TREM2 haplo-insufficiency in TREM2 R47H ki mice.

Although the R47H variant activates a cryptic splicing site in mice, no aberrant splicing was detected in human iPSC derived microglia-like cells and patient brains harboring the TREM2 R47H variant. As a result, the TREM2 mRNA level remains unchanged in human microglia derived from induced pluripotent stem cells (iMG) harboring one TREM2 R47H allele. In addition, the expression of the R47H allele is comparable to the wt allele in iMG and patient brain samples. This finding raises the possibility that the R47H variant impairs TREM2 function by different mechanisms in humans and in mice. Using a cellular splicing assay, the splicing pattern of the human and mouse TREM2 R47H variant was compared. The TREM2 R47H variant by itself is sufficient to induce aberrant splicing in mouse TREM2. However, neither the R47H variant nor silent mutations alter the splicing of human TREM2. In summary, TREM2 R47H alters TREM2 splicing in mice but not in humans. This indicates that the TREM2 haplodeficiency phenotypes found in TREM2 R47H heterozygous AD mouse models³⁰ are not translatable to humans. Thus, humanized TREM2 R47H mice with endogenous expression level should be generated to study the cellular consequence of the TREM2 R47H variant. Finally, my finding that the AD-associated variant R47H induces a mouse-specific reduction in TREM2 mRNA that does not apply to humans is highly relevant for TREM2-based therapy as ki mice are often used in pre-clinical studies.

References

1. Xiang, X. *et al.* TREM2 deficiency reduces the efficacy of immunotherapeutic amyloid clearance. *EMBO Mol. Med.* **8**, 992–1004 (2016).
2. Takahashi, K., Rochford, C. D. P. & Neumann, H. Clearance of apoptotic neurons without inflammation by microglial triggering receptor expressed on myeloid cells-2. *J. Exp. Med.* **201**, 647–57 (2005).
3. Kleinberger, G. *et al.* TREM2 mutations implicated in neurodegeneration impair cell surface transport and phagocytosis. *Sci. Transl. Med.* **6**, 243ra86 (2014).
4. Hsieh, C. L. *et al.* A role for TREM2 ligands in the phagocytosis of apoptotic neuronal cells by microglia. *J. Neurochem.* **109**, 1144–56 (2009).
5. Colonna, M., Turnbull, I. & Klesney-Tait, J. The enigmatic function of TREM-2 in osteoclastogenesis. *Adv. Exp. Med. Biol.* **602**, 97–105 (2007).
6. Cantoni, C. *et al.* TREM2 regulates microglial cell activation in response to demyelination in vivo. *Acta Neuropathol.* **129**, 429–47 (2015).
7. Zhao, Y. *et al.* TREM2 is a receptor for β -amyloid that mediates microglial function. *Neuron* **97**, 1023–1031.e7 (2018).
8. Wang, Y. *et al.* TREM2 lipid sensing sustains the microglial response in an Alzheimer's disease model. *Cell* **160**, 1061–71 (2015).
9. Parhizkar, S. *et al.* Loss of TREM2 function increases amyloid seeding but reduces plaque-associated ApoE. *Nat. Neurosci.* **22**, 191–204 (2019).
10. Mazaheri, F. *et al.* TREM2 deficiency impairs chemotaxis and microglial responses to neuronal injury. *EMBO Rep.* **18**, 1186–1198 (2017).
11. Bohrmann, B. *et al.* Gantenerumab: a novel human anti-A β antibody demonstrates sustained cerebral amyloid- β binding and elicits cell-mediated removal of human amyloid- β . *J. Alzheimers. Dis.* **28**, 49–69 (2012).
12. Lathuilière, A. *et al.* A subcutaneous cellular implant for passive immunization against amyloid- β reduces brain amyloid and tau pathologies. *Brain* **139**, 1587–604 (2016).
13. Bard, F. *et al.* Peripherally administered antibodies against amyloid β -peptide enter the central nervous system and reduce pathology in a mouse model of Alzheimer disease. *Nat. Med.* **6**, 916–9 (2000).
14. Schenk, D. *et al.* Immunization with amyloid- β attenuates Alzheimer-disease-like pathology in the PDAPP mouse. *Nature* **400**, 173–7 (1999).
15. Paradowska-Gorycka, A. & Jurkowska, M. Structure, expression pattern and biological activity of molecular complex TREM-2/DAP12. *Hum. Immunol.* **74**, 730–7 (2013).
16. Crowley, M. T. *et al.* A critical role for Syk in signal transduction and phagocytosis mediated by Fc γ receptors on macrophages. *J. Exp. Med.* **186**, 1027–39 (1997).

17. Ulrich, J. D. & Holtzman, D. M. TREM2 Function in Alzheimer's Disease and Neurodegeneration. *ACS Chem. Neurosci.* **7**, 420–7 (2016).
18. Guillot-Sestier, M.-V., Doty, K. R. & Town, T. Innate Immunity Fights Alzheimer's Disease. *Trends Neurosci.* **38**, 674–681 (2015).
19. Fuller, J. P. *et al.* Comparing the efficacy and neuroinflammatory potential of three anti- β antibodies. *Acta Neuropathol.* **130**, 699–711 (2015).
20. Sevigny, J. *et al.* The antibody aducanumab reduces A β plaques in Alzheimer's disease. *Nature* **537**, 50–6 (2016).
21. Guerreiro, R. *et al.* TREM2 variants in Alzheimer's disease. *N. Engl. J. Med.* **368**, 117–27 (2013).
22. Jonsson, T. *et al.* Variant of TREM2 associated with the risk of Alzheimer's disease. *N. Engl. J. Med.* **368**, 107–16 (2013).
23. N'Diaye, E.-N. *et al.* TREM-2 (triggering receptor expressed on myeloid cells 2) is a phagocytic receptor for bacteria. *J. Cell Biol.* **184**, 215–23 (2009).
24. Ulland, T. K. *et al.* TREM2 maintains microglial metabolic fitness in Alzheimer's Disease. *Cell* **170**, 649–663.e13 (2017).
25. Mazaheri, F. *et al.* TREM2 deficiency impairs chemotaxis and microglial responses to neuronal injury. *EMBO Rep.* **18**, 1186–1198 (2017).
26. Atagi, Y. *et al.* Apolipoprotein E is a ligand for Triggering Receptor Expressed on Myeloid Cells 2 (TREM2). *J. Biol. Chem.* **290**, 26043–50 (2015).
27. Yeh, F. L., Wang, Y., Tom, I., Gonzalez, L. C. & Sheng, M. TREM2 Binds to Apolipoproteins, including APOE and CLU/APOJ, and thereby facilitates uptake of amyloid- β by microglia. *Neuron* **91**, 328–40 (2016).
28. Sudom, A. *et al.* Molecular basis for the loss-of-function effects of the Alzheimer's disease-associated R47H variant of the immune receptor TREM2. *J. Biol. Chem.* **293**, 12634–12646 (2018).
29. Song, W. M. *et al.* Humanized TREM2 mice reveal microglia-intrinsic and -extrinsic effects of R47H polymorphism. *J. Exp. Med.* **215**, 745–760 (2018).
30. Cheng-Hathaway, P. J. *et al.* The Trem2 R47H variant confers loss-of-function-like phenotypes in Alzheimer's disease. *Mol. Neurodegener.* **13**, 29 (2018).
31. Isken, O. & Maquat, L. E. Quality control of eukaryotic mRNA: safeguarding cells from abnormal mRNA function. *Genes Dev.* **21**, 1833–56 (2007).
32. Maquat, L. E. Nonsense-mediated mRNA decay in mammals. *J. Cell Sci.* **118**, 1773–6 (2005).

Acknowledgments

I would like to express my sincerest thanks and gratitude to my supervisor Prof. Dr. Dr. h.c. Christian Haass for providing me the PhD candidate position and guiding me through my dissertation.

I thank Prof. Dr. Harald Steiner and Dr. Arthur Liesz to be members of my Thesis examination committee. They always gave me guidance and many useful suggestions. I would like to thank Dr. Gernot Kleinberger for great help and countless discussions. I must also acknowledge Dr. Kai Schlepckow, Dr. Marc Suarez, Dr. Fargol Mazaheri, Samira Parhizkar, Dr. Anja Capell, Georg Werner for their valuable suggestions. They are a fantastic team to work with. Furthermore, I am grateful for my collaborators, Dr. Bernd Bohrmann and Dr. Irene Knuesel, who provided me with the valuable antibody and shared their thoughts. I wish to thank the GSN for providing me guidance and training during my PhD period. I furthermore want to acknowledge all readers of this thesis. Last but not least, I would like to give my sincere gratitude to my family, including my husband, who always support my research and give me numerous valuable suggestions and helped me through some tough moments; my parents, who live more than ten thousand kilometers away but always give me love and supports; my little daughter, who is my motivation to be better.

Curriculum Vitae

XIANG, Xianyuan Date of birth: 08.01.1986 Nationality: P.R. China

Education

2013-2019 PhD candidate

Graduate School of Systemic Neurosciences (GSN);

Ludwig-Maximilians-University Munich (LMU), Munich, Germany

2011-2013 Master of Biology 'Molecular and Physiological Biology'

Katholieke Universiteit Leuven, KU Leuven, Leuven Belgium

2004-2008 Bachelor of Science 'Biotechnology'

Shenzhen University, Guangdong China

Research

2013-2018 PhD thesis supervised by Prof. Dr. Dr. h.c. Christian Haass

Topic: The role of TREM2 in pathogenesis and treatment of Alzheimer's disease

2011-2013 Master thesis supervised by Prof. Dr L. Arckens

Topic: The age-dependent effect of monocular enucleation on the expression pattern of cytosolic and membrane proteins in mouse visual cortex

2004-2008 Undergraduate thesis supervised by Prof. Dr. LIU, Shide

Topic: Specific Lethal Effects of Trace Neutral Red on Amoeba discoides and Trichodina

Awards

Partial scholarship from Science@Leuven

Outstanding Graduates Awards from Shenzhen University

Top Prize of Shenzhen University Scholarship

List of publications

1. **Xiang X**, *et al.*, The Trem2 R47H Alzheimer's risk variant impairs splicing and reduces Trem2 mRNA and protein in mice but not in humans. *Mol. Neurodegener.* 13, 49 (2018).
2. **Xiang X**, *et al.*, TREM2 deficiency reduces the efficacy of immunotherapeutic amyloid clearance. *EMBO Mol. Med.* 8, 992–1004 (2016).
3. K. Zhu, **Xiang X**, Filser S, *et al.*, β -Site amyloid precursor protein cleaving enzyme 1 inhibition impairs synaptic plasticity via seizure protein 6. *Biol Psychiatry.* 83(5):428-437 (2018).
4. G. Kleinberger, Brendel M, Mracsko E, Wefers B, Groeneweg L, **Xiang X**, *et al.*, The FTD-like syndrome causing TREM2 T66M mutation impairs microglia function, brain perfusion, and glucose metabolism. *EMBO J.* 36, 1837–1853 (2017).
5. Ardura-Fabregat A, Boddeke EWGM, Boza-Serrano A, Brioschi S, Castro-Gomez S, Ceyzériat K6, Dansokho C, Dierkes T, Gelders G, Heneka MT, Hoeijmakers L, Hoffmann A, Iaccarino L, Jahnert S, Kuhbandner K, Landreth G, Lonnemann N, Löschmann PA, McManus RM, Paulus A, Reemst K, Sanchez-Caro JM, Tiberi A, Van der Perren A, Vautheny A, Venegas C, Webers A, Weydt P, Wijasa TS, **Xiang X** *et al.*, Targeting Neuroinflammation to Treat Alzheimer's Disease. *CNS Drugs.*31 (2017) pp.1057-1082

Eidesstattliche Versicherung / Affidavit

Hiermit versichere ich an Eides statt, dass ich die vorliegende Dissertation 'The role of TREM2 in pathogenesis and treatment of Alzheimer's disease' selbstständig angefertigt habe, mich außer der angegebenen keiner weiteren Hilfsmittel bedient und alle Erkenntnisse, die aus dem Schrifttum ganz oder annähernd übernommen sind, als solche kenntlich gemacht und nach ihrer Herkunft unter Bezeichnung der Fundstelle einzeln nachgewiesen habe.

I hereby confirm that the dissertation 'The role of TREM2 in pathogenesis and treatment of Alzheimer's disease' is the result of my own work and that I have only used sources or materials listed and specified in the dissertation.

München, den 26.07.2019

Munich, date 26.07.2019

Unterschrift Signature Xianyuan Xiang

Declaration of author contributions

Paper I: X.X. G.K. and C.H. designed the study and interpreted the results. X.X. performed all experiments except generating mutant N9 cells, which was performed by G.W. and A.C., the quantification of cell surface Fcγ-receptors expression level was done by A.L.; B.B. and I.K. provided antibodies. R.F. generated monoclonal antibody against TREM2 (clone 5F4). F.M. and G.K. provided bone marrow cells. C.H. wrote the manuscript with input of all co-authors.

Paper II: X.X. designed and conceived the study. C.H. and X.X. interpreted the results. C.H. and X.X. wrote the manuscript with input from all co-authors. B.W. and W.W. generated the TREM2 R47H knock-in mice. G.K. and B.W. analyzed potential off-targets. X.X., K.Z. and J.H. prepared bone marrow and isolated microglia from mice. X.X. and B.B. performed RNA analyses and immunoblotting. X.X. performed RT-PCR, allele specific qPCR and cellular splicing analysis. T.P., A.M. and J.P. generated the iPSC derived microglia-like cells and performed qPCR on these cells. M.C. and W.S. provided the mouse brain samples from humanized TREM2 mice.

Munich 01.08.2018

Signature:

Xianyuan Xiang

Prof. Dr. Dr. h.c. Christian Haass